Preliminary Design Considerations for a Commercial Launch Vehicle Upper Stage

Phillip Kwabena Konadu Gyasi-Agyei

Submitted in fulfilment of the academic requirements for the degree of Master of Science in Mechanical Engineering, College of Agriculture, Engineering and Science, University of KwaZulu-Natal.

Supervisor: Dr Jean-Francois Pitot de la Beaujardiere

Co-Supervisor: Prof Michael J. Brooks

Declaration 1 – Plagiarism

I, Phillip Kwabena Konadu Gyasi-Agyei, declare that:

1. The research reported in this thesis, except where otherwise indicated, is my original research.

2. This thesis has not been submitted for any degree or examination at any other university.

3. This thesis does not contain other persons' data, pictures, graphs or other information, unless specifically acknowledged as being sourced from other persons.

4. This thesis does not contain other persons' writing, unless specifically acknowledged as being sourced from other researchers. Where other written sources have been quoted, then:

    a) Their words have been re-written but the general information attributed to them has been referenced.

    b) Where their exact words have been used, then their writing has been placed in italics and inside quotation marks, and referenced.

5. This thesis does not contain text, graphics or tables copied and pasted from the Internet, unless specifically acknowledged, and the source being detailed in the thesis and in the References sections.

Signed:

……

Mr Phillip Kwabena Konadu Gyasi-Agyei

As the candidate's Supervisor I agree/do not agree to the submission of this thesis.

Signed:

……

Dr Jean-Francois Pitot de la Beaujardiere

As the candidate's Supervisor I agree/do not agree to the submission of this thesis.

Signed:

……

Prof Michael J. Brooks

Acknowledgements

I would like to express my gratitude for the continuous guidance and advice I've received from my supervisors, Dr Michael Brooks and Dr Jean Pitot. Their leadership has allowed me to grow my potential and produce this body of work.

I'm grateful for the support, encouragement and camaraderie shown by my colleagues in the ASReG office. Their invaluable knowledge has accelerated my work and the banter has kept me sane. Special thanks to Nino Wunderlin, Duran Martin and Ryan Cooper for their work on the SAFFIRE engine, the basis of my work.

I would like to express my deepest appreciation to the DST for making funding available to sustain my research and for their continual support of the SAFFIRE programme.

To my family, who have been the wind in my sails, encouraging me to challenge myself and persevere through difficulties. To not fear my dreams.

Lastly, I would like my best friend, Bash, for her patience and words of wisdom throughout my research.

MEMENTO MORI

Abstract

The African small satellite industry (micro and nano satellites in particular) continues to grow with developments in the miniaturization of satellite technology. However, the costs and delays involved with the traditional “piggy backing” satellite launch method is unsustainable for small sat developers and has thus created a niche market for dedicated small satellite launch services. Notably, there is no satellite launch capability whatsoever in Africa, meaning all of the continent’s launch requirements are serviced by foreign providers, incurring additional cost.

As its primary objective, the University of KwaZulu-Natal’s (UKZN’s) Aerospace Systems Research Group (ASReG) seeks to enable the establishment of an indigenous small satellite launch capability in alignment with the South African Government’s goals. To this end, ASReG is currently developing the LOX/Kerosene SAFFIRE (South African First Integrated Rocket Engine) to propel a hypothetical two-stage orbital launch vehicle, termed Commercial Launch Vehicle 1 (CLV). The upper stage of the launch vehicle will use a vacuum-expanded variant of SAFFIRE called SAFFIRE-V. The upper stage for both cases must meet the design constraints of a 0.85 mass fraction and a 1.2 m outer diameter. CLV has been envisaged to deliver a 75kg payload to 400 km sun synchronous orbit.

This thesis presents a high level analysis focusing on the upper stage of CLV, which intends to guide design decisions by comparing design options based on mass, and develop a methodology for upper stage vehicle design. One of the major design decisions is the type of propellant feed system the vehicle should use; in this regard, the analysis compares an electric pump feed system to a pressure fed system. Another is the selection of propellant tank material, given that the propellant tanks constitute most of the mass of a rocket. Stainless steel (301 and Duplex), aluminium alloy (7075), aluminium-lithium (2195), carbon fibre reinforced plastic (T700/Epoxy), as well as combinations of materials were compared.

To perform the preliminary mass analysis, each of the major components/systems of the CLV upper stage were independently designed and the various design options available for each of the components/systems were compared based on mass. These systems and components include: fuel and oxidiser propellant tanks, the propellant pressurization system and the reaction control system. After the individual analyses of the variations of each component, the best suited architectures were modelled in SolidWorks® CAD software. The components were then assembled, in CAD.

The analysis found that, on a preliminary basis, the Lithium ion (Li-Ion) based electric pump fed upper stages did not meet the mass requirements while Lithium polymer (Li-Po) based upper stages achieved the mass requirements. An upper stage employing stainless steel propellant tanks was found to meet the mass requirements, but only for a pressure fed upper stage. Overall, pressure fed upper stages had lower masses compared to electric pump vehicles. The mass reduction of thin walled, low pressurized,

propellant tanks (resulting from using electric pumps) was offset by the mass of the battery packs required to power the pumps.

Contents

List of Figures

List of Tables

Nomenclature

Symbol	Description	Units
A	Area	m^2
A_t	Area of Throat	m^2
C^*	Characteristic Velocity	m/s
D	Diameter	m
Ø	Diameter	m
E	Elastic Modulus	Pa
R	Gas Constant	J / mol K
g_o	Gravitational Constant	m/s^2
L	Length	m
M	Mach Number	-
m	Mass	kg
m_1	Mass Dry	kg
m_0	Mass Final	kg
M_R	Mass Ratio	-
P	Power	W
P	Pressure	Pa
r	Radius	m
I_{SP}	Specific Impulse	s
T	Temperature	K
t	Thickness	m
t	Time	s
V	Volume	m^3

Greek Symbol	Description	Units
α	Wrap Angle or Conical Half Angle	radians
δ	Power Density	kW/kg
δ	Energy Density	Wh/kg
ϵ	Curing Factor	—
ε	Nozzle Expansion Ratio	—
η	Efficiency	—
γ	Specific Heat Capacity Ratio	—
λ	Nozzle Efficiency	—
ρ	Density	kg/m^3
σ	Tensile Strength	Pa
τ	Torque	Nm
ζ	Mass Fraction	—
ζ_d	Discharge Correction Factor	—

Subscript	Description
0	Initial
a	Atmosphere
b	Battery Pack
c	Composite
cr	Critical Failure Point
d	Dry
e	Exit
E	Engine
em	Electric Motor
f	Final
fp	Fuel Pump
ft	Fuel Tank
g	Gas
gt	Pressurant Tank
i	Internal
inv	Inverter
l	Liner
o	Outer
op	Oxidiser Pump
ot	Oxidiser Tank

Subscript	Description
p	Propellant
pu	Pumps
T	Propellant Tank
t	Throat
V	Vapour
w	Wet

Abbreviation	Description
Al	Aluminium
Al-Li	Aluminium-Lithium
ASReG	Aerospace Systems Research Group
BLDC	Brushless Direct Current Motor
CFRP	Carbon Fibre Reinforced Plastics
CLV	Commercial Launch Vehicle 1
CTG	Cold Gas Thruster
ICBM	Intercontinental Ballistic Missile
JAXA	Japan Aerospace Exploration Agency
LEO	Low Earth Orbit
Li-Ion	Lithium-Ion
Li-Po	Lithium-Polymer
LOX/LOX	Liquid Oxygen
NPSH	Net Positive Suction Head
O/F	Oxidiser-Fuel
RCS	Reaction Control System
SAFFIRE	South African First Integrated Rocket Engine
SS	Stainless Steel
SSO	Sun Synchronous Orbit
Ti	Titanium
ULA	United Launch Alliance

1 Introduction

1.1 Background

In recent years, the miniaturization of satellites has gained momentum as a design approach, especially for start-up companies who develop small, cost effective satellites with the capabilities of larger, older satellites. These miniaturized satellites fall within a mass range of 10 g to 500 kg and are further classified as follows: femtosatellites (10 g – 100 g), picosatellites (< 1 kg), nanosatellites (1 kg – 10 kg), microsatellites (10 kg – 100 kg) and small satellites (100 kg – 500 kg) (Di Mauro et al., 2018).

The challenge miniature satellite manufacturers face is getting their satellites into orbit, within a desired time frame, without the high cost associated with dedicated launches for their satellites. Traditionally, ride sharing (as a secondary payload) has been the only low cost alternative. Ride sharing, however, has the major disadvantage of potential delays, given that the launch is dependent on the primary payload's development (Doncaster et al., 2016). This has created a niche market for affordable dedicated small satellite launches, a niche that many entrepreneurs are trying to occupy in a movement called "New space". Figure 1-1, published by SpaceWorks, shows a forecast of micro and nanosatellite launches which indicates the need for more dedicated launch services for miniature satellites in the coming years.

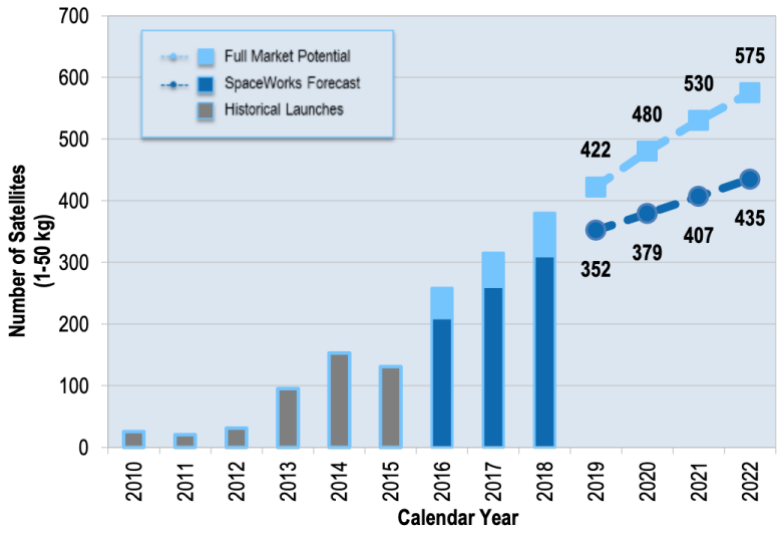

Figure 1-1: Micro/nanosatellite launch history and projections (Doncaster et al., 2016)

New space refers to the commercialisation of the space sector, led by a wave of entrepreneurs who are developing products and services for space (Nagendra, 2019). New space start up enterprises, unlike traditional space agencies (e.g. Boeing and Lockheed Martian) who wait and compete for government projects, they are privately funded and embark on their own space projects. This allows them to service a larger market and develop in shorter time frames with less bureaucracy (Berger, 2019).

One of the most important decisions of a liquid rocket launch vehicle's design is the propellant feed system it will use, this decision effects the cost, complexity and mass of the vehicle. Broadly, there are two types of liquid propellant feed systems for rocket engines. The first is a "pressure fed system" which forces the propellant out of the propellant storage tanks at the required chamber pressure, using a high pressure gas. The second is known as a "pump fed system" and uses pumps to draw the propellants from the propellant storage tanks and pressurizes them to chamber pressure. Pressure fed engines can be further categorized as either being a blow down, pressure regulated or gas-generator systems. Pump fed engines are characterized by how the turbines are driven (i.e. gas generator cycle, staged combustion cycle or expander cycle). The various pump fed rocket engine cycles are depicted in Figure 1-2 below.

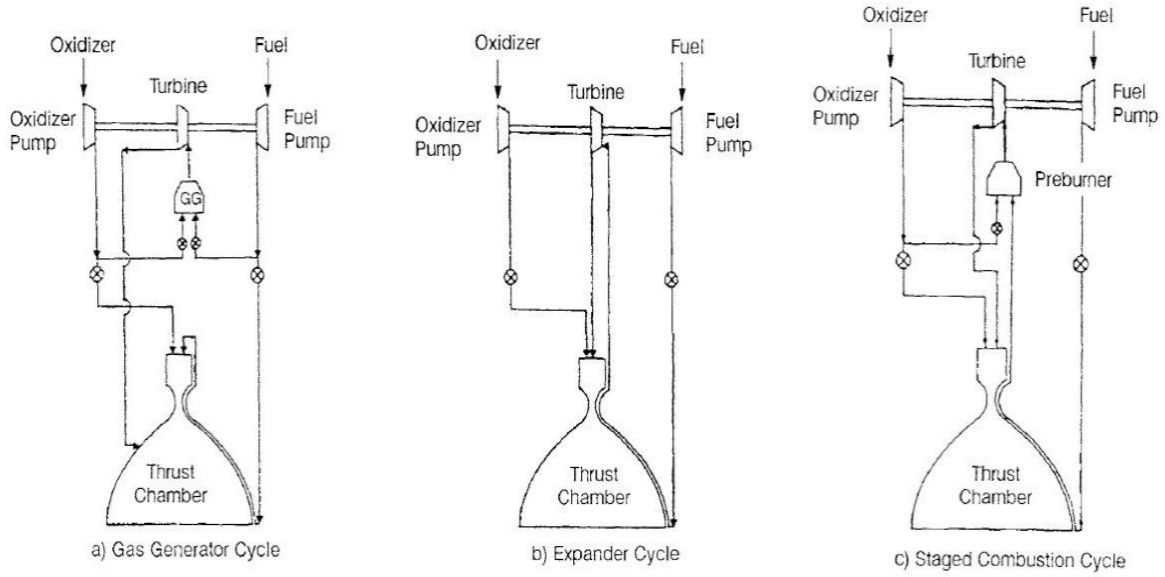

Figure 1-2: Pump fed rocket engine cycles (Huzel and Huang, 1992)

There exists a new type of propulsion cycle called an electric pump (or electro-pump) feed system, where the pumps are driven by electric motors (powered by batteries) instead of a gas turbine. Without a turbine and the associated hardware, the system design and operation of an electric pump feed system is simplified with a greater emphasis placed on software to control the motors (Kwak et al., 2018). To date, only Rocket Lab's Electron launch vehicle has successfully reached orbit with an electric pump fed system (Waxenegger-Wilfing et al., 2018). Astra Space are following Rocket Lab's lead and are developing an electric pump fed launch vehicle of their own, having tested the system in a suborbital launch (Etherington, 2020).

South Africa, and Africa as a whole, do not possess a satellite launch capability and so do not feature in the opportunity-rich "New Space" movement, where small satellite launch has gained traction as a viable market. In response to this reality, the University of KwaZulu-Natal's Aerospace Systems Research Group (ASReG) seeks to drive the development of a South African small satellite launch capability, and to this end, has conceptualised a hypothetical two-stage small satellite launcher, CLV

(Commercial Launch Vehicle 1). It has been envisaged that CLV will be powered by the SAFFIRE (South African First Integrated Rocket Engine) liquid propellant rocket engine (Wunderlin et al., 2018), which is currently being developed by ASReG. CLV's booster stage will be propelled by nine SAFFIRE engines, while the second stage will be propelled by a single vacuum-optimised variant of SAFFIRE. At the beginning of this study, CLV had the objective of delivering a 75 kg payload to 400km sun synchronous orbit (SSO); this requirement has since been updated to 300 kg to 500 km SSO.

The intention is for SAFFIRE to be fed by electric pumps, however, cost, complexity, and time may hamper this. Figure 1-3 shows the proposed electric pump feed system for the SAFFIRE engine. Each pump will be independently driven by an electric motor, allowing for precise oxidiser/fuel (O/F) ratio control.

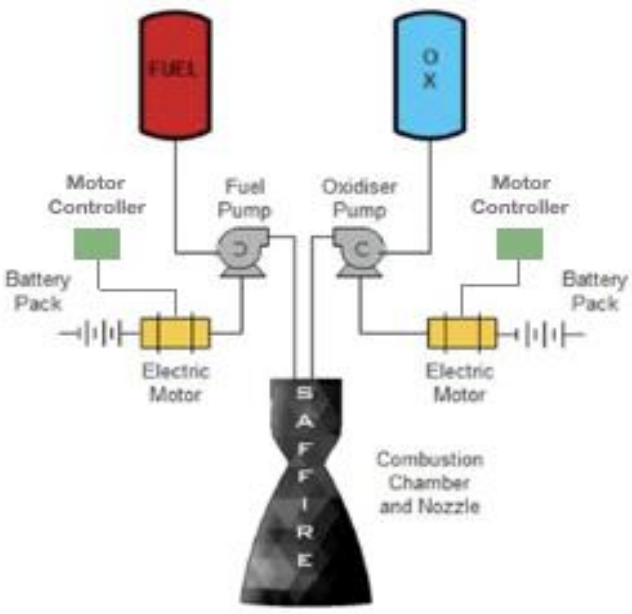

Figure 1-3: Electric pump feed system (Chetty, 2018)

At the time of this study, three other SAFFIRE based masters projects were underway conducting research related to injector design, combustion chamber design, and cold flow injector testing. In addition to this, preliminary hydrodynamic designs of the fuel and oxidiser pumps have been developed by Chetty (2018) and Singh (2018).

1.2 Problem Statement

Designing an orbital launch vehicle is a complex endeavour, complex because there are many interconnected elements. The problem faced by the SAFFIRE team is determining the performance requirements for the booster stage/1st stage. The booster stage design relies on the mass of the elements upstream (i.e. the upper stage and the payload), while the allowable mass of the upper stage is governed by the overall mass of the booster stage. It is clear that the design will be an iterative endeavour.

The SAFFIRE team have chosen the upper stage as the starting point for the iterative design process as it will be the first stage manufactured when improving the project's TRL. Following the work of Chetty (2018) and Wunderlin (2017), the upper stage must have a mass fraction between 0.84 and 0.85 to achieve the 75 kg to 400 km or 500 km SSO requirement. There is therefore need for a standard preliminary design methodology, one that allows for quick, high level iterations, of practical upper stage designs which meet specific performance requirements. The hypothetical vehicle specifications outlined by Wunderlin and Chetty are listed in Table 1-1 . Chetty (2018)'s vehicle is less refined and was used to design the pumps, while Wunderlin (2018)'s vehicle is a more accurate approximation.

Table 1-1: CLV's hypothetical specifications

Parameter	**Booster Stage**	**Upper Stage**
Wunderlin (2018)		
Payload-to-Orbit	75 kg to 400 km SSO	
Engine Thrust	25 kN (Sea Level)	27.5 kN (Vacuum)
Chamber Pressure	50 bar	12 bar
Burn Time	116 s	240 s
O/F Ratio	2.45	2.73
Propellant Mass Flow Rate	8.9 kg/s	7.9 kg/s
Mass Fraction	0.885	0.840
Feed System	Electro-Pump	Pressure Fed
Chetty (2018)		
Payload-to-Orbit [kg/km]	75 kg to 500 km SSO	
Engine Thrust	25 kN	27.46 kN
Chamber Pressure	50 bar	50 bar
Burn Time	116 s	249.4 s
O/F Ratio	2.45	2.6
Propellant Mass Flow Rate	8.64 kg/s	8.64 kg/s
Mass Fraction	0.750	0.850
Feed System	Electro-Pump	Blow Down

To achieve this the input variables (which are essentially the design constraints) which influence upper stage design must be identified. The variables such as: propellant tank maximum diameter, which effects the overall height and aspect ratio of the tanks; and engine burn time and O/F ratio, they govern the propellant requirements.

The mass estimates of upper stage design iterations will be attained by designing and modelling the major systems and components which make up an upper stage. Microsoft Excel was used to perform design calculations and SolidWorks® CAD was used to visually represent designs. Figure 1-41-4 shows a detailed breakdown of the various systems and components this thesis will focus on.

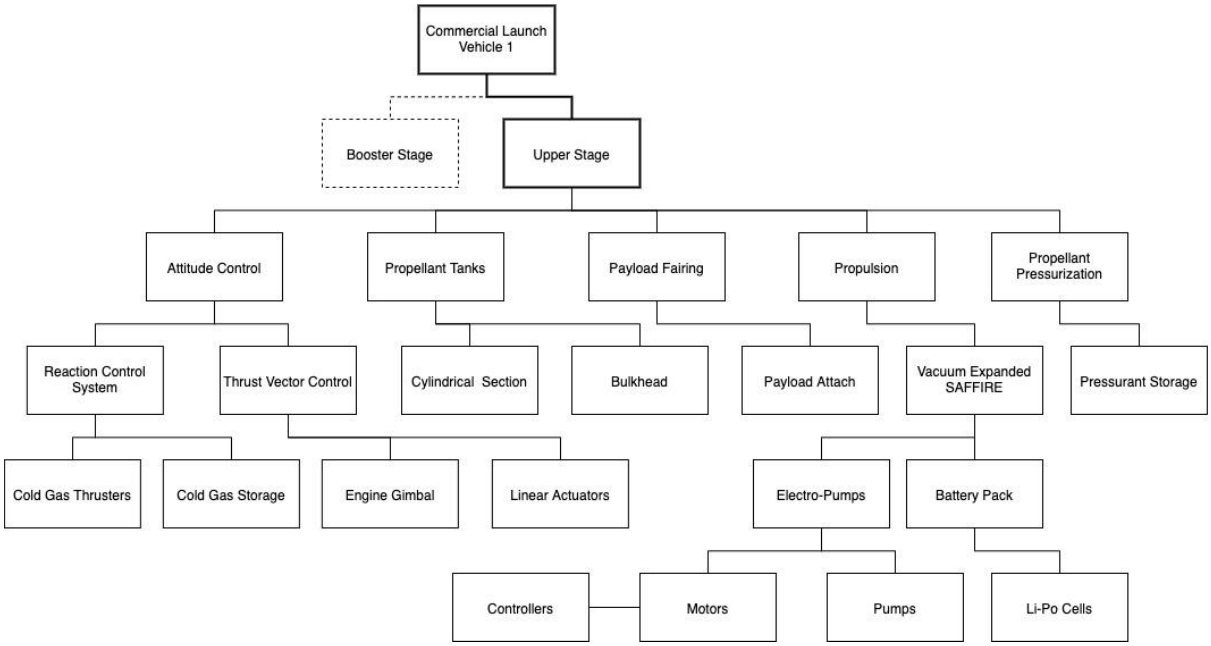

Figure 1-4: CLV upper stage feature tree

1.3 Motivation

The nano/microsatellite industry in Africa has seen growth in recent years. The reduced cost of satellite manufacture, due to the miniaturization of satellite technology, has allowed African research institutions to manufacture and launch their own satellites. By offering cost effective access to space, a dedicated small satellite launch service, based in Africa, would encourage further growth in space research and development.

Liquid rockets have been in existence since 1926 and are favourable due to their power density compared to other rockets. There is a wealth of information available on their design and operation, however, this research is in context of 1st world countries. The USA lead the space race, in part, due to the high budget allocated by the government to research and development of space technology.

In Africa, however, the majority of intellectual capital is dedicated to solid rocket research, primarily for military use. There is thus a research gap on liquid rocket design in an African context, where the design must be cost effective, simple and robust.

1.4 Research Objectives

This thesis will focus on the preliminary design of the upper stage of CLV. In addition to this it will determine whether an upper stage vehicle (using the proposed electric pump feed system) can meet the 0.85 mass fraction requirement, which was determined by Chetty (2018) based on results obtained from the Silverbird Launch Performance Calculator and a preliminary trajectory analysis. Finally, a comparison between the electric pump fed system and the simpler, more robust, pressure fed system will be made using mass as the key performance measure.

The objectives of this research are as follows:

1) Develop a preliminary design methodology for upper stage design.

   This objective seeks to provide a framework for future vehicle design in order to reduce the time and effort for creating new renditions of vehicles. It will also outline the major design decisions associated with vehicle design.

2) Compare various upper stage designs on a mass basis. Compare an electric pump fed system must also be assessed based on mass fraction.

   This objective will serve as a practical test of the methodology and will establish preliminary mass information on the various design options available for the major components of an upper stage, comparing materials and geometries.

   This objective will also advise the SAFFIRE team on the feasibility of pursuing an electric pump fed upper stage while identifying elements which produce the greatest mass.

3) Identify areas of future research based on findings.

1.5 Thesis Outline

This first chapter introduces the SAFFIRE program and its theoretical launch vehicle CLV. It also introduces the concept of NewSpace and motivates the need for South Africa to enter this market. Chapter 2 is a review of the history, trends and key concepts of upper stage vehicles. The information detailed therein focuses on the major components of an upper stage.

Chapter 3 documents the design process associated with each of the major components of an upper stage vehicle. Vehicle final design concepts are proposed in this chapter.

To determine the structural integrity of the propellant tanks, a buckling analysis was performed, comparing the critical buckling stress of various propellant tank materials, for a given configuration. Four buckling theories are compared over a range of tank wall thicknesses. The results of this analysis appear in Appendix A.

In Chapter 4, the mass estimates of the vehicle's components are compared considering various materials and configurations in order to determine the best performing system architecture. One of the vehicle concepts presented in Chapter 3 is also analysed to compare the electric pump fed and pressure fed configurations. The findings of the study are discussed within Chapter 4, and conclusions and recommendations for future work are presented in Chapter 5.

2 Literature Review

2.1 Small Launch Vehicles

Various options are available for placing a miniature satellite (also called a “small satellite”) into orbit. A satellite could have a “dedicated launch” as the primary payload of a launch vehicle. A dedicated launch is advantageous because a satellite can be deployed to an orbit specified by the operator within a flexible time frame (Crisp et.al, 2014). The convenience, however, incurs a high cost (compared to the other options) as the launch vehicle’s payload capacity is not fully utilised. Traditionally, dedicated launches are used to service medium and large satellites (Crisp et.al, 2014).

“Ride sharing” is another option, here multiple satellites of a similar size share a single launch vehicle. Ride sharing is attractive because the launch cost per satellite is reduced as the number of satellites increases (Chavez et.al, 2017). The downside is the inability for an operator to choose a specific orbit for their satellite. Satellite constellations make use of this option as they consist of multiple satellites of the same size being deployed to the same orbit (King et.al., 2016).

The third option is a “piggyback launch” as a secondary payload, the satellite occupies the excess volume available in the fairing of a larger, primary payload’s dedicated launch vehicle. The launch date and orbit is completely dictated by the primary payload’s development and operation orbit, this means the secondary payload must be flexible in terms of schedule, design (to fit into the free space) and operational orbit (Salvini et.al, 2004). Presently most miniature satellites are placed into orbit as secondary payloads via piggy backing or ride sharing.

CubeSats are currently leading the industry demand and are directly responsible for the New Space movement (Niederstrasser, 2018). Miniaturisation of technology means CubeSats have similar capabilities to their larger predecessor for a fraction of the manufacturing and development cost, this has attracted start up enterprises and educational institutions to invest in CubeSat development. The increased demand for CubeSats means operators are not satisfied with piggy backing or ride sharing due to the associated delays and orbit limitations. Operators now seek low cost dedicated launch services for their satellites (Niederstrasser and Frick, 2015).

To be cost effective, the dedicated launch of a miniature satellite requires a “small launch vehicle” or “small lift vehicle”. The cost of a dedicated launch with a medium or heavy lift vehicle would render the mission infeasible (Crisp et.al, 2014). According to Foust and Smith (2004) the Associate Administrator for Commercial Space Transportation at the Federal Aviation Administration (FAA/AST) classifies a launch vehicle as “small” when its payload capabilities are below 2268 kg to

low Earth orbit (LEO). Table 2-1 and Table 2-2, respectively, list well known small launch vehicles currently in operation and under development.

Table 2-1: Small Launch Vehicles in Operation

Manufacturer	**Launch Vehicle**	**Payload-to-Orbit**	**First Launch**	**Source**
Avio S.p.A	Vega	1 450 kg to 400 km SSO	2012	Arianespace (2014)
EUROCKOT Launch Services	Rokot	2140 kg to 200 km Circular Orbit	2000	EUROCKOT (2011)
ExPace	Kuaizhou 1A	250 kg to 500 km SSO	2017	Krebs (2018)
Japan Aerospace Exploration Agency (JAXA)	Epsilon	700 kg to 500 km LEO	2013	(JAXA, 2018)
Northrop Grumman	Pegasus XL	310 kg to 700 km LEO	1990	Orbital ATK (2015)
Rocket Lab	Electron	225 kg to 500 km SSO	2018	Rocket Lab (2016)

Table 2-2: Small Launch Vehicles Under Development

Manufacturer	**Launch Vehicle**	**Payload and Orbit**	**Source**
Firefly Space	Firefly Alpha	630 kg to 500 km SSO	(Firefly Aerospace Inc, 2018)
Generation Orbit	GO Launcher 2	45 kg to 200 km	(Generation Orbit Launch Services, Inc., 2014)
NewSpace India Limited	Small Satellite Launch Vehicle	500 kg to 500 km LEO 300 kg to 500 km SSO	NewSpace India Limited (2019)
Orbex	Orbex Prime	150 kg to 500 km SSO	(DEIMOS elecnor and OrbeX, 2018)
PLD Space	Arion 2	150 kg to 400 km LEO	Torres et al. (2018)
Vector Space Systems	Vector-R	60 kg to LEO	Vector Launch (2019)
Virgin Orbit	LauncherOne	500 kg to 230 km LEO	Virgin Orbit LLC (2019)

The trend in small launch vehicles performance leans toward launch vehicles with payload capabilities lower than 500 kg, while between 500 kg and 1000 kg no significant bias exists (Burkhardt, 2018). This is representative of the industry's demands, Niederstrasser (2018) found that 73 % of the satellites launched in 2017 fell into the 1 kg – 500 kg mass category. Despite this fact, most satellites are still launched as secondary payloads aboard medium or large launch vehicles (da Cás et al., 2019). The gap in the market is clear and many start-up enterprises and entrepreneurs are trying to stake their claim with over 131 small launch vehicles currently under development (Foust, 2019).

2.2 Multistage Launch Vehicles

Most rocket propelled vehicles are single staged and use solid rocket motors to propel them, these vehicles are generally used for military purposes where they deliver explosive payloads without the need to reach orbit (Sutton and Biblarz, 2001). To achieve the high velocities required to overcome gravity and achieve orbit (with a payload) a single stage vehicle becomes infeasible.

A multistage launch vehicle contains two or more stages, each with its own rocket engine(s) and propellant. As the launch vehicle ascends, each stage is jettisoned once its propellant is depleted, thus continuously reducing the launch vehicle's mass. The reduced mass makes it easier for the next stage —with lower thrust and less propellant— to achieve the Δv required for reaching orbit. Δv refers to the change in velocity an ideal rocket (i.e. no external forces acting on it) must produce in order to reach orbit. Equation (2-1) is Tsiolkovsky's rocket equation describing Δv where m_0 is the initial mass of the rocket, m_f is the final mass and v_e the effective exhaust velocity.

$$\Delta v = v_e \ln\left(\frac{m_0}{m_f}\right) \tag{2-1}$$

The need for staging is due to the impracticality of developing a single stage vehicle capable of producing a high enough mass ratio (m_0/m_f) to achieve the high Δv requirements for orbital insertion of a payload. Staging allows for the total Δv to be divided among the stages as Equation (2-2) shows. (Burghes, 1974)

$$\Delta v = \sum_{1}^{n} \Delta v = \Delta v_{Stage\,1} + \Delta v_{Stage\,2} + \cdots + \Delta v_{Stage\,n} \tag{2-2}$$

Two staging configurations exist: serial and parallel staging. A serial (or tandem) staged rocket is one in which the stages are stacked on top of one another, with the stages operating sequentially. A parallel staged rocket is one in which the stages are grouped alongside each other, typically operating simultaneously. Parallel staging is generally used in the first stage where "booster rockets" are strapped on to the core stage, the core stage then has multiple serial stages above it (Lopez, 2018). The two staging techniques are illustrated in Figure 2-1 below.

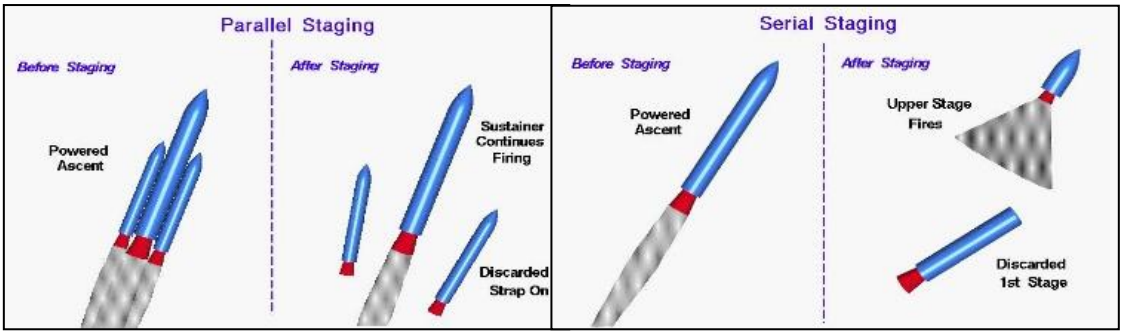

Figure 2-1: Types of Rocket Staging (Space Flight Systems, 2018)

Generally, low orbit, light payload launch vehicles are two staged with serial staging (Hadfield, 2019). The first stage, or booster stage, is the largest stage of a multistage launch vehicle. The booster stage performs the power ascent, which requires the most ΔV to accelerate the combined mass of the launch vehicle (stages and payload) (Space Flight Systems, 2018). The upper stage, which is the final stage of a launch vehicle, carries the payload (e.g. a satellite or spacecraft) into orbit by performing specific manoeuvres using thrust vector control, reaction control and attitude controls. Consecutive stages are connected by an "interstage".

The ULA manufactured Delta II launch vehicle, illustrated in Figure 2-2, is an example of a launch vehicle using parallel staging in tandem with serial staging. It has solid rockets strapped alongside the liquid engine propelled first stage, the second stage (which is the upper stage) is also liquid propelled (United Launch Alliance, 2006).

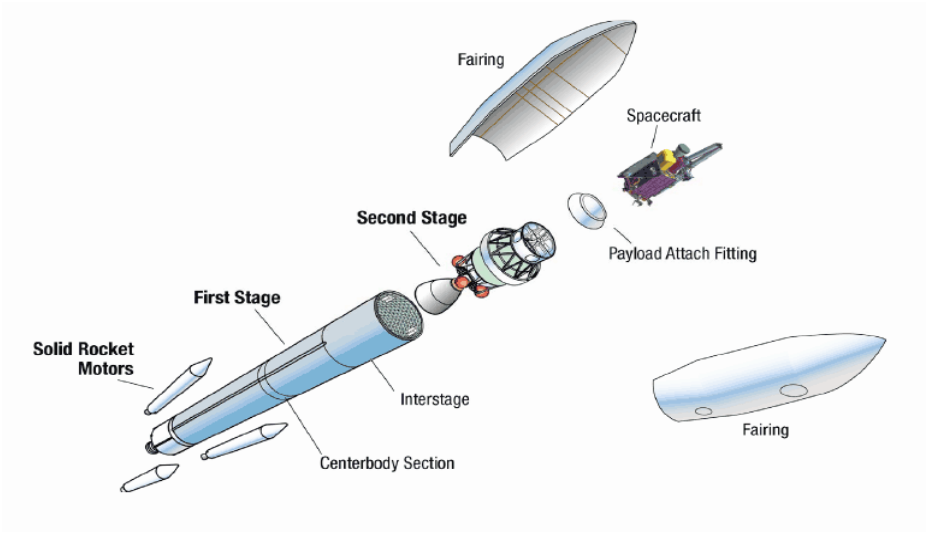

Figure 2-2: Delta II launch vehicle stages (United Launch Alliance, 2006).

The size of a launch vehicle and number of stages it will have depends on the mission requirements and budget. The cost of a launch vehicle increases with the number of stages, which also causes an increase

in launch mass and propellant requirements (Sutton and Biblarz, 2001). Table 2-3 lists modern small launch vehicles and the number of stages each has, the bias toward 2-3 stages is evident.

Table 2-3: Small launch vehicle number of stages

Manufacturer	**Launch Vehicle**	**Payload and Orbit**	**Number of Stages**
Avio S.p.A	Vega	400 km to 1 450 kg SSO	4
ExPace	Kuaizhou 1A	250 kg to 500 km SSO	3
Firefly Space	Firefly Alpha	200 kg to 500 km SSO	2
Northrop Grumman	Pegasus XL	310 kg to 700 km LEO	3
Orbex	Orbex Prime	150 kg to 500 km SSO	2
Rocket Lab	Electron	225 kg to 500 km SSO	2
Virgin Orbit	LauncherOne	500 kg to 230 km LEO	2

2.3 Small Launch Vehicle Upper Stage

The upper stage of a multistage launch vehicle is designed to operate at high altitudes where the atmospheric pressure approaches 0 Pa. The thrust requirements are relatively low, making the use of simple and reliable pressure propellant feed systems feasible. Upper stages are used to complete orbital insertions and to accelerate payloads into higher orbits unachievable by the lower stages (Sutton and Biblarz, 2001).

In addition to the standard components of a launch vehicle's stages (i.e. engine, propellant tanks and feed system, component mounts, support structures, separation mechanisms and avionics) an upper stage also consist of: small engines (or cold gas nozzles) for reaction control and attitude control (if the mission requires in space manoeuvres for orbital insertion); fairings to protect the payload during assent through the atmosphere; the payload adapter, which connects the payload to the launch vehicle; and the payload itself. A diagram of the United Launch Alliance's (ULA) AC-17 Centaur upper stage and all its parts is give below in Figure 2-3.

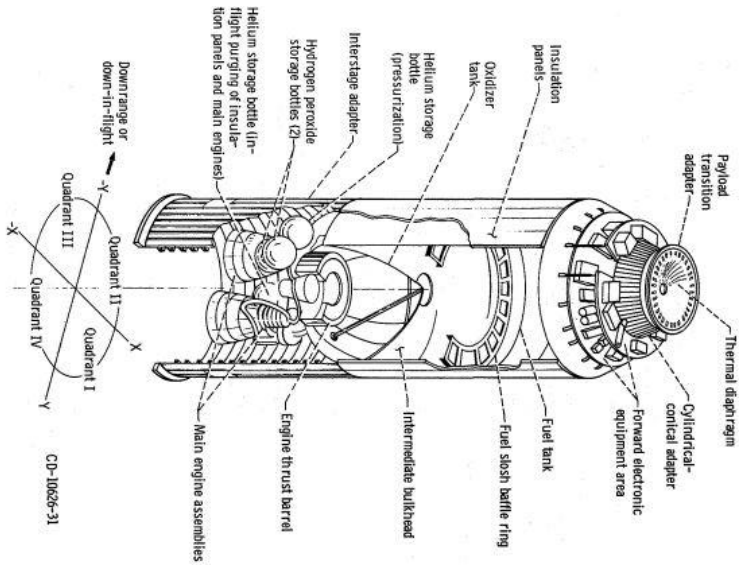

Figure 2-3: ULA AC-17 Centaur Upper Stage Diagram (NASA, 1972)

Pressure-fed liquid rocket and solid rockets are the most commonly used means of propulsion for small launch vehicle upper stages, as they are simple and meet the performance requirements (Huzel and Huang, 1992). Table 2-4 lists well known upper stages of small launch vehicles currently in operation.

Table 2-4: Small Launch Vehicle Upper Stages in Operation

Name	**Manufacturer**	**Launch Vehicle**	**Propulsion**	**Thrust (kN)**	**Burn Time (s)**	**Height x Diameter (m)**
AVUM	Avio S.p.A	Vega	Pressure Fed: N_2O_4 / UDMH	2.42	317	1.74 x 2
Briz-KM	EUROCKOT	Proton-M and Rokot	Gas Generator: 14D30	20	3000	2.6 x 2.5
Electron 2nd Stage	Rocket Lab	Electron	Electric Pump: LOX / Kerosene	22	160	2.4 x 1.2
KM-V2c	JAXA	Epsilon	Solid Rocket: HTPB	99.8	90	2.3 x 1.4
Kuaizhou 1A 4th Stage	ExPace	Kuaizhou 1A	Pressure Fed: N_2O_4 / MMH	6.5	765	- x 1
Orion 38	Northrop Grumman	Pegasus XL	Solid Rocket: QDL-1, HTPB, and 19% aluminium	34.31	63.8	2.08 x 0.97

The remaining sections of this chapter will discuss the major components, mentioned above, of which an upper stage vehicle is composed.

2.4 Payload Fairing

A launch vehicle's payload is housed within the payload fairing. Also known as a heat shield (Avio, 2017), it serves to protect the spacecraft from the large aerodynamic loads (≈6.9 MPa), heating, and the acoustic vibration experienced during the launch vehicle's ascent through the atmosphere. It also has the function of reducing the launch vehicle's drag coefficient, thus reducing the mission's thrust requirements.

Fairings are typically made up of two halves or three sectors connected by fasteners along the length of the interfaces. Upon reaching the upper atmosphere, where the air is too thin to impart significant aerodynamic forces on the payload, the fairing's parts are separated and jettisoned clear of the upper stage's flight path, thus exposing the payload for orbital insertion (Mathew et al., 2016).

Fairings consist of a face panel that is stiffened on the inside (facing the payload) by longerons and bulkheads, a method typical of aerodynamic structures as it provides mass reduction compared to using thick plates. Longerons run longitudinally and provide axial stiffness, while the bulkheads transverse the body and provide bending stiffness. Other stiffening techniques exist and are discussed below.

Aluminium is the most common face material used for fairing construction, this is due to its workability, relative low cost, heat resistance and low mass (Mathew et al., 2016). Composite fairings are the alternative also due to its high strength-to-weight ratio and heat resistance. In addition to this, it is easier to manufacture doubly curved structures (like a parabolic fairing) from composite materials, however, composite fairings (especially CFRP) are more expensive to manufacture compared to their aluminium counterparts (Shen and Pope, 1990).

An ogive shaped fairing (e.g. ESA's Ariane 5 launch vehicle) is the most aerodynamic shape, the conical shape (e.g. the Briz-M, manufactured by Khrunichev State Research and Production Space Centre) are less complex to manufacture (Crowell, 1996), while bi-conical fairings bridge the gap between aerodynamics and manufacturability . A fairing's structure may consist of up to three sections, namely: the boat tail, barrel or cylindrical section, and the nose cone (Ramamurti et al., 2001). Figure 2-52-5 shows these different sections on Northrop Grumman's Minotaur IV's bi-conical fairing.

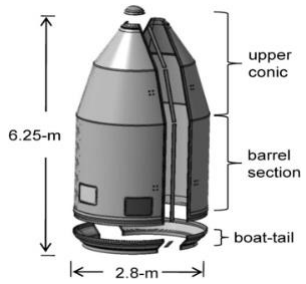

Figure 2-4: Minotaur IV bi-conic payload fairing sections (Lane et al., 2011)

Wegner et al. (2002) explored the use of composites for the construction of fairings. They investigated different structural configurations and fabrication methods in order to produce large, low cost structures, specifically for the Minotaur IV's payload fairings. They also sought to find a solution to the moisture absorption associated with honeycomb reinforcements. The moisture absorbed is discharged (a phenomenon called sweating) and gets trapped between the honeycomb and the metal it reinforces, thus causing corrosion and mass gain (Tuttle, 2009). They concluded that using "advanced grid stiffened structures (AGS)" eliminates the problem of moisture uptake associated with the traditional honeycomb integrally stiffened panel. The AGS configuration consists of longitudinal and helical CFRP ribs, which form a repeating triangular pattern, as illustrated in Figure 2-5. The fibres are orientated along the rib direction to exploit the high specific strength and stiffness of unidirectional CRFP.

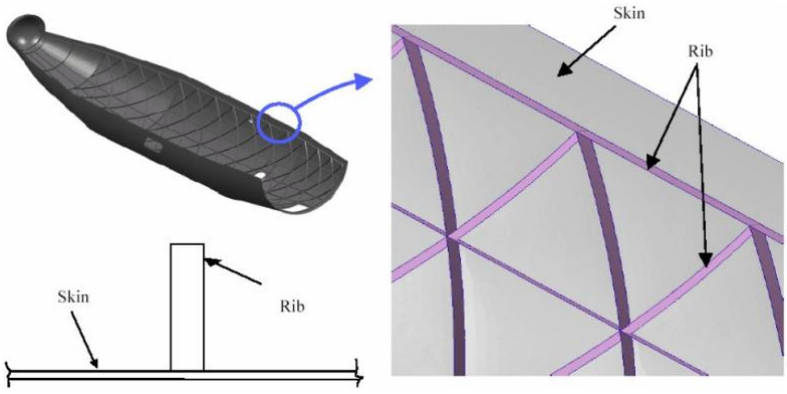

Figure 2-5: Minotaur AGS composite structure (Biskner and Higgins, 2005)

In another paper, Biskner and Higgins (2005), mention a pitfall of the AGS design. The Minotaur's final fairing required thick skin to reduce the strain experienced between the skin and ribs due to the relative rotation between the ribs and skin. They investigated the effectiveness of placing light foam inserts in between the ribs (i.e. in the triangular gaps). The foam, Rohacell 71 IG in particular, improved the strain response and allowed a skin thickness reduction from 12 plies to 8 plies.

Krivanek and Yount (2012) investigated the effectiveness of 8 different composite construction technologies in a bid to optimise (i.e. decrease drag and increase strength-to-weight) the dry structures

of NASA's - now cancelled - Ares V Heavy Lift Vehicle, which includes the payload fairing. The concepts were ranked by key characteristics which include: mass, development risk due to technology readiness level (TRL) maturity, damage tolerance, cost, acoustic transmissibility, thermal tolerance, joining, and inspectability. Using IM7/977-3 graphite/epoxy pre-impregnated fabric: the hat stiffened panel, fibre reinforced foam core, and honeycomb sandwich concepts obtained the best overall scores. Figure 2-6 shows the different concepts that were analysed.

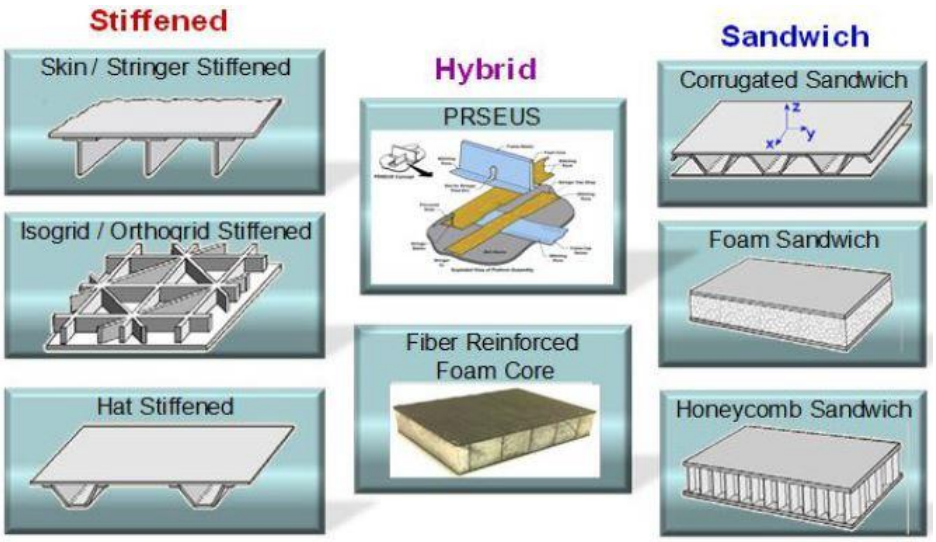

Figure 2-6: Composite construction concepts (Krivanek and Yount, 2012)

Various manufacturing techniques exist and the choice depends on the material used and the shape desired. Most fairings made of aluminium are biconical, as creating a doubly curved structure (e.g. ogive) is difficult to achieve with metals. The aluminium fairings are often stiffened with stringers or used as a honeycomb sandwich. The aluminium sheets are bonded to the stringers with rivets or welding.

Composite fairings can be manufactured using a hand layup or automated tape layup, which are the easiest methods for creating curves but have the disadvantage of being labour and time intensive. Filament winding, pultrusion and resin transfer molding are less labour and time intensive but require complex machines and are often unable to produce large components (Shen and Pope, 1990). Composite fairings can also be stiffened; the face sheet is bonded to the stiffeners with an adhesive. Figure 2-7 illustrates the manufacturing methods used for composite fairings.

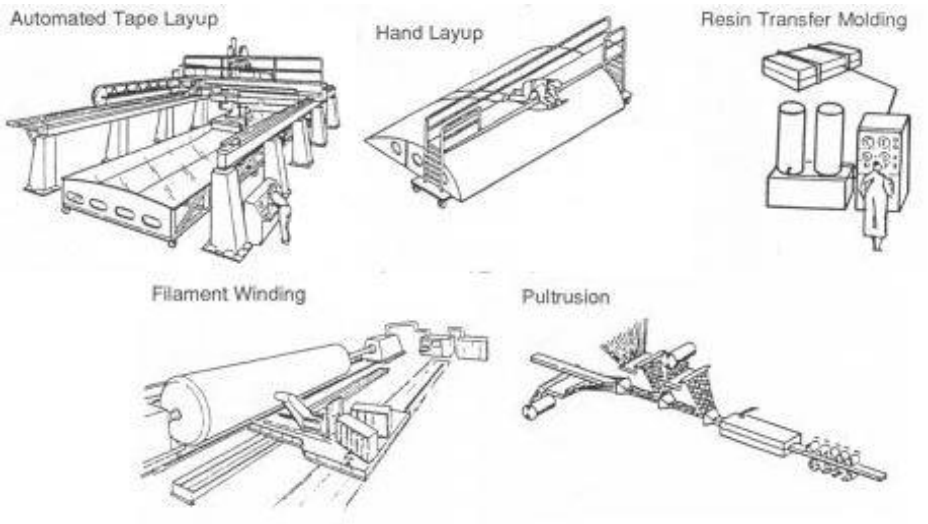

Figure 2-7: Composite fairing manufacturing methods (Shen and Pope, 1990)

2.5 Payload Interfaces

A payload requires a way to attached itself to the launch vehicle, while also isolating the payload from the vibrations imparted on it during the launch vehicle's ascent. A payload interface serves this requirement, it consists of three components: the payload attach fitting (PAF), payload adapter (PLA), and payload separation system (PSS) (Delta IV Launch Services User's Guide, 2013).

The PAF is typically bolted to the launch vehicle's upper stage. Its design depends on the payload's dimensions but it is generally tapered to connect the small diameter of the payload's mounting point to the fore end of the larger diameter upper stage. The PAF used on ESA's Ariane 5 launch vehicle is depicted in Figure 2-8, it is constructed of composite and aluminium (Fink et.al, 2010).

Figure 2-8:Ariane 5 payload attach fitting (Fink et.al, 2010)

The payload adapter (PLA) connects the payload to the PAF and provides the required electrical interfaces. The design of this component takes on many different forms, influenced by the characteristics of the payload (geometry, weight, and sensitivity to vibrations and heat). For instance, the United Launch Alliance offers six different designs for the Delta IV launch vehicle's PLA.

MOOG CSA Engineering have developed the Evolved Expendable Launch Vehicle (EELV) secondary payload adapter (ESPA) ring. It is a multi-payload adapter (MPA) whose function is to facilitate the launch of secondary payloads by utilizing the space unoccupied by the primary payload. MPA's are the most efficient way to maximize a launch vehicles lift capacity (Biskner et.al., 2007).

The ESPA ring is connected to the launch vehicle's payload attach fitting, and above the ESPA mounts the large primary payload; the secondary payloads mount on the ESPA's side wall. Constructed out of aluminium, it can launch 6 secondary payloads and a 15 000 lb (6 803 kg) primary payload (Goodwin and Wegner, 2001).

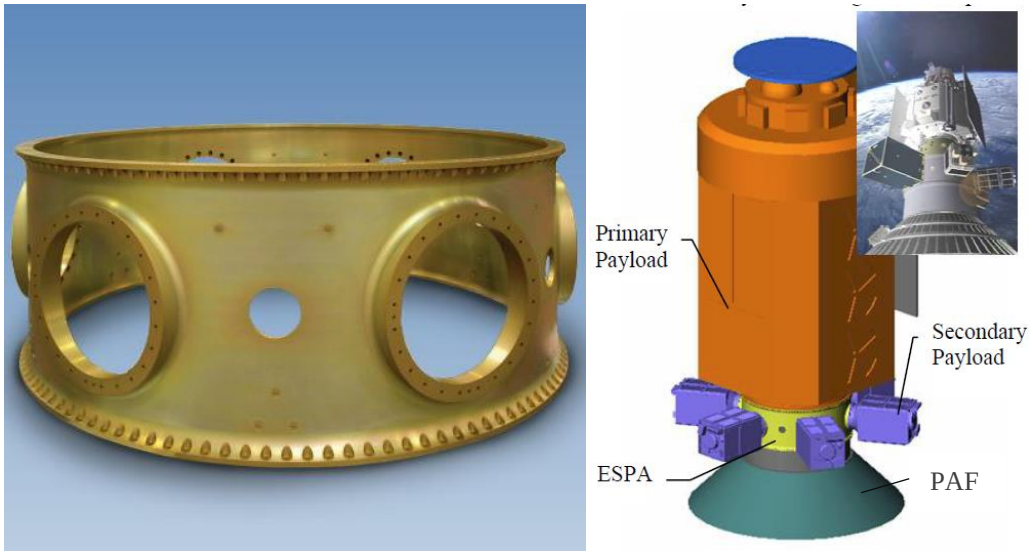

Figure 2-9: ESPA payload adapter ring (left) (Moog Inc., 2018), and Populated ESPA payload adapter ring (right) (Biskner et.al., 2007)

The payload separation system resembles that of a stage separation system, only the components are smaller. Most vehicles use Marmon band (or V-band) clamps, which are fastened by explosive bolts, to lock the payload and the adapter together during launch. A spring mechanism then separates the payload from the upper stage when the bolt is severed on command. Separation mechanisms are further discussed in Section 2.9.

2.6 Liquid Propellant Feed Systems

Liquid propellant rockets are chemical rockets that work by exploiting Newton's third law of action and reaction. The "action" is the ejection of high speed gases through the exit of a De Laval nozzle, the "reaction" is the propulsion of the rocket in the opposite direction of the exhaust gases. To produce the gases, the engine burns an oxidiser and a fuel. Unlike a car, which burns petroleum as a fuel and the

surrounding air as the oxidiser, a launch vehicle must also store oxidiser as the air in the atmosphere dissipates as the launch vehicle ascends.

Liquid-propellant rockets are favoured in applications were a high specific impulse "I_{SP}" and high thrust are required (Humble et al., 2007). I_{SP} (measured in seconds) is a performance measure describing how efficiently a mass of propellant is used to produce thrust, it is similar to the fuel economy (km/l) of a car (Sutton and Biblarz, 2001). Being in the liquid state means liquid propellants can be easily throttled; the engine flame can also be extinguished and restarted provided the ignition system is suitable, giving them great flexibility. These capabilities make liquid propellants particularly useful compared to solid rockets.

The penalty for greater performance, thrust and operational flexibility is an increased system complexity, storage difficulties (low temperatures for cryogenic propellant) and operational danger (toxicity of storable propellants). The complexity comes from the fact that LREs need a mechanism to feed the propellants into the rocket engine's thrust chamber at the flow rate, mixture ratio and pressure necessary to meet the thrust requirements which means complex valves and plumbing, further complicated by use of cryogenics. Cryogenic propellants are those with boiling points lower than -150 °C (Pallardy, 1998).

There are two types of propellants used in industry: monopropellants and bipropellants. Monopropellants consist of a single chemical while bipropellants are a mix of two chemicals, bipropellants are further classified into hypergolic (which igniting upon contact between oxidiser and fuel) and non-hypergolic. The propellants used depend on the I_{SP} the engines must produce and the storability of the propellants (i.e. corrosiveness, cryogenic etc.). Table 2-5 and Table 2-6 list common propellants used in launch vehicles.

Table 2-5: Common bipropellant combinations Isp

Fuel	**Oxidiser**	**Isp at Vacuum (s)**
Kerosene (RP-1)	Liquid Oxygen (LOX)	304
Liquid Hydrogen (LH_2)	Liquid Oxygen (LOX)	453
Unsymmetrical dimethyl hydrazine (UDMH)	Dinitrogen tetroxide (N_2O_4)	313

Table 2-6: Common monopropellants Isp

Propellant	**Isp at Vacuum**
Hydrazine (N_2H_4 with catalyst)	245
Hydrogen Peroxide (H_2O_2)	144
Nitrous Oxide (N_2O with Rhodium catalyst)	131

Broadly, two types of propellant feed systems are used in space launch vehicles (Sutton and Biblarz, 2001), pressurized and pump fed. The pressurized (or pressure fed) system uses inert gases (usually helium or nitrogen) to force the propellants out of their respective tanks at the requisite chamber pressure. Another type of pressure fed system, described by Ewig (2009), uses propellants with high vapour pressure (e.g. nitrous oxide and methane), which force themselves out of their containers due to the internal energy of the saturated vapours that boil off the stored liquid propellant; this is known as "self-pressurization". The tanks of pressure fed systems tend to be heavy given that the propellants are stored above chamber pressure.

The second propellant feed system makes use of pumps to draw the propellants and pressurize them; this allows very high chamber pressures and flow rates to be achieved. Pumps allows for low pressure propellant storage, which corresponds to lighter propellant tanks. Pumps driven by gas turbines, called turbopumps, are used almost exclusively in pump-based feed systems. A detailed organogram of liquid propellant feed systems is depicted in Figure 2-10 below.

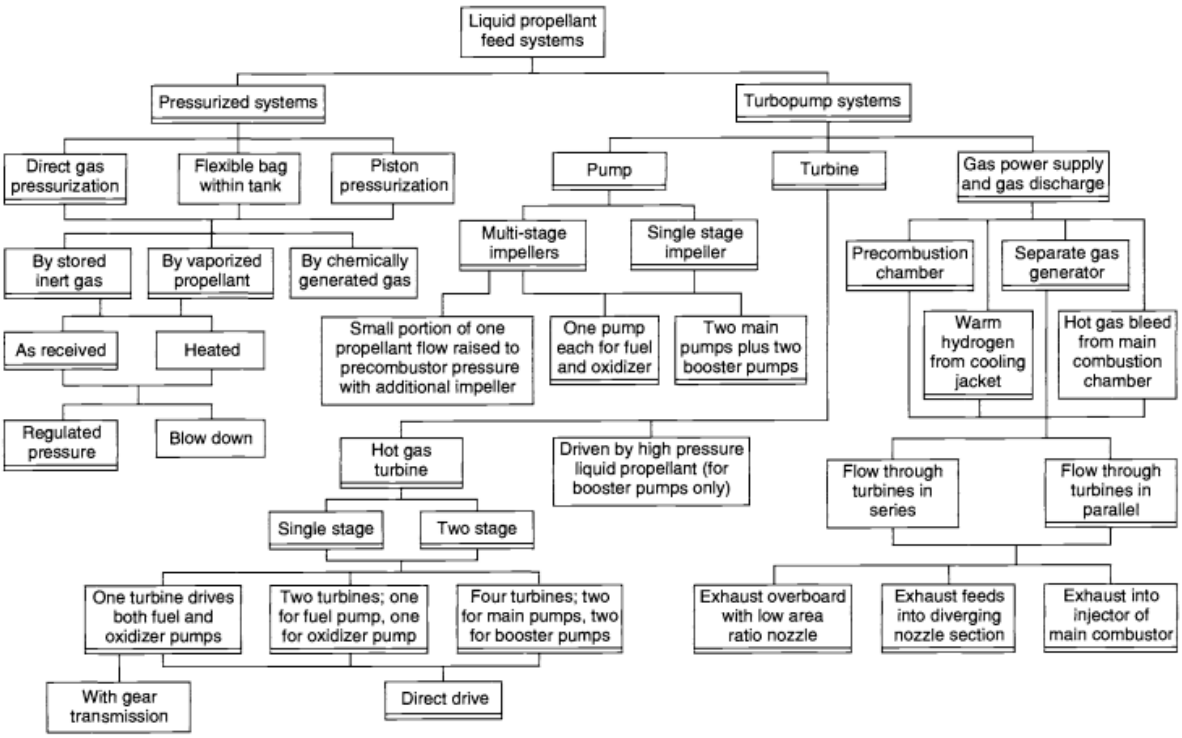

Figure 2-10: Liquid propellant feed systems classification (Sutton and Biblarz, 2001)

Pump-fed rockets are generally used for the booster stage of a launch vehicle where high propellant flowrates are required in order to produce the high thrust levels needed for the initial stage of flight. Pressure-fed systems are used when the thrust requirements are relatively low, for example, the upper stages of launch vehicles, for spacecraft reaction control and their orbital manoeuvring systems (Huzel and Huang, 1992).

According to Huzel and Huang (1992), there are seven major subsystems that make up a liquid-propellant rocket engine: thrust chamber assembly, propellant feed system, pumps and drive system (turbine or electric motor), propellant flow control system, electric and pneumatic control systems, thrust-vector control (TVC) system, interconnect components and mounts.

2.7 Liquid Propellant Storage

Liquid propellants are known for the high specific impulse they produce, while their liquid state has the benefit of allow straightforward throttling of engine thrust. The variety of liquid propellants and propellant combinations (in the case of bi-propellant systems) means that rocket motors can be designed to meet a broad spectrum of operational requirements. Rockets, however, burn copious amounts of propellant to meet ΔV requirements, as a result storing these propellants requires large tanks which may occupy most of a launch vehicle's structure, accounting for up 60-70% of a rocket's dry weight (Morino et al., 2001).

The walls of the propellant tanks are an integral part of the launch vehicle's structure, they must withstand internal pressure from the propellants, the dynamic loads imparted during flight and buckling stresses (Sutton and Biblarz, 2001). To improve structural stability of a launch vehicle, especially for the larger booster stage, propellant tanks are integrally stiffened with stringers, similar to the stiffening of payload fairings (see Section 2.4). Stringers can reduce the overall mass of a propellant tank, the reinforcing allows the tank walls to be thinner (Huzel et al., 1992). Figure 2-11 below shows a typical booster stage propellant tank arrangement.

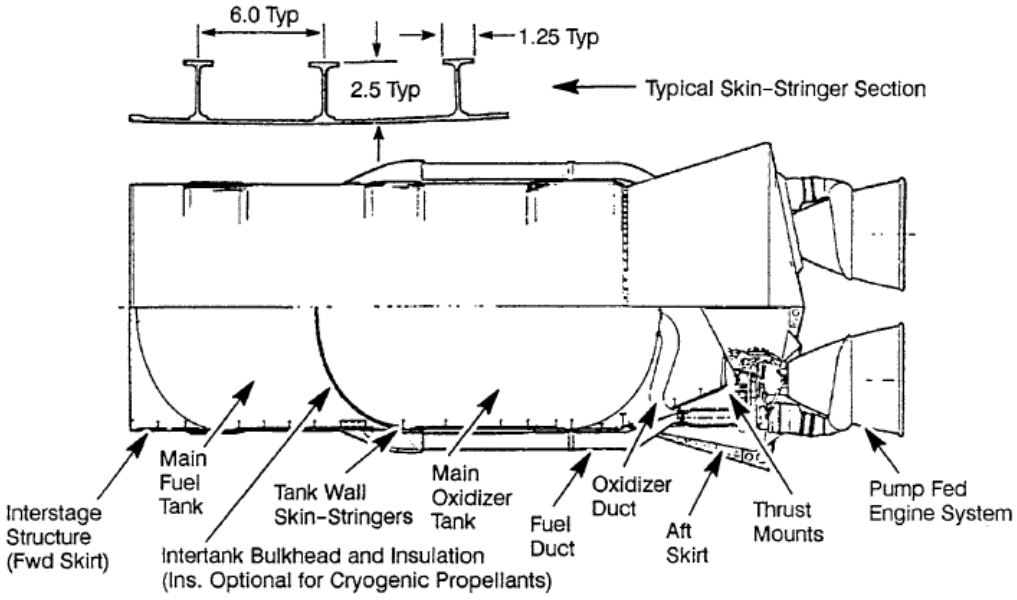

Figure 2-11: Stringer stiffened booster stage propellant tank (Huzel et al., 1992)

Upper stage propellant tanks are often pressure fed and shrouded by a cylindrical shell. The tanks have support rings which are used to bolt them to the shell. The aft section of the tanks are conical to improve

propellant drainage (Huzel et al., 1992). Figure 2-12 illustrates the typical tank configuration of a pressure-fed upper stage, note the conical aft ends and the cylindrical shroud.

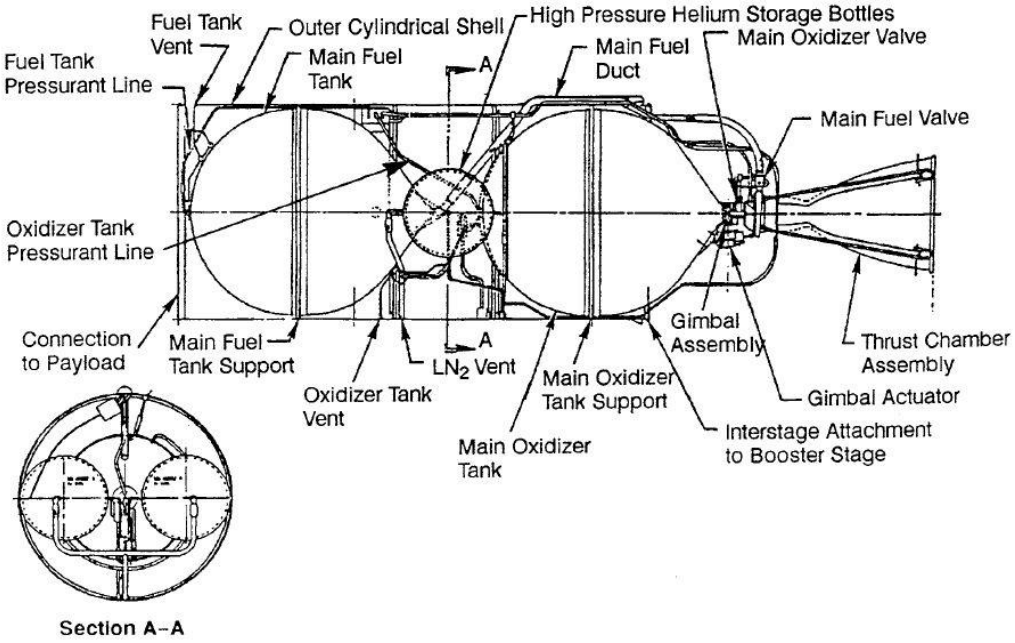

Figure 2-12: Pressure fed upper stage propellant tank configuration (Huzel et al., 1992)

The size (or volume) of a propellant storage tank depends on the propellant O/F ratio, propellant flow rate and engine burn time. The thickness of the tank is determined by the storage pressure of the propellant, which, in a pressure fed system, is determined by the required chamber pressure and feed line pressure loss. In such systems, storage pressures typically range between 6 and 27 bar. Pump fed systems have thinner walls given that the propellants can be stored at a relatively low pressure, typically between 2 and 6 bar, as the pumps pressurize the propellants to the combustion chamber pressure (Humble et al., 2007). In pump fed systems, the tank pressurisation is required to prevent pump cavitation.

A launch vehicle's range is a function of the propellant mass fraction (propellant mass / launch vehicle take-off mass) (see Section 4). To maximize this ratio, it is of primary importance to minimize the propellant tank mass, which occupy a significant portion of the mass budget. The tanks should also be easily serviceable, handled and stored; of reasonable cost; have smooth contours to improve drainage of the liquid propellants; they should be well aligned to adequately transmit thrust, as a misalignment will cause stress concentrations; and be compatible with the propellant, to avoid corrosion and permeability (Ross and Young, 1948).

The shape of a propellant tank has a significant influence on its height and mass. The three most common shapes of propellant tanks are: spherical, cylindrical section with ellipsoidal bulkheads and cylindrical section with spherical bulkheads. Bulkheads (also referred to as end caps) can also be convex, concave, flat, or unsymmetrical. According to Ford (2007), flat bulkheads are disadvantageous

as they must be made thicker compared to convex or concave bulkheads for adequate strength, and as they lack a low point for optimal outlet positioning. Convex bulkheads increase tank length and require additional support structures to keep the tank from buckling. Concave bulkheads also result in increased tank length and decreased volumetric efficiency, in addition to lacking a low point. Figure 2-13 shows the various tank bulkheads.

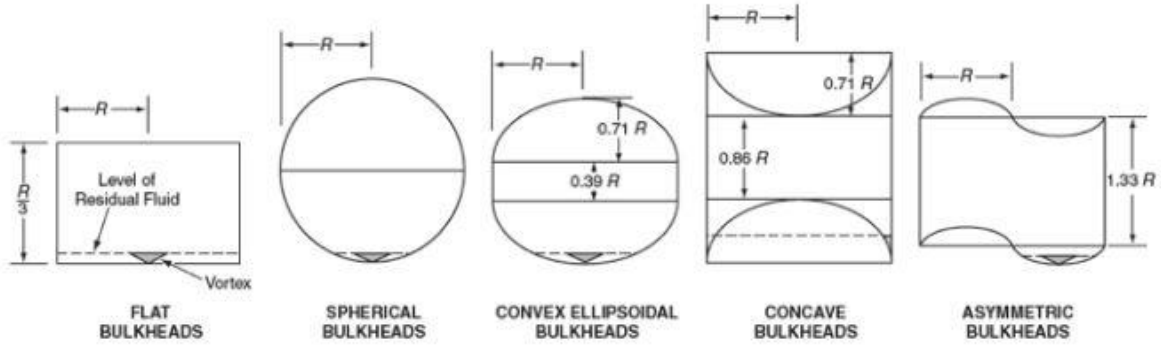

Figure 2-13: Pressure vessel bulkheads (Ford, 2007)

The tank configuration is another design factor, the tanks may be arranged in tandem as separate tanks, in tandem with a common bulkhead (essentially making them one tanks) or concentrically. Figure 2-14 below, shows the various configurations.

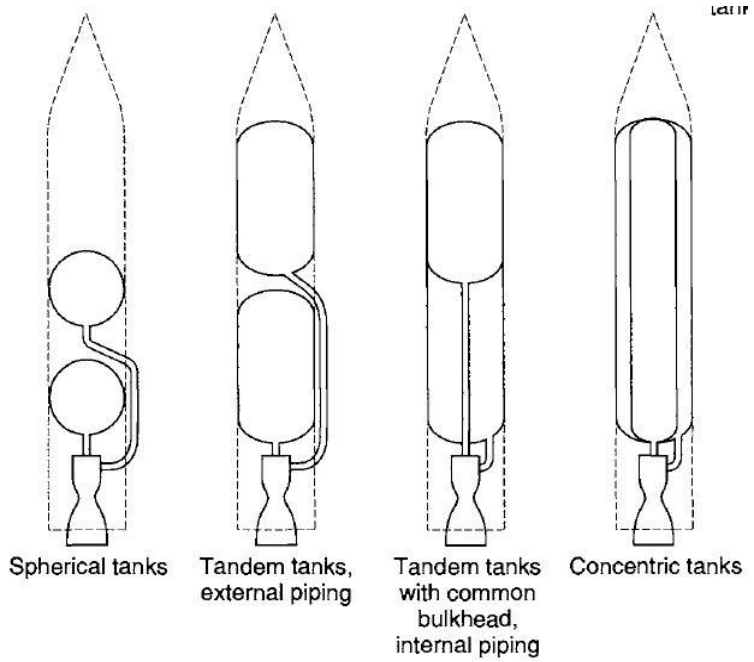

Figure 2-14: Propellant tank configurations (Sutton and Biblarz, 2001)

Generally, upper stage tanks are arranged in tandem with a common bulkhead such that the fuel tank is below the oxidiser tank (Scarr, 1992), this configuration reduces mass and reduces the vehicle's overall length. The common bulkhead is concaved on the fuel side, while convex on the oxidiser side to improve drainage of the oxidiser (Scarr, 1992). The common bulkhead that separates the propellants must

withstand the pressure of the propellants while ensuring no cross flow between each tank and minimal inter-tank heat transfer, especially when cryogenic and non-cryogenic propellant combinations are stored (Scarr, 1992). Figure 2-15 below shows an upper stage concept with common bulkhead tanks.

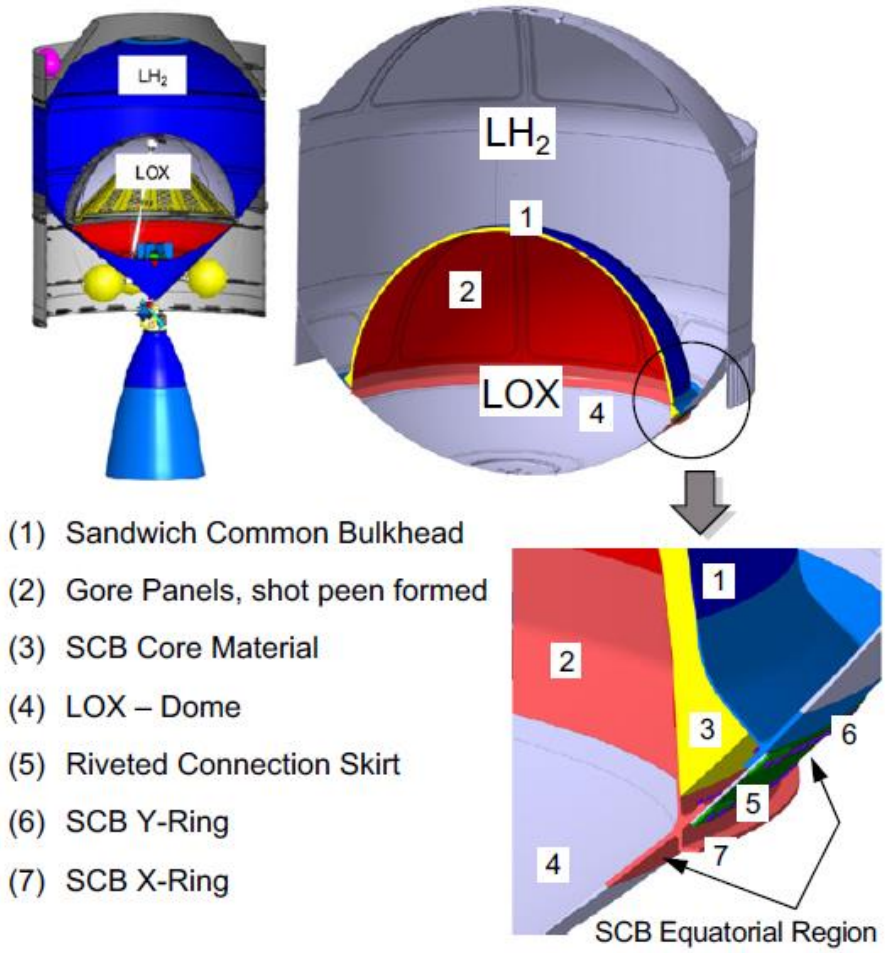

Figure 2-15: Upper stage common bulkhead propellant tank (Szelinski et al., 2012)

Geometry of the tanks also affects a parameter known as the "packing efficiency" which is a measure of the unoccupied space in a launch vehicle. This is why elliptical bulkheads are preferred to spherical bulkheads as the flatter geometry reduces the free space around the bulkhead (Tam et al., 2006).

For booster stages, spherical tanks (although lighter) are impractical as their diameter cannot be constrained, as a result cylindrical tanks, in tandem, with elliptical ends are a popular propellant tank configuration. The cylindrical section allows the diameter to be constrained while the elliptical end caps reduce the tank's height compared to a hemispherical end cap. The elliptical ends also create less free space compared to the larger hemispherical end caps. (Huzel and Huang, 1992)

Cylindrical tanks with a common bulkhead provide the greatest height and mass savings. However, a common bulkhead presents insulation complexities when a cryogenic propellant is used with a non-cryogenic (e.g. LOX/Kerosene). Internal piping is required for this configuration and has the benefit of

giving the rocket a smoother design but, creates sealing and assembly complexities. Another configuration is the nested tank, which is similar to a common bulkhead but with a gap between the tanks for insulation, the configuration is depicted in Figure 2-16. (Tam et al., 2006)

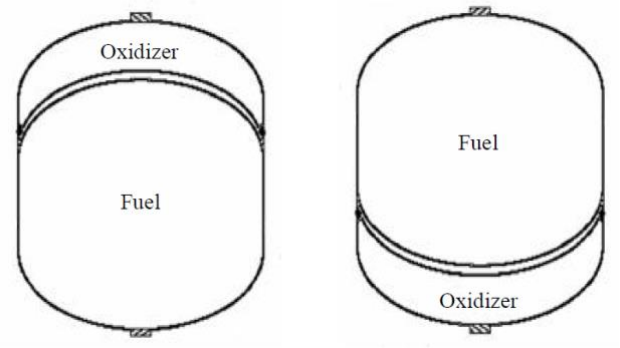

Figure 2-16: Nested tanks (Tam et al., 2006)

The type of propellant used influences the material selected to construct the tank and the configuration used. Bi-propellant systems are the most commonly used type of liquid propellant system for large launch vehicles given the high specific impulse and thrust achievable, compared to solids (Ward, 2010. Monopropellants are primarily used for spacecraft propulsion and, by their nature, have lower specific impulses than bi-propellants.

The most commonly used oxidisers include: nitrogen tetroxide (N_2O_4), liquid oxygen (LOX), nitric acid (HNO_3), and hydrogen peroxide (H_2O_2) (Sutton and Biblarz, 2000). Tanks that store HNO_3 are vulnerable to corrosion; LOX is the most commonly used for launch vehicles (Ward, 2010), the tanks require materials that can withstand low temperatures and remain impermeable; and H_2O_2 requires materials that do not promote its decomposition. N_2O_4, the most common oxidiser, is hypergolic with fuels and can spontaneously combust with paper, wood and leather (Sutton and Biblarz, 2000).

Corrosion resistance isn't generally a factor when considering fuel storage materials. Fuels commonly used are alcohols, hydrocarbons (e.g. Jet A and Rocket Propellant 1), and amines, neither of which being corrosive; the only complication is that fuels tend to be good solvents, which affects the design of gaskets and other plastic components.

NASA and the U.S. Air Force used stainless steel (SS) tanks for the Atlas ICBMs (manufactured by Covair) and the Centaur upper stage (manufactured by ULA) (Rudman and Austard, 2002). To offset the mass gain when using SS, compared to aluminium and composites, the tanks rely on internal pressurization to maintain their shape. Tanks of this nature are referred to as "balloon tanks" and are unattractive as a drop in pressure will cause the tank to collapse. The main advantages are: its strength at both cryogenic (increases by 50%) and high temperatures, particularly SS 301; and its low cost and workability. SS has re-gained its relevance recently with SpaceX opting to use it for their BFR, mostly

due to advances in cold forming, a process that imparts additional strength to a material during manufacture.

Table 2-7: Propellant tank characteristics of small launch vehicle upper stages

Manufacturer	Vehicle	Tank Material	Tank Configuration
Rocket Lab [(1)]	Electron	Linerless Carbon Fibre Composite	Tandem Ellipsoidal End Caps
Vector Space Systems [(2)]	Vector R	Carbon Fibre Composite	Tandem
Orbex [(3)]	Orbex Prime	Carbon Fibre Composite	Coaxial
Avio S.p.A [(4)]	AVUM	Titanium	Adjacent Spherical Tanks
Virgin Orbit [(5)]	LauncherOne	Composite with spray on foam insulation	Tandem Ellipsoidal End Caps

Rocket Lab (2016) [(1)], Vector (2018) [(2)], Orbex Vehicle (2021) [(3)], Avio (2019) [(4)], Virgin Orbit LLC (2019) [(5)].

From Table 2-7 there is clearly a trend towards composite propellant tanks with ellipsoidal end caps. This allow the upper stage to have a low aspect ratio (i.e. length/diameter) (Sutton and Biblarz, 2000), while using composites (especially linerless carbon fibre) greatly reduces the tank mass. Composite tanks are discussed in the coming sections (2.7.1 and 2.7.2).

2.7.1 Composite Tanks

The next generation of launch vehicles have to be lightweight to obtain high mass fractions which will improve payload-to-orbit capabilities and pave the way for manned deep space exploration. To achieve these high mass fractions, the strength-to-weight characteristics of composite materials must be exploited. Zheng (2018), predicts that the structural components of future launch vehicles will consist solely of composite materials.

A launch vehicle's dry mass is dominated by the propellant tanks and so great emphasis is placed on composite tank design and manufacture, particularly for cryogenic propellant storage (LOX, LH_2 and LCH_4). The difficulty of composites tank design is that no design standards exist due to insufficient data, data which is closely guarded by manufactures.

Cryogenic LH_2 composite tanks have been researched extensively and are the standard for NASA heavy lift vehicles. The SLS will use Cytec's CYCOM 5320-1 prepreg for the LH_2 tank and have tested a 5.5 m diameter sample, depicted in Figure 2-17 (Jackson et.al., 2015).

Figure 2-17: NASA 5.5 m LH_2 tank (Messier, 2014).

Mallick et al. (2004) investigated the plausibility and challenges of ultralight linerless composite tanks (ULLCTs), they based the success of a tank on a He leakage rate less than 10^{-4} scc/sec at 1% biaxial strain. They found that ULLCTs could yield a 50% mass saving and 80% cost saving compared to metal-lined tanks. They conclude that – at the time – no commercially available resin could achieve a low enough He leakage rate at pressures exceeding 350 bar, at 150 bar a tank made with CTD 7.1, a "toughened epoxy resin," met the requirements. Figure 2-18 below compares the strength-to-weight efficiencies of composite tanks of varying liners and overwrap materials. The efficiency compares the design pressure, volume and mass of the tank $\left(\text{where } \eta = \frac{Pressure \times Volume}{Weight}\right)$.

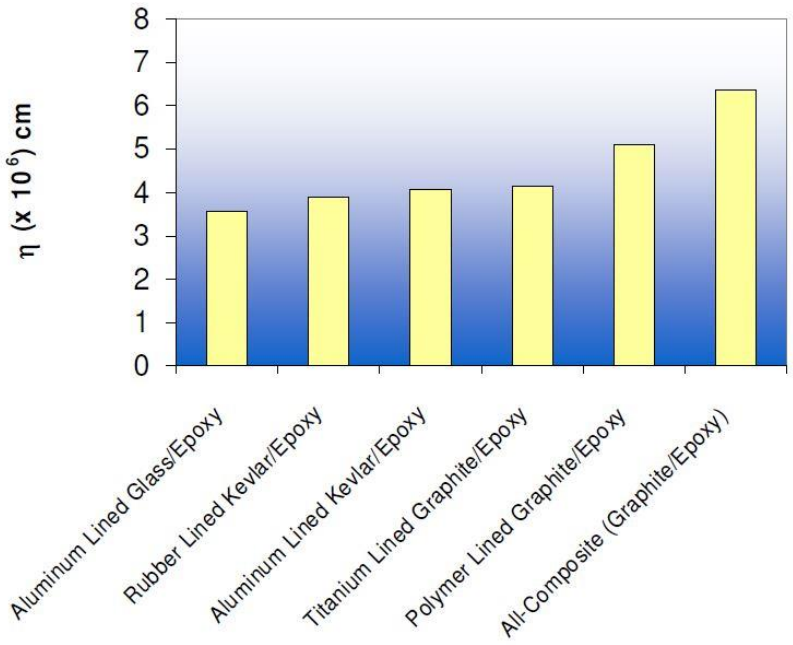

Figure 2-18: Composite tank efficiencies (Mallick et al., 2004).

Linerless composite LOX tanks are not common and lack the research heritage of linerless LH_2 tanks. The difficulty is material compatibility, however, NASA and Lockheed Martin performed compatibility and permeability tests on various composite materials (Graf et.al., 2000). They claim to have developed

a LOX compatible composite. The composite was likely composed of a toughened resin, according to Zheng (2018) toughened resins have improved ignition resistance.

In 2016, SpaceX completed the fabrication and testing of the all composite LOX tank which was intended for the interplanetary transport system (ITS). With a 12 m diameter, it was the largest composite tank ever constructed at the time. The SpaceX and the SLS composite tanks are depicted in Figure 2-18 below.

Figure 2-19: SpaceX 12 m LOX tank (Gardiner, 2017)

To date, Rocket Lab's Electron is the only all composite launch vehicle and the only with a linerless composite LOX tank in service, the weight saving allow the vehicle to achieve a mass fraction of 0.9. The key to LOX compatible linerless tanks lies in identifying the composition of suitable matrixes to bind the fibres.

2.7.1.1 Composite Overwrapped Pressure Vessels

Composite materials tend to form micro cracks at high pressure cryogenic conditions, this is due to the difference in thermal expansion coefficients of the resin compared to carbon fibre. These cracks cause leakage of liquid propellants (Zelenka et al., 2012). The issue can be solved by using a liner to form a tough, impermeable layer between the propellant and the tank wall. The liner can then be "over-wrapped" by a composite to form the finished tank, the fibre overwrap will bear the stress from the tank's internal pressure. Common liner materials include: aluminium, rubber, titanium and polymers (e.g. PEEK, FEP, PFA, PET and ETFE).

Liners simplify tank manufacture by providing a permanent base for the composite shape, but more importantly they offer a solution to LOX/composite incompatibility and LH_2 permeability. Unfortunately, a liner adds to the mass and thickness of an overwrapped tank, constituting up to 50 % of its mass. The filament winding process used to manufacture COPVs is depicted in Figure 2-20 below.

Figure 2-20: COPV filament winding process (McLaughlan et.al., 2011)

Both Tam (2002) and Kawahar (1996) chose Toray T1000 for their overwrapped tanks due its high strength-to-weight with an Epon 826 resin system. They both selected commercially pure titanium CP-3 for the liner, CP-3 has better weldability and higher tensile strength compared to aluminium 6061-T6. Titanium CP-3 has a tensile strength of 462 MPa elastic modulus 104 GPa, and density of 4 510 kg/m^3 (United Performance Metals, 2019).

T1000 carbon fibre has a tensile strength of 6 370 MPa, density 1800 kg/m3 and elastic modulus 294 GPa. With an unspecified epoxy resin at 60 % fibre volume the composite has a tensile strength of 1 570 MPa (60 MPa at 90 °), and elastic modulus 165 GPa (T1000G Data Sheet, 2019). The properties of other laminates are presented in Table 2-8 below.

Table 2-8: Mechanical properties of aerospace composite laminates (Zheng, 2018)

Mechanical Property	**IM7/5320-1**	**IM7/997-2**	**IM7/8552**
0 ° Tensile Strength (MPa)	2703	2690	2650
0 ° Tensile Modulus (GPa)	156	165	168
90 ° Tensile Strength (MPa)	81	75	-
90 ° Tensile Modulus (GPa)	9.7	7.6	-
0 ° Compressive Strength (MPa)	1737	1580	1690
0 ° Compressive Modulus (GPa)	143	152	150
Poisson's Ratio	0.34	-	-

2.7.2 Propellant Tank Pressurization

Both pressure fed and pump fed propellant systems require pressurization of the propellants, in pump fed systems this is done to meet NPSH demands and prevent impeller cavitation. Huzel et al. (1992) list four types of pressurization systems characterised by the gas source: stored gas, propellant evaporation, non-propellant evaporation, and chemical reaction.

Stored gas propellant systems are the most widely used for upper stage vehicles and have been in use since WWII for the V-2 rocket's propulsion system. Stored gas systems can be further classified as cold gas or hot gas. Cold gas systems are heavier due to the high density of the stored gas, hot gas systems are more complex and require heat exchangers to warm the gas during the vehicle's ascent.

These systems can be further classified based on the gas delivery mechanism, which can either a blow down or a regulated system. Blow down systems simply expel the gas into the propellant tanks without any pressure regulation; they are simple to implement, however, they cannot maintain a constant delivery pressure which in turn means the thrust will decrease over time. Regulated systems can maintain a constant pressure, but require additional components. Figure 2-21 shows the various pressure feed system configurations.

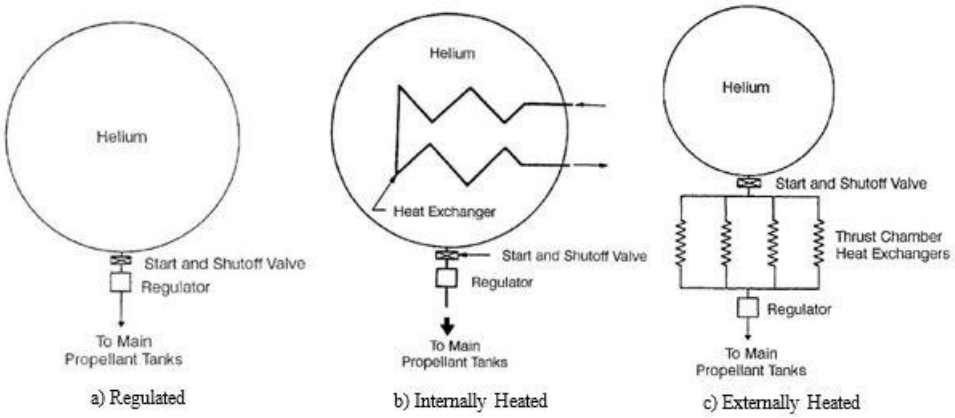

Figure 2-21: Pressure Feed System Configurations (Huzel et al., 1992)

2.7.3 Buckling of Thin-Walled Cylindrical Shells

Buckling is a major concern when designing propellant tanks which double up as the vehicle's structure. In trying to make the walls as thin as possible, the designer should consider buckling as a failure mode in addition to ruptures from internal pressure and bending from external pressure.

Buckling in thin-walled circular cylinders can be analysed in various ways. One method, described by Bruhn (1973) and used for propellant tanks, is based on the Kirchoff-Love hypothesis, where the value of the buckling coefficient (K_c) is obtained empirically from Figure 2-22.

The formula for critical stress is given by equation (2-3), where σ_{cr} is the critical compressive buckling stress; E is the materials modulus of elasticity; υ is Poisson's ratio; and t/L is the ratio of wall thickness

to height. Equation (2-4) is used to calculate the Batdorf parameter (Z) which is used with the cylinder's aspect ratio (*r/t*) to find K_c (Bruhn, 1973). The material properties necessary for the buckling analysis of common tank materials are listed Table 2-9.

Table 2-9: Buckling analysis material properties

Material	**Modulus of Elasticity (GPa)**	**Poisson's Ratio**
Aluminium (7075-T6)	71.7	0.33
Stainless Steel (301)	193	0.27
Titanium (Ti6Al4V)	114.5	0.34

$$\sigma_{cr} = K_c \frac{E\pi^2}{12(1-v^2)}\left(\frac{t}{L}\right)^2 \tag{2-3}$$

Where

$$Z = \frac{L^2}{rt}\sqrt{1-v^2} \tag{2-4}$$

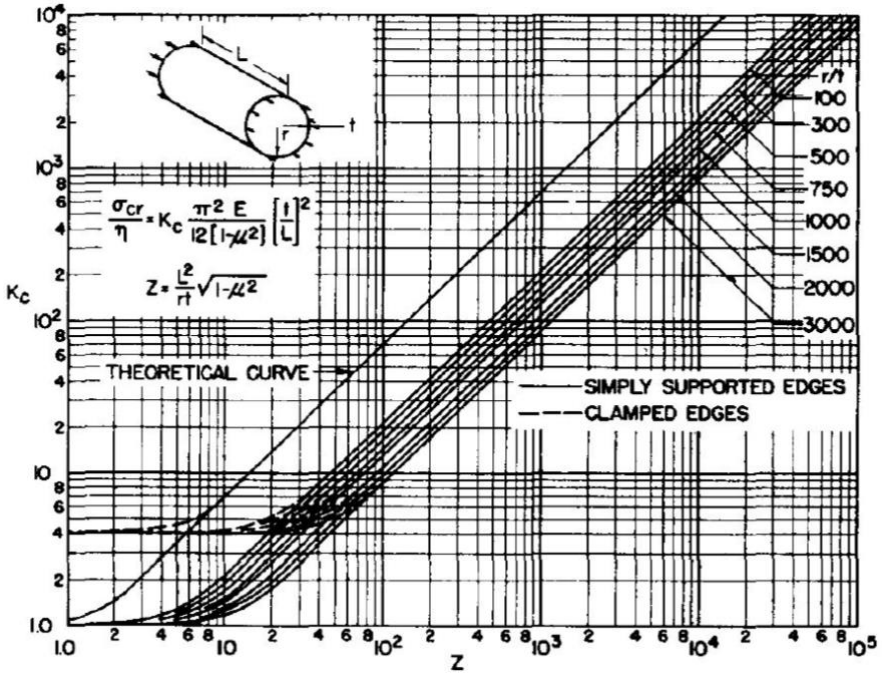

Figure 2-22: Buckling coefficient for cylinders (Bruhn, 1973)

Many methods exist for determine the buckling characteristics of thin walled sections, the classical method along with three commonly used methods including the work of: Sechler (1959), Pisacane (2005), Brauhn (1973) are presented.

Sechler (1959) approaches buckling analytically, although it does not completely capture the phenomenon, it is good for initial guesses for parameter estimation from experimental data. For the case where a thin-walled tank has no internal pressurization (tank pressure = atmosphere), equation (2-5) applies.

$$\frac{\sigma_{cr}}{E} = 9\left(\frac{t}{R}\right)^{1.6} + 0.16\left(\frac{t}{L}\right)^{1.3} \tag{2-5}$$

With internal pressure (tank pressure > atmosphere) the following equations apply.

$$\sigma_{cr} = \left(K_o + K_p\right)\frac{Et}{R} \tag{2-6}$$

where:

$$K_o = 9\left(\frac{\mathrm{t}}{\mathrm{R}}\right)^{1.6} + 0.16\left(\frac{\mathrm{t}}{\mathrm{L}}\right)^{1.3}\left(\frac{t}{R}\right)^{0.3} \tag{2-7}$$

$$K_p = 0.191\left(\frac{p}{E}\right)\left(\frac{R}{t}\right)^{2} \tag{2-8}$$

Pisacane (2005) uses an altered version of the classical buckling formula for the case where there are no end restraints on the cylindrical section. The classical equation (equation 2-9)is similar to Pisacane's only without the factor, "γ".

$$\sigma_{cr} = \frac{E}{\sqrt{3(1-\nu^2)}}\frac{t}{r} \tag{2-9}$$

$$\sigma_{cr} = \frac{\gamma E}{\sqrt{3(1-\nu^2)}}\frac{t}{r} \tag{2-10}$$

where

$$\gamma = 1 - 0.901\left(1 - e^{\phi}\right) \tag{2-11}$$

and

$$\phi = \frac{1}{16}\sqrt{\frac{\overline{r}}{t}}\ ; \quad \text{for } \frac{r}{t} < 1500 \tag{2-12}$$

Each theory produces different values and is effective across a limited range of wall thicknesses. Pisacane's method stands out as being the least conservative prediction of buckling strength, which may result in overestimations.

A comparison of outputs from the various methods (i.e. Bruhn, Pisacane, Sechler and classical) for estimating critical buckling stress of a 301 stainless steel (fully hardened) cylinder is presented in Figure 2-23. From the figure, the variation in critical buckling stress results between the methods can be seen,

also, the possible overestimation of Pisacane's theory is visible. The variation makes it difficult to select an appropriate method, these techniques are better suited for parameter initialisation for developing numerical models based on experimental data.

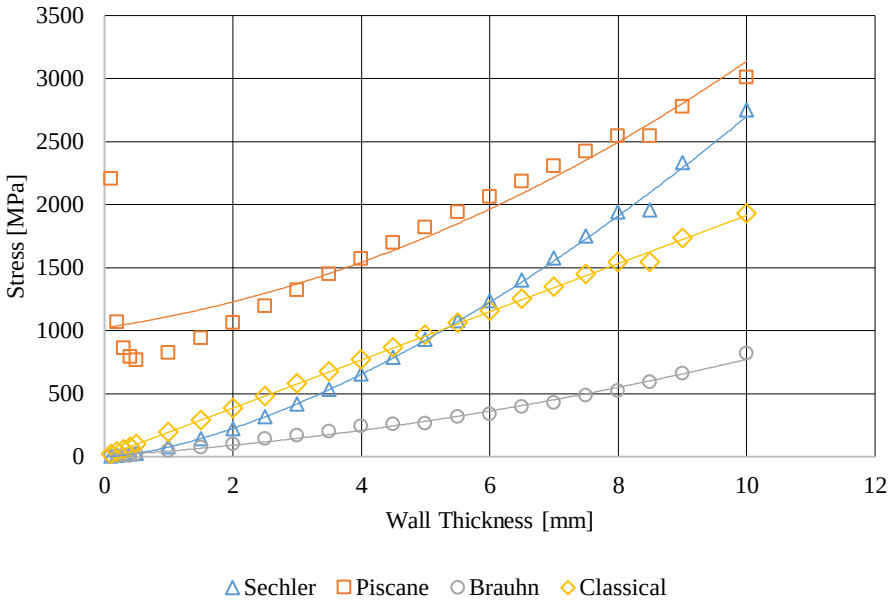

Figure 2-23: Comparison of buckling theories for a 301 FH stainless steel cylinder

2.8 Attitude Control System

A spacecraft's attitude is defined as its rotational orientation in relation to a reference coordinate system (Grobekatthöfer and Yoon, 2012).

2.8.1 Cold Gas Propulsion System

The attitude control of spacecraft and satellites requires a propulsion system is that produces quick, low I_{SP} bursts of thrust. The system should also be highly reliable, simple in design and must not rely on combustion for fear of contaminating a spacecraft's vital surfaces e.g. solar panels (Fatehi et al., 2015).

Lev and Herscovitz (2017) explain that cold gas propulsion systems (CGPS) satisfy the design criteria for spacecraft engines, they work by expanding a pressurized gas through a nozzle. There are three types of cold gas propulsion systems: gas pressurized systems, which store pressurized gas and simply allow it to expand through a nozzle; liquefied systems store liquid phase propellants at their vapour pressure, the propellant flows into a plenum tank where it is vaporized (by expansion or external heating) and then out to space through a nozzle; and finally, heated gas systems, which are non-conventional and operate by heating the storage tank to vaporize the liquid propellant before each firing of the thruster(s).

Cold gas propulsion systems consist of a highly pressurized propellant tank, containing a liquid or gas; pressure regulator; solenoid valves; tubing and fittings; thrusters; and various sensors to monitor the propellant (Anis, 2012). Figure 2-242-24 illustrates the base components of a CGPS.

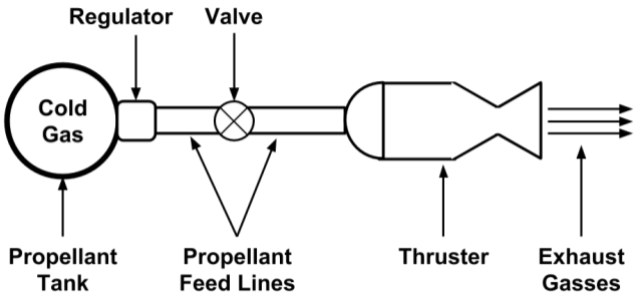

Figure 2-24: Cold Gas Propulsion System Schematic (Anis, 2012).

Monopropellant systems have also been used for spacecraft propulsion. They produce significantly higher I_{SP}, but they are often toxic and carcinogenic while the products of their decomposition also pose health risks, e.g. hydrazine is toxic and decomposes into harmful ammonia gas as a product (Nothnagel et al., 2011).

2.8.1.1 Propellants

Selection of a propellant revolves around two parameters: specific thrust and molecular weight (or density). High specific thrust propellants tend to have a low molecular weight (e.g. helium and hydrogen) this means the tank volume and thus the weight will be increased (Anis, 2012). Nitrogen is the most common propellant due to its balance between density and thrust as well as the lack of contamination concerns.

Ammonia and carbon dioxide would perform well, however the toxicity of CO_2 and the corrosive nature of ammonia makes their use undesirable. Commonly used propellants and their properties are listed in Table 2-6 below.

Table 2-10: Properties of Common Cold Gas Propellants (Ketsdever and Micci, 2000)

Gas	**Molecular Weight (g/mol)**	**Specific Impulse (s)**
Air	28.9	74
Argon	39.9	57
CO_2	44.0	67
Helium	4.0	179
Hydrogen	2.0	296
Nitrogen	28.0	80
Methane	16.0	114

2.8.1.2 Propellant Tank

Spherical tanks are typically used for cold gas propulsion systems, given the low quantity of propellant required the space requirement associated with spherical tanks is less of an issue. Spherical tanks are known for their ability to store contents at higher pressures with thinner walls than cylindrical tanks, this means for the same pressure a spherical tank will be lighter. The drawback is that spherical tanks are more expensive than cylindrical tanks (Wermac.org, 2018).

As per ASME Section VIII Division 1 2011 the wall thickness for a spherical tank is given by equation 2-13. *"P"* is the design pressure, "r_i*"* is the internal corroded radius, "σ*"* is the maximum allowable stress at design temperature, and *e* is the joint efficiency.

$$t = \frac{P \times r_i}{2\sigma e - (0.2\ to\ 0.6)P} \tag{2-13}$$

2.8.1.3 Thruster

The thruster is nothing more than a CD nozzle designed for relatively low thrust, I_{SP}, and infinite expansion (i.e. vacuum, where ambient pressure is 0 Pa). These nozzles are extremely small compared to the main engines of a rocket, an attitude/reaction control system will consist of multiple thrusters to cater for the various manoeuvres the system will perform.

2.9 Separation Systems

A separation system is responsible for holding two different stages together during a multistage launch vehicle's ascent until a separation event occurs. At this point the mechanism releases the stages, along a separation axis, and provides actuation to separate them. A separation system can be broken up into two mechanisms: the "release mechanism", that holds stages together until the separation event and the "separation mechanism", which provides relative actuation between stages. The main separation events of a launch vehicle, include:

1) Rocket stage separation, which occurs when a stage has depleted its propellant and is ejected, allowing the subsequent stage's engine(s) to fire.
2) Payload fairing separation, this occurs when the launch vehicle has ascended to an altitude where the atmosphere is too thin to impart significant aerodynamic loads on the payload.
3) Payload separation occurs once the mission orbit has been reached; the payload is separated from the upper stage of the launch vehicle and begins operation.

In addition to those listed above, the activation of the launch escape system and the ejection of strap on boosters are also considered separation events. For this section a "stage" refers to an object participating in a separation event (e.g. spent rocket stage, subsequent rocket stage, payload fairing and payload itself).

Various industry techniques exist for achieving separation. One approach is to use a V-clamp (or Marman clamp), fastened by an explosive bolt, as a release system (Li et al., 2014). A V-clamp is made of two segments, or "bands", consisting of multiple V-clamps attached to each band segment. Figure 2-26 is a top and cross-sectional view of the V-clamp band used on the CALT manufactured Long March launch vehicle.

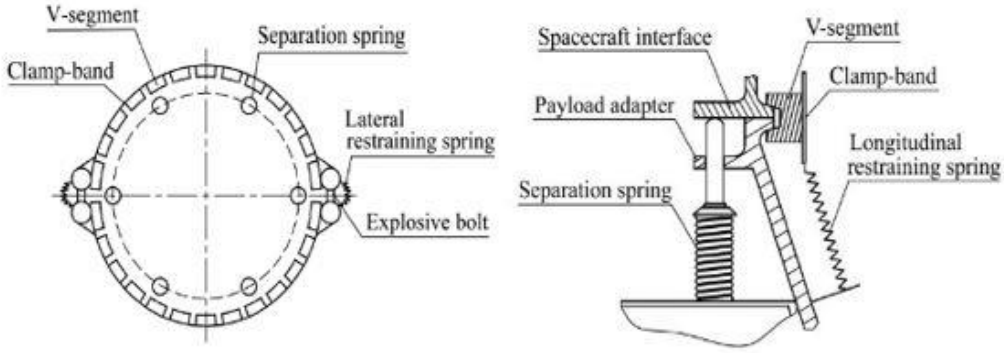

Figure 2-26: V-clamp band (left) and spring loaded lock system (right) (Li et al., 2014)

Once the bolt is severed, the separation mechanism activates and applies a separation force between the stages, either by using a spring mechanism; expanding a diaphragm; by pressurization of an interstage; extending pneumatic or electric actuators (for low shock separation); the firing of retrograde thrusters attched to the stages; the ignition of the next stage's engine(s); or a combination of the above (Mitchell, 1970).

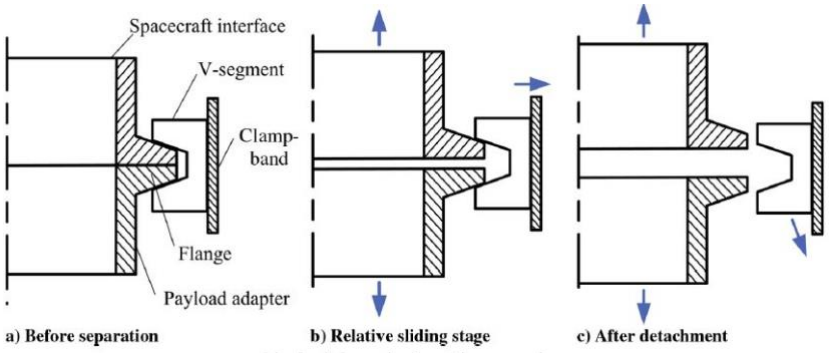

Figure 2-27: V-clamp separation process (Li et al., 2014)

Pneumatic and electric locks are a low shock alternative to explosive bolts, especially for payload and fairing separation. ESA's Vega launch vehicle utilises hinged locks as a release mechanism and pneumatic actuators as a separation mechanism for its fairing, the system is depicted in Figure 2-27 below. Pneumatic/electric systems have the advantage of being tested before flight and can be reused if recovered, potentially reducing manufacturing costs compared to explosive bolts which must be replaced after each launch or test.

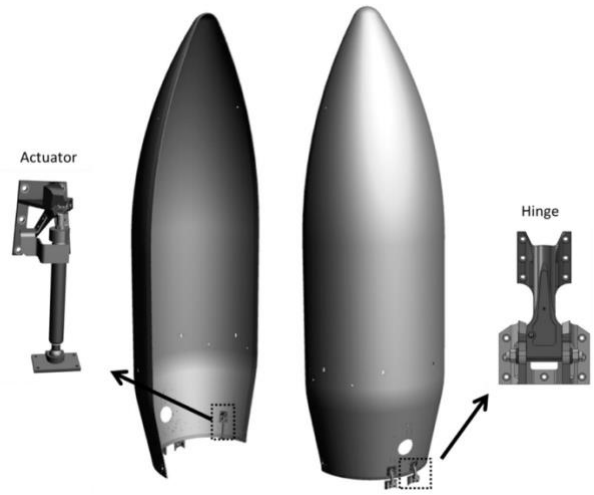

Figure 2-28: ESA Vega fairing separation system (United Space in Europe, 2019)

2.10 Electric Motors

A motor is an electrical machine that produces mechanical energy by means of electromagnetics (Zhao and Yangwei, 2011). In an Electro-pump engine cycle, electric motors provide the torque for the pump impellers as opposed to traditional gas turbines *et.al.*, 2018).

The motor must produce high speed, the rotational speeds of rocket engine centrifugal range from 20, 000 to 100, 000 rpm, and require high-power output (Waxenegger-Wilfing *et.al.*, 2018). Table 11 lists the pump speed of modern small lift liquid rocket engines, from the shaft speeds we can deduce that an electric motor must rotate at speeds in excess of 20, 000 RPM and produce upwards of 30 kW of power to meet the engine requirements of a small lift launch vehicle.

Table 2-11: Pump Shaft Speeds of Modern Launch Vehicle Engines

Engine	Impeller Shaft Speed (RPM)
Reaver (Firefly Aerospace) [(1)]	26, 000
Prime Launcher Engine (OrbeX) [(2)]	25, 000
Rutherford (Rocket Lab) [(3)]	40, 000 (at 32kW)

[(1)] Kovacs (2018), [(2)] Orbex (2019), [(3)] Morring and Norris (2015)

When the density and outlet requirements of both propellants are similar, it is possible to drive the propellant pumps with one shaft (Haidn, 2008). This could present a cost and mass reduction as only one motor (and gear set) per engine would be required to drive both pumps.

2.10.1 Types of motors

Electric motors fall into two broad categories: Alternating Current (AC) motors and Direct Current (DC) motors, who differ based on the type of voltage each requires (Gopal, 2020). AC motors are the

most common type in heavy industry, owing to their rugged design, whereas DC motors are preferred for applications that require precise speed control (Alnaib, 2019).

AC motors can be classified by the rotor's construction and nature of its rotation, namely: asynchronous (i.e. induction motor) and synchronous (i.e. permanent magnet motors).

According to Teschler (2013) an induction motor's rotor consists of conductive bars imbedded in slots (similar in construction to a cage), current passes through the stator coils to "induce" a rotating magnetic field whose flux interacts with the conductive bars of the rotor to produce rotation in the direction of the magnetic field. The nature of the assembly means the rotor's mechanical speed lags behind the stator's rotating magnetic field speed, a feature called slip. This is where the term "asynchronous" motor comes from (Rawlins, 2019).

In a permanent magnet motor the rotor has magnets imbedded on or into the shaft, these magnets become north and south poles (Detloff, 2017). The magnetic field produced in the stator will thus attract or repel the poles of the rotor to produce rotation, so there's no magnetic induction of a conductor. Given the direct magnet-to-magnet interaction, the rotor speed and stator magnetic field rotate synchronously (Rawlins, 2019).

Motor mass relies on power density (see Equation 3-45). Figure shows the densities of various motors which are discussed below.

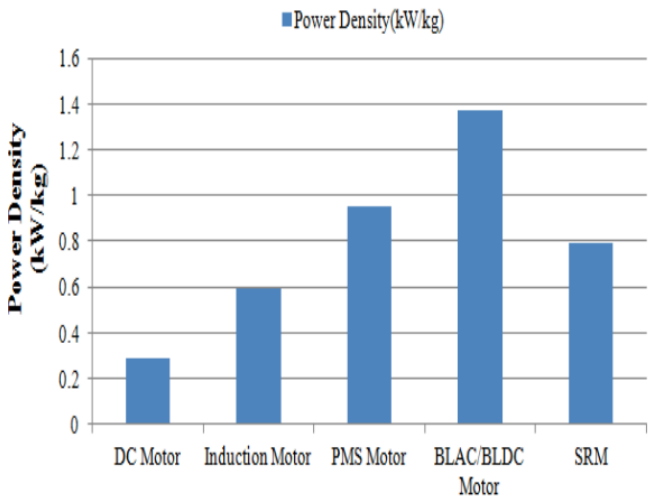

Figure 2-29: Power density comparison of various motors (Chaudhari 2020)

2.10.1.1 Direct Current Motor

This is a classic motor that has been in use for many years. Electrical power, for rotation, is transferred to the rotor via stationary brushes which contact commutator segments (Gopal, 2020). The arrangement converts incoming DC current to AC (Zhao and Yangwei, 2011).

There are 3 types of DC motors: shunt, series and compound, they differ mainly due to the position of the field windings in relation to the armature (Alnaib, 2019). Shunt has the windings in parallel and have good speed control but poor starting torque. Series have the windings connected in series and can produce high starting torque. Compound have series windings with a separately excited shunt field, this combines the characteristics of shunt and series configurations (i.e. high starting torque and good speed control) (Shrivastava, 2016). The equivalent circuits of each configuration are depicted in Figure 2-30

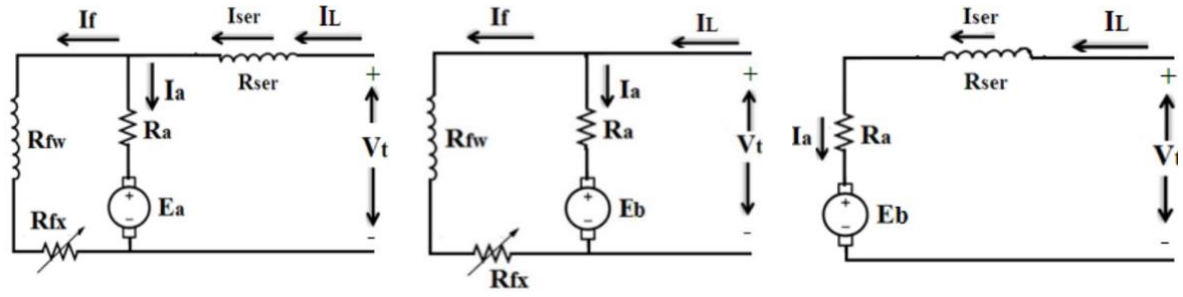

Figure 2-30: DC motor equivalent circuits - compound (left), shunt (centre), and series (right) (Alnaib, 2019).

The commutator and brushes, although simple, present a maintenance challenge and are often the cause of breakdowns in DC motors (Gopal, 2020).

2.10.1.2 Brushless Direct Current Motor

A BLDC can be considered a permanent magnet DC motor (Gopal, 2020). They are commutated by means of power switches and not brushes, unlike DC motors (Zhao and Yangwei, 2011). The switches activate based on the rotor's position which is determined electronically, usually with hall sensors (Zhao and Yangwei, 2011). BLDC motors can also be considered a type of permanent magnet AC motor fed with trapezoidal currents (Cao *et al.*, 2012).

There are three types of BLDC motors which are classified by the type of power each uses, they include: single-phase, two-phase and three-phase (Zhao and Yangwei, 2011); a schematic of the most common, single-phase and three-phase, are depicted in Figure 2-31.

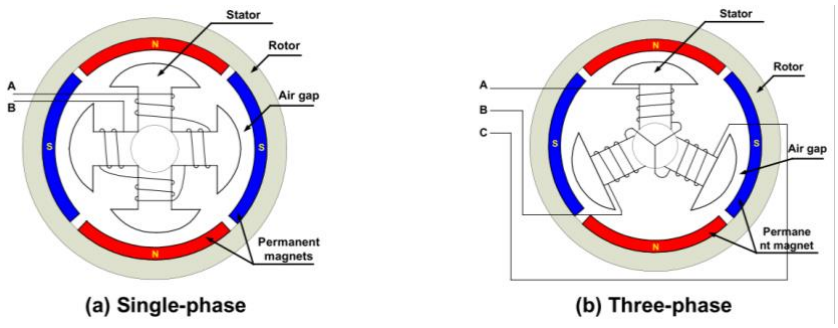

Figure 2-31: Simplified BLDC cross section (Zhao and Yangwei, 2011)

According to Zhao & Yangwei (2011), BLDC motors possess excellent speed vs torque characteristics, a wide operating speed range, high power densities, high efficiency, and fewer maintenance issues (due to the lack of brushes). The lack of brushes also eliminates the sparking issues associated with DC motors (Gopal, 2020). (Wang, 2012) adds that they are low-noise and compact. The high efficiency of permanent magnet motors, in general, is due to the lack of rotor copper losses given that the permanent magnets negate the need for electrical excitation via windings (Yazdi *et.al.*, 2020).

2.10.1.3 Induction Motor

Induction motors are the most prevalent AC motor in industry, this is due to their rugged construction, low maintenance requirements and high efficiency (85 – 97 %) (Gopal, 2020). Their main disadvantages are their low starting torque, rotor losses at high speed, and narrow speed range for maximum power output (Gopal, 2020).

2.10.1.4 AC Permanent Magnet Synchronous Motor

PMSM (a.k.a. brushless AC motors) are increasingly replacing AC induction motors (Karunamoorthy and Dhivyaa, 2017) as they boast advantages like reliability, high efficiency, and high power density (Gopal, 2020). The main disadvantage, as stated by Kwak *et.al.* (2018), is overheating, especially for the relatively small motors likely to be used for small lift launch vehicles. The heat causes demagnetization of the permanent magnets which greatly reduce the motor's performance. Another pitfall is the high cost of the rare earth elements, like neodymium, used in their construction (Gopal, 2020).

Two types of PMSM categories exist, interior (IPMSM) and surface-mounted (SPMSM), differentiated by where the permanent magnets are placed on the rotor (Pellegrino *et al.*, 2012).

For SPM the magnets are mounted on the outer periphery of the rotor; this configuration produces the highest flux density in the air gap but is less robust. Surface mounted are best suited for low speed applications and give the highest power density (Balashanmugham and Maheswaran, 2020).

IPMSM have the magnets embedded in the rotor laminations, which is difficult and costly to construct. This configuration is suited for high speed applications (Balashanmugham and Maheswaran, 2020).

A third type, surface inset permanent magnet, combines surface and interior architectures and has the magnets mounted on the outer periphery but facing inwards (towards the centre of the rotor), thus providing robustness and high speed capabilities (Rycroft, 2018). The various magnet configurations are presented in Figure 2-32.

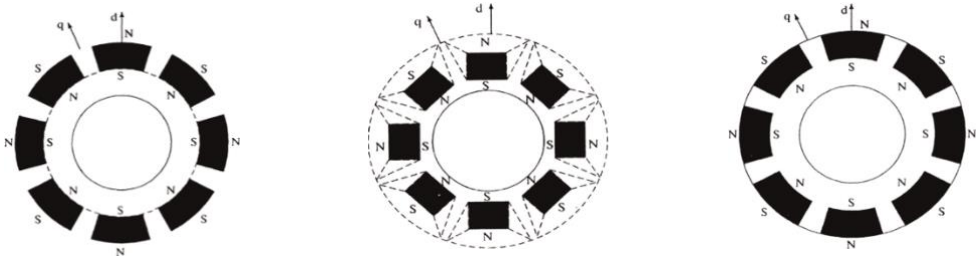

(a) Surface-mounted (b) Interior (c) Surface inset

Figure 2-32: PMSM magnet positions on rotor (Balashanmugham and Maheswaran, 2020)

2.10.1.5 Axial-Flux PMSM

Axial-flux permanent magnet (AFPM) motors are gaining popularity in the light electric vehicle industry owing to their high efficiency, improved heat removal, and superior torque and power densities compared to their radial-flux permanent magnet (RFPM) counterparts (Yu *et.al.*, 2016). They are suited to direct drive applications, nullifying the need for a gearbox in EV applications (Yang and Lee, 2012).

Two types exist namely Kaman and Torus, they differ based on the position and quantity of stators and rotors. Torus has a stator sandwiched by two rotors, whereas the Kaman has a rotor sandwiched by two stators (Yang and Lee, 2012).

The structure of AFPM motors affords them a higher diameter-to-length ratio compared to RFPM motors meaning they are generally shorter and compact (Mei *et.al.*, 2020). As a result, these motors are also referred to as "pancake" motors (Clemens, 2018). Figure 2-33 compares the structure of axial and radial flux motors.

Another advantage of AFPM motors is that the direct drive capability allows for multiple motors to be stacked (i.e. modularity) in order to achieve higher power or torque requirements (Chaker *et al.*, 2009).

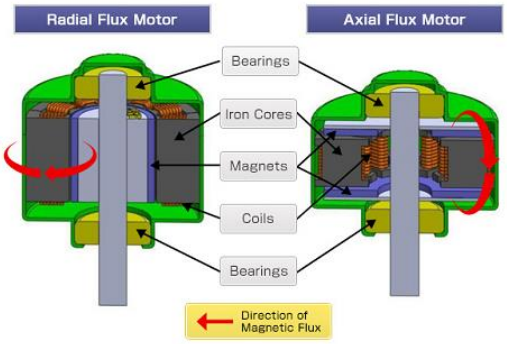

Figure 2-33: Components of axial and radial flux motors (Fahem, 2020)

2.10.2 Motor Control

According to Jaszczolt (2017), in most cases, controlling the speed of an AC motor is done by a variable frequency drive (VFD). Although many scenarios involve the use of VFD and stator winding induction motors to generate a rotating magnetic field, they can also use position or speed feedback sensors as a

reference for the VFD to achieve precise speed control. In some cases, relatively accurate speed control can be obtained without a feedback sensor. This can be achieved using a permanent magnet (PM) motor and a process called "high frequency signal injection method".

2.10.3 Best for propellant pumps

Cost, performance (i.e. speed and power), efficiency (i.e. losses), power density (which influences mass), maturity of the technology, and ease of control are the factors generally considered when selecting an electric motor (Gopal, 2020). For an electric pump, the required speed, power, and mass will be the greatest influences on the selection.

Derammelaere *et. al.* (2017) performed a quantitative comparison between DC, BLDC, and PMSM motors. They conclude that BLDC is best suited for high speed applications (especially smaller motors with little inertia) while PMSM give the best overall performance (i.e. efficiency, torque density, and power density). DC motors can still be useful as they don't require a motor drive. Figure 2-34 compares the motors based on speed, power, and cost.

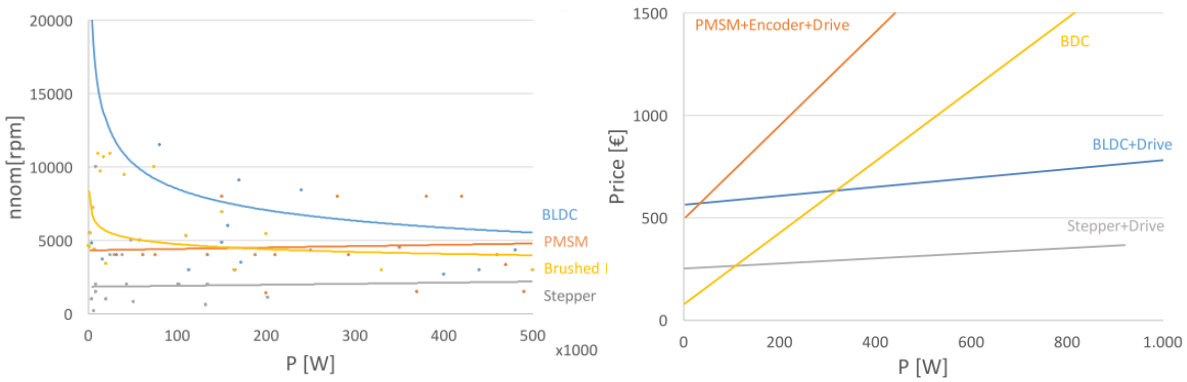

Figure 2-34: Motor speed vs power (left) and price vs power (right) (Derammelaere *et. al.*, 2017)

According to Kwak et al. (2018), the permanent magnet synchronous motor (PMSM) is a promising candidate for driving propellant pumps due to their high operating speeds. Their main concern was cooling the motor, specifically the permanent magnets which have a maximum operating temperature of 403 K (Kwak *et.al.*, 2018). Waxenegger-Wilfing et al. (2018) describes the high power density of PMSM motors as the most attractive feature for small lift vehicle applications.

Figure 2-35 depicts the turbo pump power and speed of various rocket engines, the red line represents experimental PMSM data from Kolondzovski et al. (2011). Figure 2-34 shows that PMSM motors can meet the operating requirements of some liquid rocket engines.

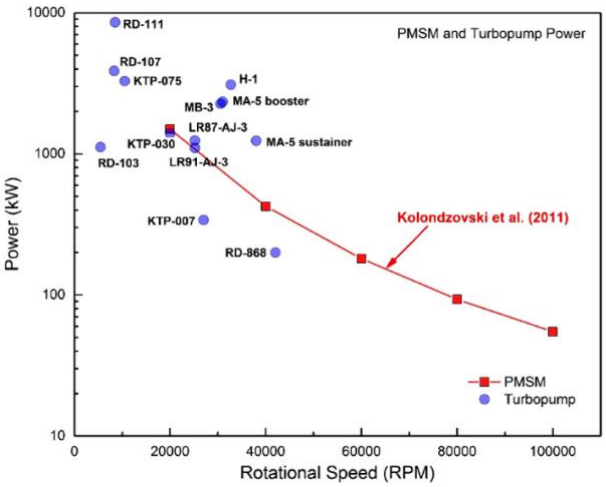

Figure 2-35: Power and speed requirements of various rocket engine turbopumps (Kwak *et.al.*, 2018).

Another candidate are BLDC motors, Rocket Lab currently use BLDC motors for the Rutherford engine's propellant pumps (Henry, 2016). They have a similar construction and operation to PMSM motors (Gopal, 2020), the main difference between the two motors is the type of voltage they receive, the flux wave form, and the method of rotor positioning. Štefan et al. (2019), who used a BLDC motor for their theoretical electric pump design, cite the higher cost and complexity compared to DC motors as the main flaw of BLDC motors. BLDC and PMSM motors are compared in Table 12.

Table 2-12: Comparison of PMSM and BLDC motors (Sakunthala et.al, 2018).

BLDC	**PMSM**
Synchronous machine	Synchronous machine
Fed with direct currents Trapezoidal back emf	Fed with sinusoidal currents Sinusoidal back emf
Stator flux position commutation each 60°	Continuous stator flux position variation
Only two phases ON at the same time	Possible to have three phases ON at the same time
Torque ripple at the commutation	No torque ripple at the commutation
Low order current harmonics in the audible range	Fewer harmonics due to sinusoidal excitation
High core losses due to harmonic content	Less core loss
Less switching losses	High switching losses at the same switching frequency
Control algorithms are relatively simple	Control algorithms are mathematically intensive
Easier to control (six trapezoidal states)	More complex control (continuous 3Φ sine wave)
Better for lower speed	Higher maximum achievable speed
Noisy	Low noisy
Doesn't work with distributed winding	Work with low-cost distributed winding

2.11 Battery Pack

The battery pack is one of the most crucial parts of the electro-pump fed system. It accounts for most of the electro-pump feed system's mass and is the source of all the vehicle's power requirements.

A battery pack is composed of "modules" which contain single cells arranged in series, parallel or a combination to achieve the voltage, current, and power requirements (Vezzini, 2014). Cells are essentially a storage medium made up of two electrodes in an electrolyte. The electrolyte serves as a medium for ionic exchanges, between the cathode and anode, which produces electricity (Miao, Y. et al., 2019). A battery pack also has a battery management system which monitors the cells and ensures their safe operation (temperature, state-of-charge and safe discharge/charge) (Vezzini, 2014).

The most important parameters of cells are their energy density and power density. High values correspond to a lower system mass. So, the question is: what is the best battery? The decision is heavily influenced by the engine burn time, which determines how long cells are discharged and thus, how much energy is required; another factor is the combustion chamber pressure, this influences the pump power required and thus the cell power required. More energy or power constitutes a heavier battery pack for a particular cell type.

In general, there are no cells that provide both high power and energy densities (Ki et al., 2020), but from Figure 2-36, it is evident that the choice of cell type for an electro-pump feed system falls between Li-Po and Li-Ion cells as they represent the upper end of the energy density spectrum. This translates to lighter battery packs

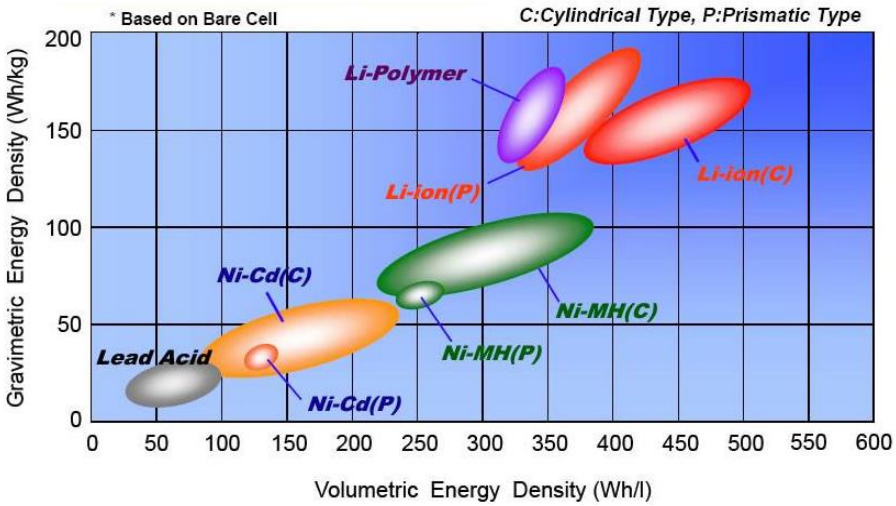

Figure 2-36: Specific specific energy of various cells (Nguyen, 2018).

According to Mirza (2013), Li-Ion refers to a family of cells which use lithium and some metal oxide as a cathode. Traditionally cobalt dioxide (CoO_2) or manganese oxide (Mn_2O_4) have been used, but iron

phosphate ($FePO_4$) has gained recent attention as a safe and chemically stable addition to the family. Table 2-11 lists the most common Li-ion cathode chemistries and their characteristics.

Table 2-13: Properties of Cathode Chemistries (Linden, 2010).

Material	**Chemical Formula**	**Comments**
Lithium cobalt oxide (LCO)	$LiCoO_2$	Original commercial type; expensive raw materials
Nickel cobalt aluminium (NCA)	$LiNi_{0.8}Co_{0.15}Al_{0.05}O_2$	Highest energy density per unit mass
Nickel manganese cobalt (NMC)	$LiNi_{1-x-y}Mn_xCo_yO_2$	Safer and less expensive than LCO
Lithium manganese oxide (LMO)	$LiMn_2O_4$	Safer and less expensive than LCO, but poor high temperature stability
Lithium iron phosphate (LFP)	$LiFePO_4$	Very safe, high power, but lower energy density. Best high-temperature stability

Li-Po are cells which use a non-conducting solid polymer composite (polyacrylonitrile) electrode, their performance is lower than Li-Ion cells however they have a significantly lower volume which makes the popular for consumer and hobby electronics. The cells can be formed into a variety of shapes limited by the designer's imagination but they can cost 10-30% more than Li-Ion cells to manufacture (Heydecke, 2018). One can conclude that Li-Ion and Li-Po cells have similar performance where Li-Ion cells better suited for power and energy constrained designs while Li-Po cells are suited for space constrained designs. Table 2-12 shows the performance of various commercially available cells.

Table 2-14: Performance Specifications of Commercially Available Cells

Model (Manufacturer)	**Type (Configuration)**	**Energy Density (Wh/kg)**	**Power Density (kW/kg)**
ABLP8474170H320 (Amicell) [(1)]	Li-Po (Pouch)	325	0.65
PSP11102313 (LJ Technology) [(2)]	Li-Ni-Mn-CoO (Pouch)	255	-
NCR18650PF (Panasonic) [(3)]	Li-Ion (Cylindrical)	207	-
Licerion® Cell (Sion Power) [(4)]	Li-Metal (Pouch)	650	8

[(1)] (Lee et al., 2020), [(2)] (LJ Global Technology, 2020), [(3)] (Panasonic, 2013), [(4)] (Mikhaylik et al., 2018)

New cell chemistries continue to be developed which are set to revolutionize the aerospace battery industry, offering nearly double the specific energy and more than triple the specific power density of current Li-Ion cells. American based Sion Power revealed their Licerion® Li-Metal cell technology at the 2018 NASA Workshop on Batteries (Mikhaylik et al., 2018). Li-Metal cells are not new, but were plagued by lithium dendrite formation which led to hazardous operation and limited life. Sion Power have overcome the challenges to develop a cell that produces specific energy and power of 650 Wh/kg and 8 kW/kg respectively (Mikhaylik et al., 2018). Hydrogen fuel cells (a.k.a. proton exchange membrane cells) are also a contender, especially for launch vehicles using hydrogen as a propellant (Brey, 2017).

2.12 Miscellaneous

2.12.1 Ignition Systems

The ignition system is responsible for releasing the energy stored in propellants, be it the main propellant mixture exiting the injector or for igniting gas generators and turbo-pumps (Huzel and Huang, 1992).

The ignition of the propellants must be well timed. According to Fletcher and Morrell (1960), liquid rocket engines are particularly sensitive to the effects of faulty or improperly timed ignition. The high propellant flow rates within a relatively small combustion chamber and high concentrations of reactants close to the stoichiometric ratios all create an environment for transient phenomenon, upon ignition, which can destroy the engine.

Figure 2-37 shows the start-up sequence of an unspecified open-cycle engine, notice the short delay (less than 0.6 s) between main oxidiser valve (MOV) opening and propellant ignition.

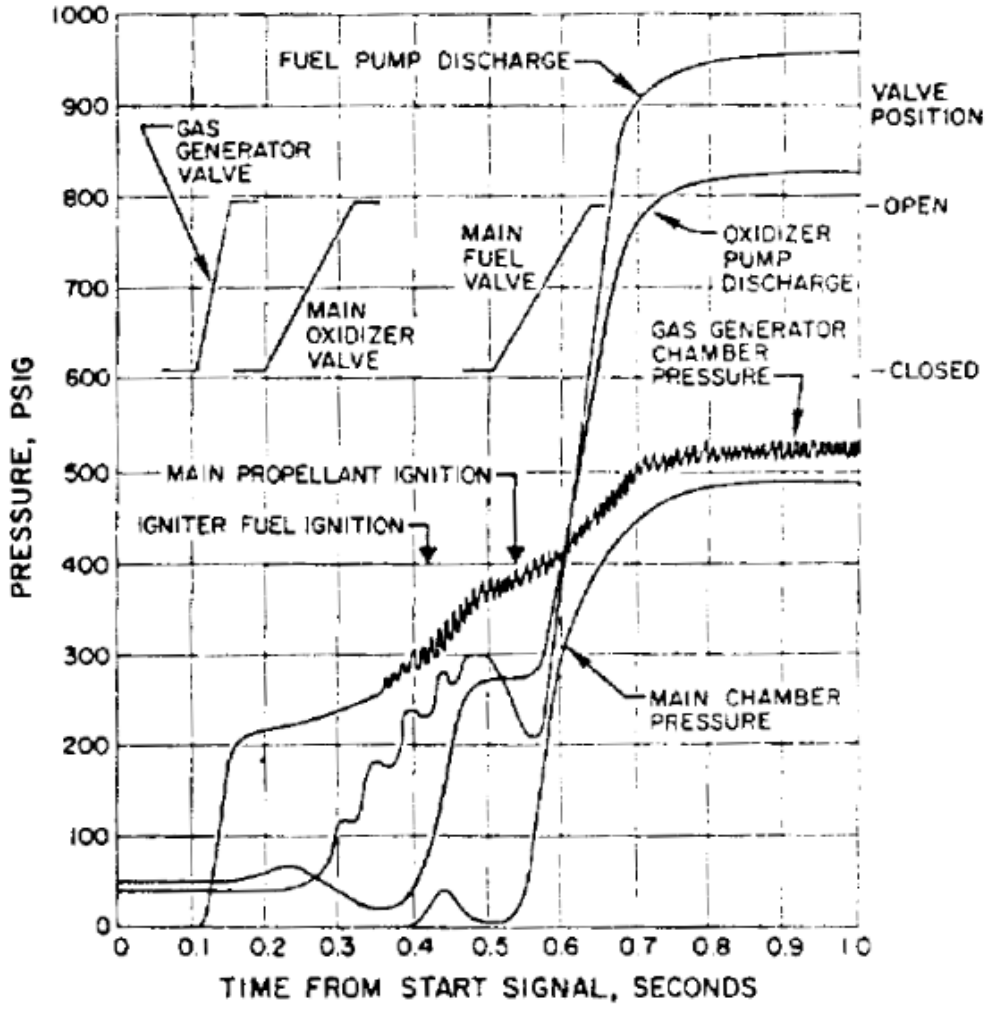

Figure 2-37: Startup Transient of an Open-cycle Engine (Park, 2017)

Late ignition can cause the combustion chamber to flood with propellants, ignition of a flooded chamber causes an explosion, known as a "hard start", which produces high pressures that can destroy the engine (Marques, 2016). Hard starts can be prevented by careful ignition and valve timing, varying the O/F ratio to limit the maximum pressure, or supplying an ignition source before propellants enter the chamber (Crone, et al., 1993).

The ignition system selected is dependent on the type and phase of propellant(s) (i.e. monopropellant vs bipropellant), if an altitude start is need, need for restarts, and the overall weight (Huzel and Huang, 1967).

Pyrotechnic igniters are essentially explosives detonated electronically or with a laser (Huzel and Huang, 1967). They are designed to burn slowly, with a sufficiently hot flame, lasting long enough to ignite the propellant. They are typically placed in the combustion chamber -in multiple units- aimed radially outwards for improved heat distribution. They can be mounted directly on the injector, or inserted from the aft end via the nozzle (Rabbitte and Mohs, 2020)

Pyrotechnic igniters have lost favour in industry as they don't scale up well, do not support engine restarts., and they struggle to ignite cryogenic propellant, causing ignition delays, thus increasing the risk of hard starts (Rabbitte and Mohs, 2020).

Hypergolic igniters, as the name suggests, generate heat from mixing a hypergolic propellant combination or a hypergolic and catalyst (typically a salt) in a cartridge. Hypergolic igniters should not be confused hypergolic ignition where the rockets hypergolic propellant combination (oxidiser/fuel) combust upon contact, in this case a physical igniter is not necessary (Gündüz *et al.*, 2005).

These ignitors work by placing a substance -which is hypergolic with one of the main propellants (generally oxygen)- in a cartridge. Upon activation, the substance is injected and mixes with the propellant, creating a hypergolic ignition. The "hot" propellant then enters the combustion chamber and subsequently ignites the main propellants. This ignition strategy is particularly popular with LOX/RP-1 rocket engines, where RP-1 poses ignition difficulties when using pyrotechnics (Ballard, 2019).

For propellant ignition in its Merlin engines, Space X uses a pyrophoric mixture of triethylaluminium (TEA) and triethylboron (TEB) (Belluscio, 2016). The Atlas rockets (LOX/RP-1) used a 15 % triethylaluminium (TEA) and 85 % triethylboron (TEB) mixture (Sutton and Schneider, 1965). A distinction must be made between the terms pyrophoric and hypergolic, "pyrophoric" is a safety classification for compounds that ignite upon contact with air (e.g. iron sulphide), all pyrophorics are hypergolic, however, not all hypergolics are pyrophoric (Glassman et.al., 2015).

One disadvantage of hypergolic igniters is that the cartridges are finite, limiting the amount of engine starts. Unlike spark-torch igniters where restarts are limited to the amount of propellant. Another is the mass incurred by the cartridges.

Spark-torch igniters, also called "augmented spark igniters (ASI)," have a similar principle of operation as the spark ignition process that occurs in an internal combustion engine; a spark plug ignites a fuel/oxidiser mixture (usually the engines main propellants) in a pre-combustion chamber, the hot expanding gas then enters the main combustion chamber and ignites the main propellant mixture (Huzel and Huang, 1967). Figure 2-38 depicts an ASI firing, notice high temperature blue flame produced.

Figure 2-38: LOX/RP-1 Spark-Torch Igniter (Ermini and Kaiser, 2002)

ASIs have the advantage of repeatability both in terms of multiple starts and reusability, unlike other ignition systems an ASI doesn't need to be replaced after each mission, a useful feature for the future state-of-the-art reusable vehicles (Wiesehan and Villegas, 2018). ASIs are popular with LOX/LH_2 rocket engines (Ballard, 2019). Figure 2-39 shows a cross sectional drawing of an ASI.

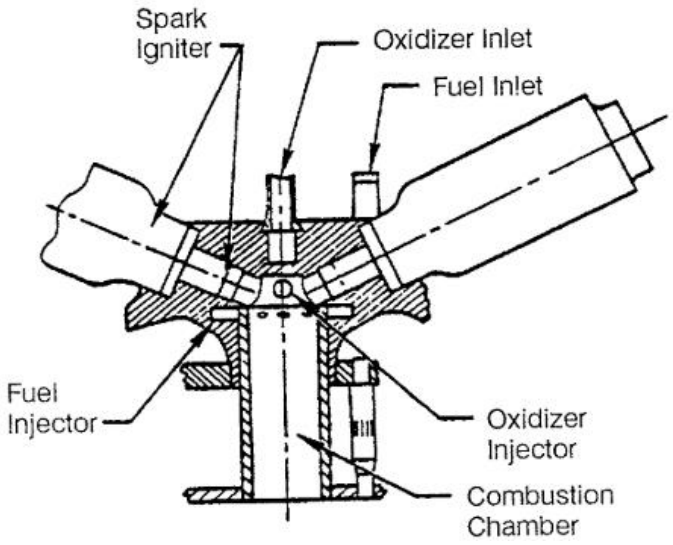

Figure 2-39: Augmented Spark Igniter Cross-Section (Huzel and Huang, 1992)

2.12.2 Avionics

Avionics (a.k.a. aviation electronics) systems form the information backbone of an aerospace vehicle. The systems sense, control, and communicate with virtually all of a vehicle's flight systems and the ground-based mission controllers (Atkins, 2010).

Vehicle guidance, which is the process of collecting and applying information in order to generate manoeuvre commands, relies on the avionics system to provide real-time information regarding the vehicles orientation, acceleration, velocity, and forces acting on the vehicle to reach a set target. Essentially, it represents the closure of a control feedback loop (Draper et al., 1965).

Chindambaram et al. (2003) divide launch vehicle electronics into two categories: Navigation, Guidance and Control (NGC); and Telemetry, Tracking and Command (TTC). The NGC system steers the vehicle to the mission target through a predetermined flight path; the TTC system monitors the state of the vehicle's sub-systems (e.g. fuel level and system temperatures and pressures) and its position, the system can also perform self-destruct commands.

2.12.2.1 Navigation, Guidance and Control System

The NGC system is the brain of the launch vehicle enabling the vehicle to reach the target apogee for satellite/spacecraft orbital insertion. NGC systems are realised in two ways, either as a simple preprogramed open loop guidance system or a complex but highly accurate closed loop guidance system.

Open loop guidance uses an attitude reference system (ARS) and auto pilot to control the vehicle's trajectory by implementing preprogramed pitch and yaw commands/profiles, the commands simplify the system as no onboard computations are required. The disadvantage of this guidance scheme is the inaccuracy given that variations in the vehicles operating conditions (e.g. variations in the propulsion system) are not accounted for.

Closed loop guidance requires sophisticated hardware and software. The ARS in open loop control is replaced by an inertial navigation system (INS) while computers perform the navigation, guidance and control functions through software. An INS in addition to measuring the attitude rates it also measures position, velocity and acceleration.

3 Component and System Sizing

From Chapter 2, it is clear that an upper stage consists of many systems and components that require enormous effort and resources to research and successfully develop. The aim of this chapter is to present the processes for followed for sizing the main systems and components of an upper stage. The considered components and systems include: propellant tanks, propellant pressurization system, reaction control system, and electro-pump system. The key output from each of the sized components is mass (m), which is required to the analysis in Chapter 4.

For the analysis (in Chapter 4) to hold value, a decision-making methodology was required to ensure the components and subsequent conceptual vehicles were practical. The methodology required various factors to be considered, including South Africa's technological capabilities and budget constraints. Figure 3-1 is a flow chart detailing the decision making methodology employed in this study.

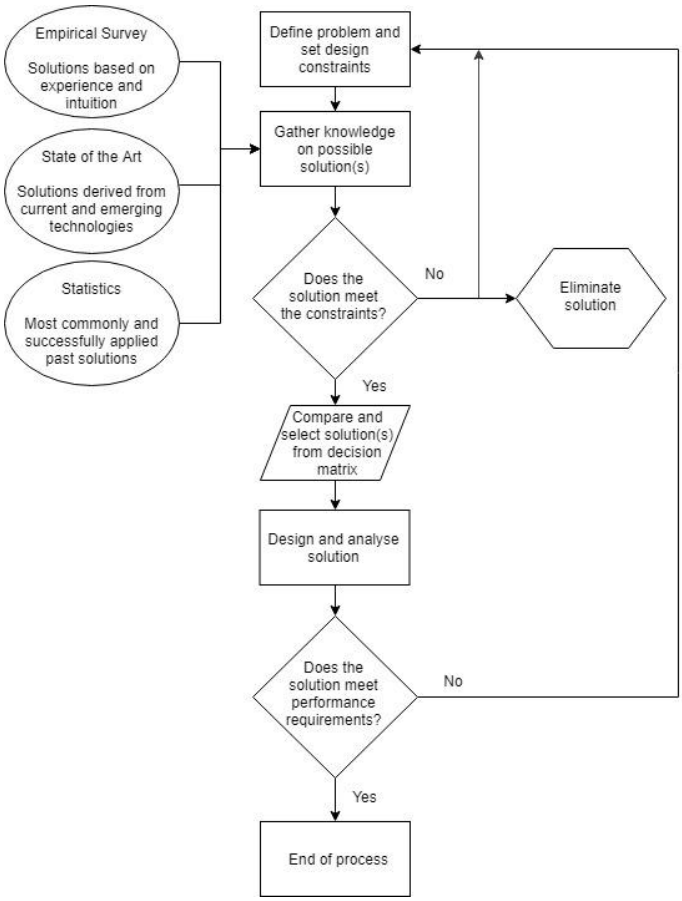

Figure 3-1: Design decision making process

The upper stage will be powered by a vacuum optimised variant of the SAFFIRE engine, which will be referred to as "SAFFIRE-V". The engine is still under development and, as a result, some design parameters (i.e. engine length and mass) were approximated from the work of Wunderlin (2019).

During the time of writing, the SAFFIRE-V had the theoretical performance specifications presented in Table 3-1. The engine cycle to be used was still undetermined and one of the aims of this project was to guide that decision. Furthermore, the chamber pressure may change in future, pending the results of detailed trajectory studies and engine testing. At present, a 12 bar chamber pressure has been specified for a pressure fed SAFFIRE-V (Wunderlin, 2019), whereas a 50 bar chamber pressure is specified for the electro-pump fed version, based on the pump designs of Singh (2018) and Chetty (2018).

Table 3-1: SAFFIRE-V specifications

Parameter	**Symbol**	**Value**	**Units**
Fuel	-	Kerosene	-
Oxidiser	LOX	Liquid Oxygen	-
Engine Cooling	-	Ablative	-
Specific Impulse	I_{sp}	353	s
Oxidiser-Fuel Ratio	$O/_F$	2.73	-
C-Star	C^*	1729.27	m/s
Total Propellant Mass Flow Rate	$\dot{m}$	7.94	kg/s
Engine Burn Time	t_b	240	s
Thrust	F_e	27.5	kN
Nozzle Expansion Ratio	ζ_n	68.6	-
Throat Area	A_t	0.011442	m^2
Length	L_e	1.8	m
Exit Diameter	d_e	1	m
Engine Mass	m_{engine}	85	kg
Combustion Chamber	p_c	12	bar
Feed System Pressure Drop	p_{fs}	1.9	bar
Injector Pressure Drop	p_i	4	bar
Propellant Storage Pressure (Pressure-Fed)	p_{tp}	20	bar
Propellant Storage Pressure (Electro-Pump)	p_{te}	5	bar
Pressurant Storage Pressure	p_c	200 - 300	bar

3.1 Storage Vessels

The design process, for the propellant tanks, began by calculating the required mass of each propellant based on the engine burn time and propellant mass flow rates. Additional propellant is required to compensate for tank ullage and propellant trapped in the plumbing lines. From the mass a minimum required volume can be determined based on each propellant's density, which depends on the storage temperature and pressure. The design process for the upper stage's storage vessels, including the pressurant storage vessels, is illustrated in Figure 3-2.

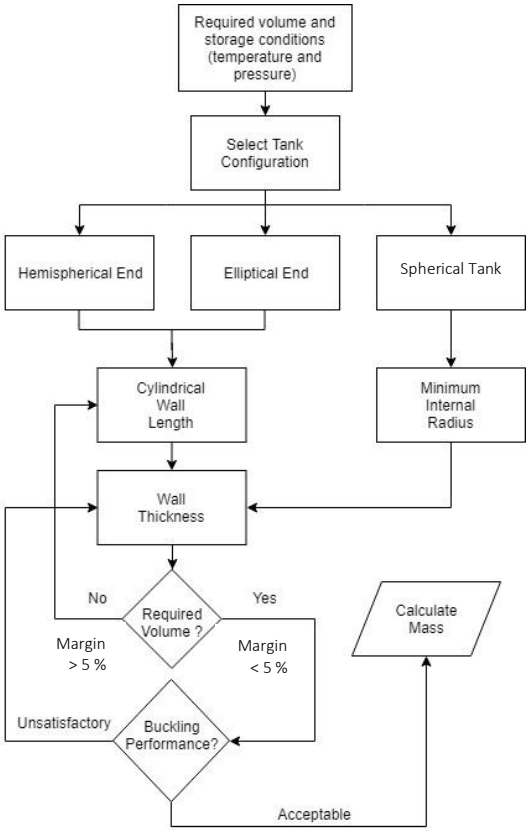

Figure 3-2: Propellant tank design process

For cylindrical propellant storage vessels, the cylindrical section length "*l*", for hemispherical or elliptical end cap, was determined via iteration. The outer diameter was set to a value of 1.2 m; a common diameter for small satellite launch vehicles such as Rocket Lab's Electron, Vector Space's Vector H, Orbex's Prime and Virgin Orbit's LauncherOne.

The wall thickness, based on internal pressure, is calculated using the equations in Table 3-2 which were obtained from Huzel and Huang (1992). They incorporate a (K) factor, which represents the reduced stress experienced by spherical surface areas compared to flat areas. (k) is the ellipse ratio taken as the major over minor axis. (t) is the minimum required thickness; (P) the design pressure; (r) inner

radius; (S) allowable stress; and (E) the weld joint efficiency. Allowable stress is determined by dividing the tank material's yield strength by a safety factor (1.4 - 1.5 for aerospace applications). The United States' aerospace industry has employed a 1.5 ultimate safety factor since 1930 (Modlin and Zipay, 2014), and there have been instances where it was reduced to 1.4 (e.g. Boeing X-20 Dyna-Soar program) and 1.1 for spaceflight applications, where low mass is paramount (Modlin and Zipay, 2014).

Table 3-2: Wall thickness formulae from Huzel et.al.

Tank Section	Equation
Cylindrical shell	$t = \frac{Pr}{SE}$ (3-1)
Ellipsoidal head	$t = \frac{Pr\left(\mathrm{K} + \frac{k}{2}\right)}{2SE}$ (3-2)
Hemispherical head	$t = \frac{Pr\mathrm{K} + \frac{1}{2}}{2SE}$ (3-3)
Spherical shell	$t = \frac{Pr}{2SE}$ (3-4)

For a spherical shell k = 1 and K = 0.5, making it the most stress resilient shape; for hemispherical ends k = 1 and K = 0.67. Elliptical end tanks usually have k = 1.375, 1.5 or 2 corresponding to K = 0.8, 0.85 and 1.20 respectively. Table 3-4 provides a range of k - K combinations useful for the wall thickness equations.

Table 3-3: Stress factor "K" for various elliptical ratios "k"

k	1	1.125	1.25	1.375	1.5	1.625	1.75	1.875	2
K	0.67	0.7	0.75	0.8	0.85	0.9	0.95	1.05	1.2

To determine the mass (m) of a storage vessel, it is split into various sections: end caps, cylindrical section, and tank skirts. The equations in Table 4 were used to calculate the mass of a vessel, depending on its configuration (e.g. cylindrical with hemispherical end caps). Spherical vessels were assumed to only consist of hemispherical end caps and skirts - without a cylindrical section. For the mass expressions below: (t) is the wall thickness, (r_o) the vessel's outer radius, (ρ) the material density, (h) the ellipsoidal height (i.e. minor axis radius), and (l) is the cylindrical section length. The variables are the wall thickness (t) and material density (ρ), both are material dependant.

Table 3-4: Storage vessel section mass expressions

Tank Section	**Formula**
Cylindrical Section	$m = \pi l \rho [r_o^2 - (r_o - t)^2]$ (4-3)
Ellipsoidal End Cap	$m = \frac{4}{3}\pi\rho[r_o^2 h - (r_o - t)^2(h - t)]$ (4-4)
Hemispherical End Cap	$m = \frac{4}{3}\pi[r_o^3 - (r_o - t)^3]$ (4-5)
Tank Skirt	$m = \pi l \rho [r_o^2 - (r_o - t)^2]$ (4-6)

The propellant tanks make up the majority of a launch vehicle's the mass budget, making material selection a crucial decision. The material must have high specific strength (i.e. high strength and low density), be commercially available, and resistant to corrosion from the stored propellant. Table 3-5 lists the density and strength of the materials that were considered for propellant storage.

Table 3-5: Comparison of possible tank materials

Material	Density (kg/m^3)	Tensile Strength (MPa)
Carbon Fibre Reinforced Plastic T700/Epoxy	1600	1600
Aluminium-Lithium 2195	2685	608
Aluminium 6061	2700	310
Aluminium 7075-T6	2810	572
Titanium Ti6Al4V	4420	1000
Duplex Steel*	7810	770
Stainless Steel 301 FH	7880	1276

3.1.1 Composite Overwrapped Pressure Vessels

A highly structurally efficient class of pressure vessel exists where composite reinforcement is wrapped over a metal or polymer shell called a "liner". This is done to simplify the formation of the vessel's structure and to mitigate any potential compatibility issues between the composite and certain fluids (e.g. LOX and liquid hydrogen) (Thesken *et.al.*, 2007).

3.1.1.1 Liner

To meet load equilibrium, the applied internal pressure (p) must equal the sum of the individual pressures the liner (p_l) and composite overwrap (p_c) carry (Thesken et.al., 2007).

$$p = p_l + p_c \quad (3\text{-}13)$$

$$\therefore\ p_c = p - p_l \quad (3\text{-}14)$$

The liner thickness (t_l) is constrained by welding requirements and is typically set to 1.5mm for aluminium. Thin shell theory was used to calculate the liner load and estimate the thickness of the overwrap. The pressure carried by the liner based on a given thickness (t_l), outer radius (r_l), and material tensile strength (σ_l) was calculated using the formulae in Table 3-6.

Table 3-6: Liner load equations

Tank Section	**Formula**
Spherical Tank/Section	$p_l = \frac{2\sigma_l t_l}{r_l}$ (3-15)
Cylindrical Section	$p_l = \frac{\sigma_l t_l}{r_l}$ (3-16)

3.1.1.2 Composite Overwrap

Continuing with the thin shell analysis described by Thesken *et.al.* (2007), the minimum required thickness of the overwrap is estimated using the equation in Table 3-7. (t_c) is the composite overwrap thickness, (p_c) the pressure the composite must withstand, (r_c) the inner radius of the composite and (σ_c) the composite's tensile strength.

Table 3-7: Composite overwrap thickness equations

Tank Section	**Formula**
Spherical Tank/End Cap	$t_c = \frac{p_c r_c}{2\sigma_c}$ (3-17)
Cylindrical Section	$t_c = \frac{p_c r_c}{\sigma_c}$ (3-18)

Following the thin wall theory based estimation, netting analysis is used to determine the ply thickness of the composite over wrap with more accuracy. In netting analysis, as described by Radhika (2016), the composite is treated as a net of fibres and the influence of the resin on structural performance is ignored. This means the tensile loads are assumed to be distributed along the length of the fibres. The assumption is only valid when internal pressure is the dominant stress, as is the case for a storage vessel.

The first step is to determine the winding angle (α), if geodesic winding is used for the end cap then the wind angle is determined using equation 3-11. Where (r) and (r_o) are the storage vessel's inner and outer radii respectively.

$$\alpha = \sin^{-1}\left(\frac{r_o}{r}\right) \quad (3\text{-}11)$$

The total ply thickness "t_{total}" of the fibres is determined from the minimum required helical "$t_{helical}$" and hoop "t_{hoop}" thicknesses using equations 3-12 to 3-14. Where "σ_c" is the longitudinal tensile strength of the fibre used, "r_c" the inner radius of the composite layer.

$$t_{helical} = \frac{p_c r_c}{2\sigma_c \cos 2\alpha} \tag{3-12}$$

$$t_{hoop} = \frac{p_c r_c (2 - \tan 2\alpha)}{2\sigma_c} \tag{3-13}$$

$$t_{total} = t_{hoop} + t_{helical} \tag{3-14}$$

3.2 Propellant Pressurization System

Before the pressure vessels containing the propellant pressurant gas can be designed, the gas requirements must be determined. If the system is in operation for a short time and the pressurant, propellant, and hardware are at the same temperature, external heating can then be neglected and equation 3-17, from Huzel and Huang (1992), is used to determine the required pressurant mass.

"W_g" is the required pressurant weight; "P_T" and "V_T" are the maximum propellant tank pressure and expelled volume; "R_g" and "T_g" are the pressurant's gas constant and mean temperature; "Z" is the compressibility factor of the pressurant.

$$W_g = \frac{P_T V_T Z}{R_g T_g} \tag{3-17}$$

When the pressurant's temperature is high compared to the propellant, heat transfer occurs at the pressurant-propellant interface and the vaporization effect on the propellant must be considered. With the heat transfer and vaporization considered equation 3-26 is obtained.

$$W_g = \frac{P_T V_g Z}{R_g T_u} \tag{3-26}$$

$$where\ V_g = V_T - V_V \tag{3-27}$$

$$and\ \ V_v = \frac{W_v R_p T_u Z}{P_t} \tag{3-28}$$

"V_g" is the volume of pressurant after expulsion; "V_V" volume of vaporized propellant; "T_u" is the gas temperature after expulsion.

Sutton and Biblarz (2001) use an alternate approach to estimate the pressurant requirements. First, the required propellant mass flow rate "$\dot{m}$" is determined from equation 3-29, where "ζ_d" is the discharge correction factor; "F" the thrust; and "c" the exhaust exit velocity.

$$\dot{m} = \frac{\zeta_d F}{c} \tag{3-29}$$

The mass flow rate is then multiplied by the rocket engine's operating time to determine the total mass of expelled propellant. Next, the propellant volume (V_p) is determined by simply dividing the mass (m_p) by its density (ρ_p). The required mass of pressurant gas can then be determined using equation 3-30.

$$m_0 = \frac{p_p V_p}{R T_0}\left[\frac{k}{1-\frac{p_g}{p_0}}\right] \tag{3-30}$$

Here, p_p and V_p are the pressure and volume of the propellant; T_0 and p_0 are the initial temperature and pressure in the pressurant vessel; p_g is the instantaneous vessel pressure; R and k are the pressurant's gas constant and specific heat ration. The vessel volume can be calculated from the ideal gas relation, with an allowance given for the excess gas (> 5 %) required to account for the volume of gas occupying the rest of the pressurisation system.

The conditions within the pressurant vessel can be obtained by assuming the gas expansion process is isentropic (provided there's no internal tank heating).

$$\frac{T_p}{T_0} = \left(\frac{p_p}{p_0}\right)^{\frac{n-1}{n}} \tag{3-31}$$

The process for both methods is depicted in Figure 3-3. Both methods produced similar results but Huzel and Huang was ultimately used as it accounts for external heating effects, in case this becomes an issue downstream.

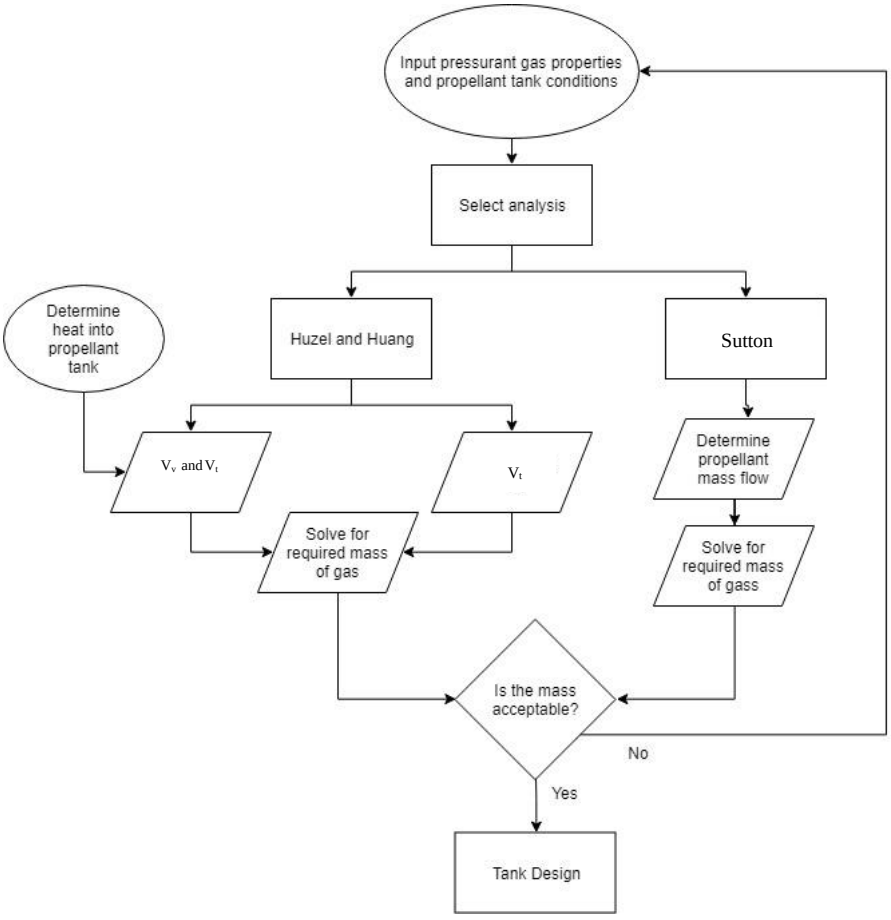

Figure 3-3: Pressurization system design process

3.3 Reaction Control System

CLV will use a cold gas-based RCS system for roll control. Cold gas thrusters (CGTs) are essentially De Laval nozzles designed for vacuum expansion, where the exit pressure (p_e) is zero. Roll control's primary function on CLV is to prevent spin during flight. Equations 3-32 to 3-34, from Humble (2007), apply specifically to the case of zero exit pressure.

$$F = \dot{m}c^*\gamma\left[\left(\frac{2}{\gamma-1}\right)\left(\frac{2}{\gamma+1}\right)^{\frac{\gamma+1}{\gamma-1}}\right]^{\frac{1}{2}} \tag{3-32}$$

$$\dot{m} = \frac{F}{c^*\gamma}\left[\left(\frac{2}{\gamma-1}\right)\left(\frac{2}{\gamma+1}\right)^{\frac{\gamma+1}{\gamma-1}}\right]^{-\frac{1}{2}} \tag{3-33}$$

$$I_{sp} = \frac{F}{g_0\dot{m}} = \frac{c^*}{g_0}\gamma\left[\left(\frac{2}{\gamma-1}\right)\left(\frac{2}{\gamma+1}\right)^{\frac{\gamma+1}{\gamma-1}}\right]^{\frac{1}{2}} \tag{3-34}$$

The required thrust is determined by setting the desired angular acceleration the thrusters must achieve based on their mounting position (i.e. lever arm) and the moment of inertia of the vehicle. Equations 3-35 and 3-36 were used to calculate torque "τ" and subsequent thrust "F" where "I_{xx}" is the longitudinal moment of inertia, "a" the angular acceleration and "r" the distance of the applied force from the centre (Marghitu et al., 2001).

$$\tau = I_{xx}a \tag{3-35}$$

$$F = \frac{\tau}{r} \tag{3-36}$$

The required propellant mass (m_p) and tank volume (V_p) are calculated from equations 3-37 and 3-38, where Δt is the total burn time and p_c is the thruster chamber pressure.

$$m_p = \dot{m}\Delta t \tag{3-37}$$

$$V_p = \frac{m_p RT}{p_c} \tag{3-38}$$

The design process revolves around the nozzle expansion ratio (ε), where the exit area is set based on available space.

$$\varepsilon = \frac{1}{M_e}\left[\left(\frac{2}{\gamma+1}\right)\left(1+\frac{\gamma-1}{2}{M_e}^2\right)\right]^{\frac{\gamma+1}{2\gamma-2}} \tag{3-39}$$

$$\frac{p_e}{p_c} = \left[1+\frac{\gamma-1}{2}{M_e}^2\right]^{\frac{\gamma}{1-\gamma}} \tag{3-40}$$

Equation 3-39 was used to solve for the exit Mach number "M_e" and thus the pressure ratio $\left(\frac{p_e}{p_c}\right)$ over a range of expansion ratios from 5 to 150. The specific impulse "I_{sp}" was calculated using equation 3-41 over the range of pressure ratios. The expansion ratio of 60 was selected based on I_{sp} and final nozzle geometry (i.e. throat and exit diameters).

$$I_{sp} = \frac{c^*}{g_0}\gamma\left[\left(\frac{2}{\gamma-1}\right)\left(\frac{2}{\gamma+1}\right)^{\frac{\gamma+1}{\gamma-1}}\left\{1-\left(\frac{p_e}{p_c}\right)^{\frac{\gamma-1}{\gamma}}\right\}\right]^{\frac{1}{2}} \tag{3-41}$$

To determine the nozzle's dimensions, equations 3-42 to 3-44 were used to compare the effect of chamber pressure on throat diameter "D_t" and exit diameter "D_e".

$$A_t = \frac{\dot{m}c^*}{p_r} \tag{3-42}$$

$$A_e = \varepsilon A_t \tag{3-43}$$

$$D = 2\sqrt{\frac{A}{\pi}} \tag{3-44}$$

Figures 3-4 and 3-5 depict the relationships described above for a 94 N nitrogen cold gas thruster.

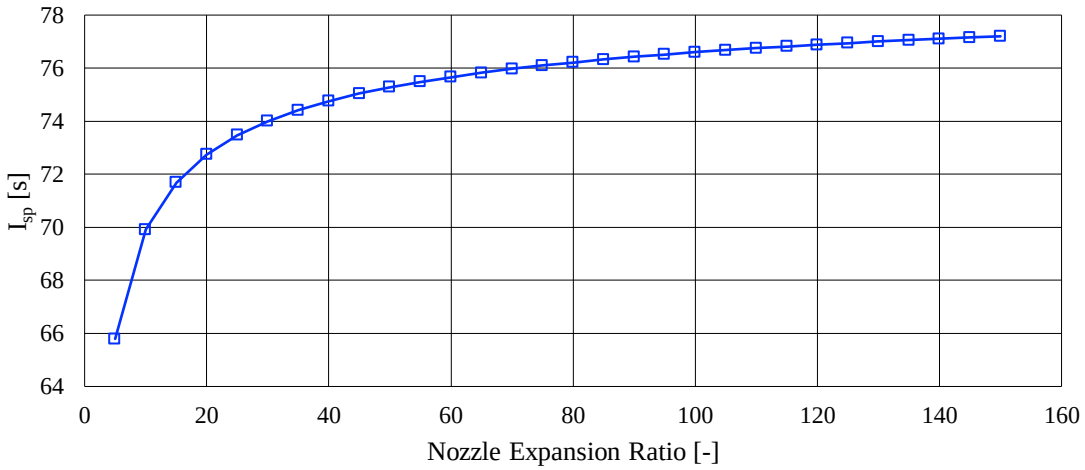

Figure 3-4: Specific Impulse vs Nozzle Expansion Ratio

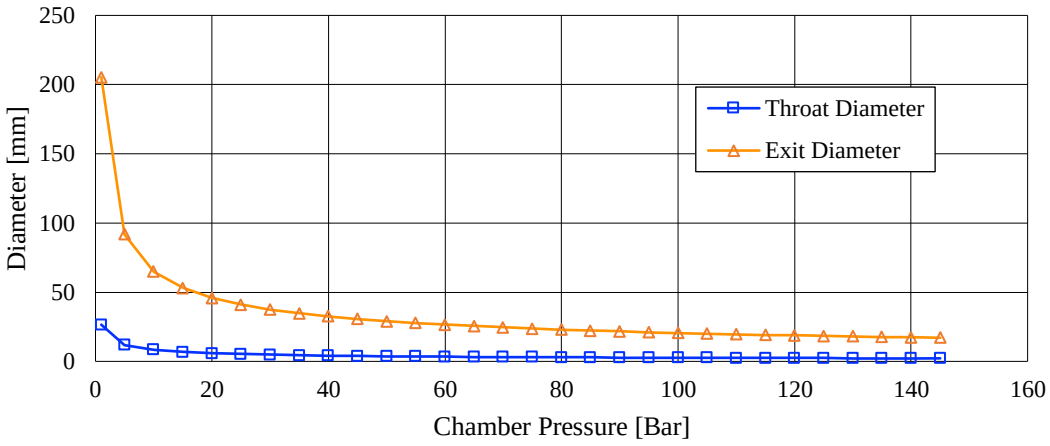

Figure 3-5:Thoat and Exit Diameter vs Chamber Pressure

Based on the parameters chosen, the real performance of the system can be determined. First, the mass of residual propellant "m_r", when the vessel internal pressure "p_i" is less than chamber pressure "p_c", is calculated by solving equations 3-45 and 3-46 simultaneously for vessel volume "V" and residual propellant mass. Total required propellant mass is given by equation 3-47.

$$p_c V = m_r R T \tag{3-45}$$

$$p_i V = (m_r + m_p) R T \tag{3-46}$$

$$m_t = m_r + m_p \tag{3-47}$$

Secondly, the real thrust and specific impulse are calculated from equations 3-41 and 3-48, where "λ" is the nozzle efficiency.

$$F = \lambda \left\{ A_t p_c \gamma \left[\left(\frac{2}{\gamma - 1} \right) \left(\frac{2}{\gamma + 1} \right)^{\frac{\gamma+1}{\gamma-1}} \left\{ 1 - \left(\frac{p_e}{p_c} \right)^{\frac{\gamma-1}{\gamma}} \right\} \right]^{\frac{1}{2}} \right\} \tag{3-48}$$

Reaction control thrusters generally have either conical or bell shaped nozzles (Sutton & Biblarz, 2001). For simplicity, a conical shape was assumed, the geometric parameters of which are depicted in Figure 3-6.

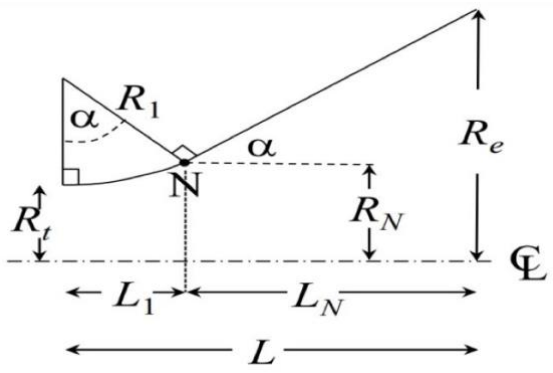

Figure 3-6: Conical nozzle geometric parameters (Seitzman, 2012)

"R_e" is the nozzle exit radius, "R_t" is the throat radius, "α" is known as the conical half-angle, and "N" denotes the beginning of the conical diverging section. The design process followed for the reaction control system, in this thesis, is illustrated in Figure 3-7.

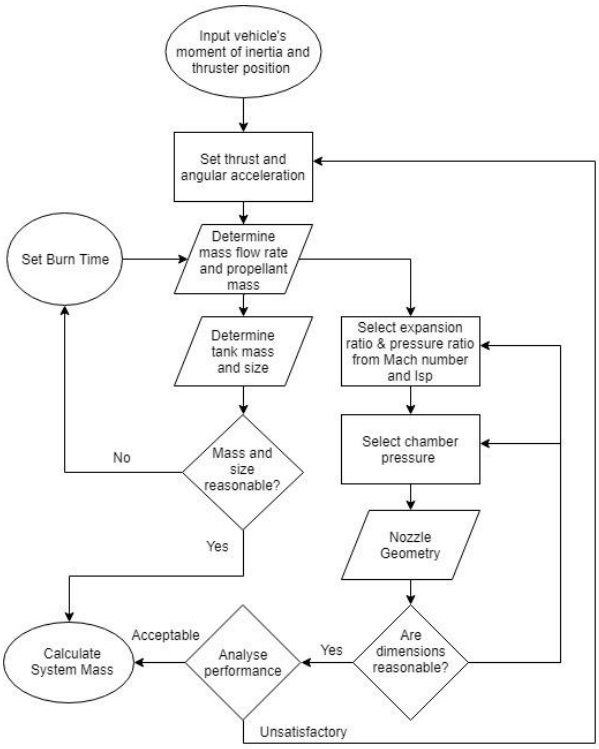

Figure 3-7: Reaction control system design process

A 94 N nitrogen cold gas thruster was designed to meet the performance specifications listed in Table 3-8. Figure 3-8 is a drawing showing the nozzle geometry of the designed nozzle. It was assumed that the thrusters must have the capacity to fire throughout the launch, more research is required to determine the exact burn time.

Table 3-8: 94 N nitrogen cold gas thruster concept performance specifications

Specification	**Symbol**	**Value**	**Unit**
Nozzle Expansion Ratio	ε	60	-
Propellant Mass Flow Rate	$\dot{m}$	0.127	kg/s
Burn Time	Δt	200	s
Chamber Pressure	p_c	25	bar
Specific Impulse	I_{sp}	75.95	s
Thrust	F	94.37	N
Lever Arm	r	0.6	m
Exit Mach Number	M_e	6.71	-
Moment of Inertia	I_{xx}	8067.28	kg m^2

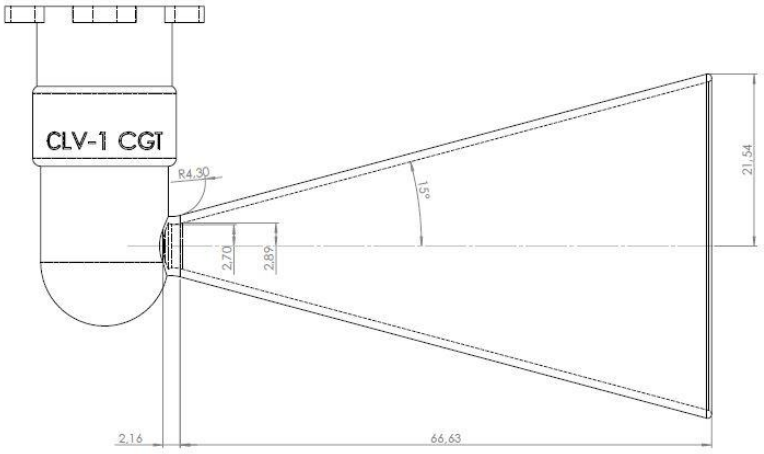

Figure 3-8: CLV CGT geometry

The 94 N thrust was selected, in part, based on Moog's triad thruster which produces 109 N of thrust and is used on the Vega launch vehicle's upper stage (Crone, 2021). The magnitude of thrust directly affects the angular acceleration achievable (for a given inertia), more thrust means more acceleration which means faster roll response. The thrust also has a large influence on the total system mass, higher thrust requires a higher propellant mass flow rate which in turn means more propellant is required.

3.4 Electric-Pump Feed System

To attain a mass estimate for the system, the individual components were sized based on the performance specifications of the propellant pumps. The dry mass of an electric-pump feed system ($m_{EPS_{dry}}$) consists of the following individual component masses: pressurant storage vessel (m_{gt}), fuel tank (m_{ft}), oxidiser tank (m_{ot}), oxidiser and fuel pumps (m_{pu}), electric motors (m_{em}), inverter (m_{inv}), and the batteries (m_b). The components of an electro-pump feed system (excluding the storage vessels) are depicted in Figure 3-9. Of these components, the motor and battery pack have the highest mass contribution. Equation 3-43 was used to calculated the system's dry mass.

$$m_{EPS_{dry}} = m_{gt} + m_{ot} + m_{ft} + m_{pu} + m_{em} + m_{inv} + m_b \tag{3-43}$$

A permanent-magnet synchronous motor (PMSM) or brushless DC motor (BLDC) would most likely be used, as they have high power densities and efficiencies compared to other motors. They can also match the speeds and power output achieved by traditional turbo-pumps (Dlugiewicz *et al.*, 2012).

The battery pack consists of a battery management system (circuits and software), wires, casings, and a thermal management system which is key for efficient battery operation. The battery pack comprised Li-Ion cells which offer high discharge voltages, high energy and power densities (Stenzel et al., 2014). Data for the Panasonic NCR 18650PF cell is used for the Li-Ion analysis. Lithium Polymer cells are also considered and the results of each cell type are compared in Chapter 4.5.

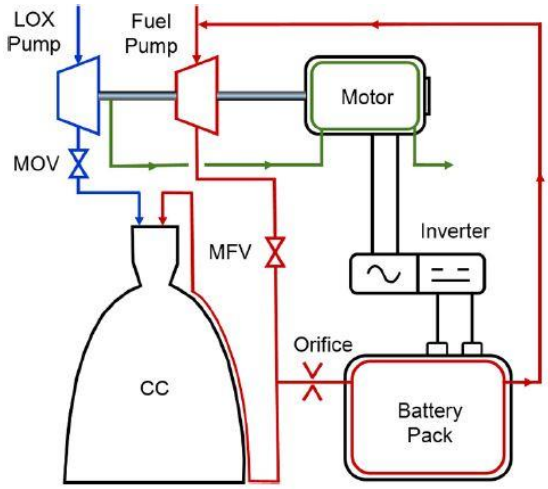

Figure 3-9: Electric pump cycle schematic (Kwak et al., 2018)

3.4.1 Motor Mass

The electric motor's mass (m_{em}) depends on the motor power requirements ($P_{em,out}$) which depend on the power requirements of the pumps which, in turn, depend on the head rise (Δp) and mass flow rate ($\dot{m}$) each pump produces. Motor power and mass are given by equations 3-44 and 3-45 respectively.

$$P_{em,out} = P_{pu} = P_{op} + P_{fp} = \frac{\Delta p_{op}\dot{m}_{op}}{\rho_o \eta_{op}} + \frac{\Delta p_{fp}\dot{m}_{fp}}{\rho_f \eta_{fp}} \tag{3-44}$$

$$m_{em} = \frac{P_{em,out}}{\delta_{em}} = \frac{\left(P_{op} + P_{fp}\right)}{\delta_{em}} \tag{3-45}$$

3.4.2 Pump and Inverter Mass

The term "δ" represents output power density, which is a type of efficiency that compares a machine's mechanical power output to its weight. The masses of the pumps (m_{pu}) and inverter (m_{inv}) can be computed by using each component's power density and power requirements.

$$m_{pu} = \frac{P_{pu}}{\delta_{pu}} = \frac{P_{op}}{\delta_{op}} + \frac{P_{fp}}{\delta_{fp}} \tag{3-46}$$

$$m_{inv} = \frac{P_{inv,out}}{\delta_{inv}} = \frac{P_{em,out}}{\eta_{em}\delta_{inv}} = \frac{\left(P_{op} + P_{fp}\right)}{\eta_{em}\delta_{inv}} \tag{3-47}$$

3.4.3 Battery Pack Mass

The battery pack has two limiting factors: the power density ($\delta_{b,P}$) and the energy density ($\delta_{b,E}$). The mass estimate depends on which factor is higher. Generally long burns require high energy density while short burns favour high power density.

For a power constrained battery pack, the mass "$m_{bp,P}$" is based on the power the pack must produce. For this case equations 3-48 and 3-49 are used. "k_{bp}" is a structural margin to account for sub component masses (e.g. battery management system, wires, and battery pack case).

$$P_{bp} = P_{inv,in} = \frac{(P_{op} + P_{fp})}{\eta_{inv}\eta_{em}} \tag{3-48}$$

$$m_{bp,P} = k_{bp}\frac{(P_{op} + P_{fp})}{\delta_{b,P}\eta_{inv}\eta_{em}} \tag{3-49}$$

For an energy constrained pack, the required energy "E_{bp}" determines the pack mass "$m_{bp,E}$". "η_E" is the battery energy efficiency.

$$E_{bp} = \frac{P_{bp}t_b}{\eta_E} = \frac{(P_{op} + P_{fp})t_b}{\eta_E\eta_{inv}\eta_{em}} \tag{3-50}$$

$$m_{bp,E} = k_{bp}\frac{(P_{op} + P_{fp})t_b}{\delta_{b,E}\eta_E\eta_{inv}\eta_{em}} \tag{3-51}$$

3.4.4 Analysis Parameters

The control variables for the mass analysis, and the outputs they affected, are depicted in Figure 3-10.

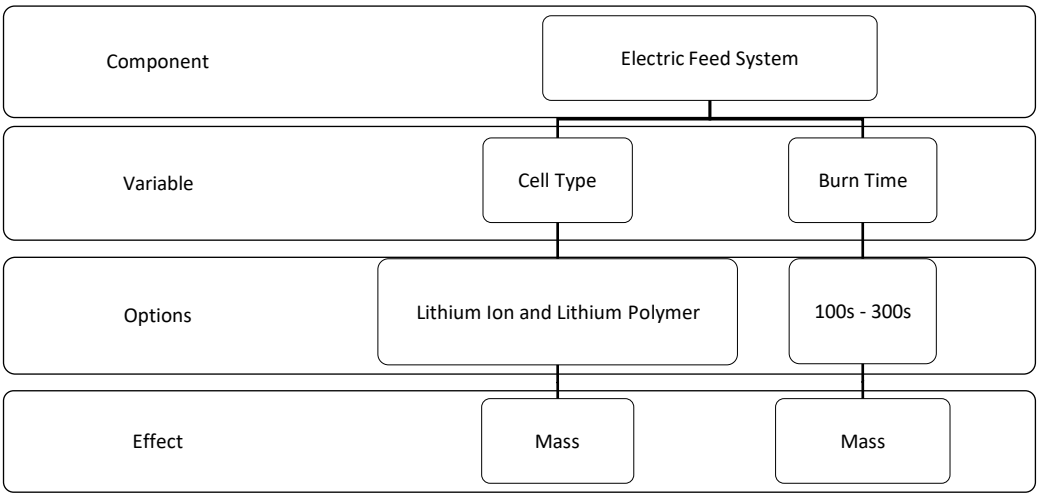

Figure 3-10: Electric pump feed system variables and effects

Key to the electric feed system's analysis are the assumptions made for the various component performance specifications, Table 3-9 lists the assumptions made.

Table 3-9: Parameter values for mass analysis

Parameter	Value	Comment
P_{op}	51.96 kW	SAFFIRE LOX pump specs (Singh ,2018)
P_{fp}	31.6 kW	SAFFIRE kerosene pump specs (Chetty, 2018)
δ_{op}	22 kW/kg	Extrapolated from Titan rocket data (Rachov, 2014)
δ_{fp}	15 kW/kg	Author's reference data (Kwak, 2018)
δ_{em}	5.3 kW/kg	Reported PMSM specific power (Duffy, 2015)
δ_{inv}	60 kW/kg	Author's reference data (Kwak, 2018)
$\delta_{b,P}$ (Li-ion)	2.5 kW/kg	Li-Ion specific power based on energy density (Stenzel et al., 2014)
$\delta_{b,E}$ (Li-ion)	213 Wh/kg	Panasonic NCR 18650PF datasheet
$\delta_{b,P}$ (Li-Po)	3.7 kW/kg	Experimental data (Chu et.al.,1996)
$\delta_{b,E}$ (Li-Po)	700 Wh/kg	Experimental data (Chu et.al.,1996)
η_{op}	60.8 %	SAFFIRE LOX pump specs (Singh ,2018)
η_{fp}	62.12 %	SAFFIRE kerosene pump specs (Chetty, 2018)
η_{em}	85 %	Values range between 0.8 - 0.95 (Kwak, 2018)
η_{inv}	85 %	Authors' data (Kwak, 2018) and (Rachov, 2014)
η_E	80 %	Average for Li-Ion (Eftekhari, 2017)
k_{bp}	1.2	Authors' data (Kwak, 2018) and (Rachov, 2014)

3.5 CLV Upper Stage Configuration

A base design for the upper stage was required in order to compare the different variations of the upper stage's components. The design was modelled in SolidWorks™ CAD, which aided in determining a mass estimate for the structural components not accounted for including: the thrust frame, engine gimbal, plumbing, tank attachments, payload fairing, and the payload attach. The CAD also allowed for the upper stage's moment of inertia to be estimated.

Some of the upper stage's characteristics are kept constant for the mass analysis such as the payload fairing, which is parabolic and constructed with CFRP/Epoxy composite material. The propellant pressurization storage vessels are located in the engine bay and the pressurant is also used for pneumatics. The main pressurant line runs on the periphery of the upper stage. The RCS nitrogen storage vessels are spherical, constructed of CFRP overwrapped aluminium, and designed for 300 bar storage pressure. The RCS bay is located between the LOX tank and payload fairing. Figure 3-11 is a render of the upper stage in the pressure fed configuration.

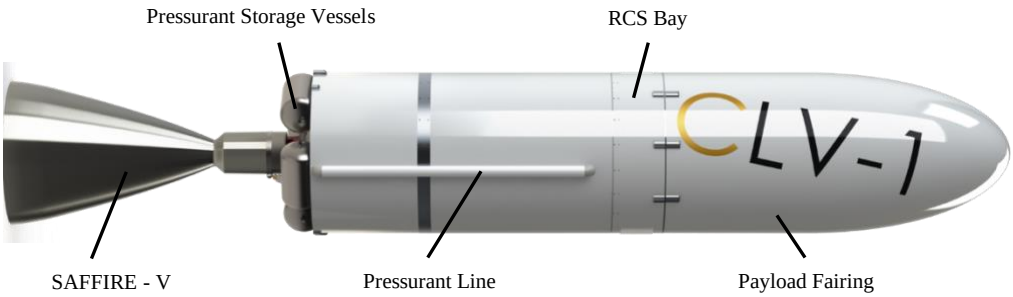

Figure 3-11: CLV upper stage render (pressure-fed configuration)

The propellant tank configuration, however, was a variable. A cross-section of the upper stage, in the separate tandem propellant tank configuration and a pressure fed system, is depicted in Figure 3-12. In this case, the tanks have elliptical ends, while the Main LOX line runs through the kerosene tank. It is preferable that the LOX run through the kerosene, if the reversed, the LOX may boil-off due to the heat addition from the warm kerosene line.

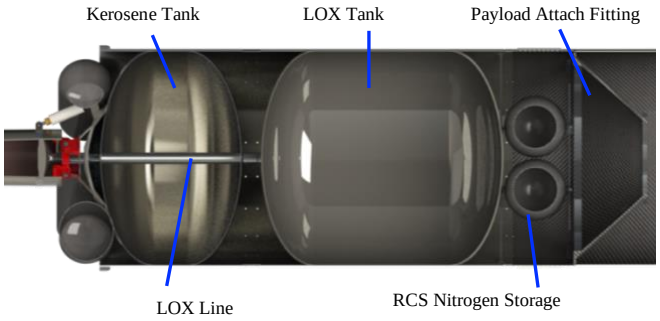

Figure 3-12: CLV upper stage cross-section render (pressure-fed configuration)

Figure 3-13 depicts the engine bay configuration for the electric-pump feed system. There are fewer pressurant storage vessels as the tanks are at a lower pressure when pumps are used. The battery packs are also located in the engine bay.

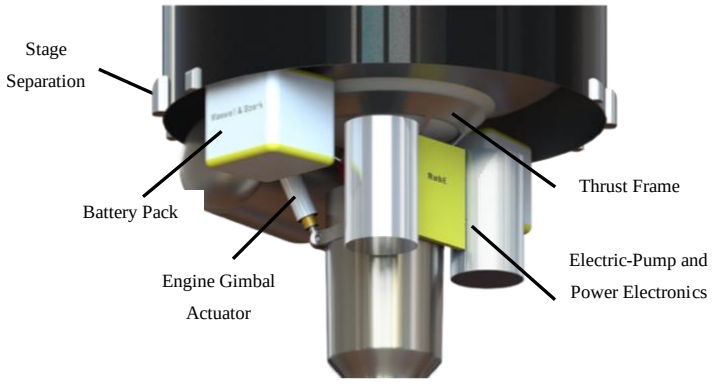

Figure 3-13: CLV upper stage engine bay render (electric-pump configuration)

4 Mass Analysis

This chapter presents the mass analysis for the CLV upper stage and its major components. The component masses are compared based on varying design parameters; generally the construction material and geometry. The results are analytically determined (using the methods described in Chapter 3) with the aid of Microsoft Excel and will provide a base for future, more refined, studies.

For a launch vehicle, two mass properties are of interest: the propellant mass fraction and the mass ratio. Propellant mass fraction (ζ) is a measure of how much of the vehicle's lift-off mass (m_0) comprises propellant mass (m_p); the higher this value, the more efficient the design of the vehicle. Mass ratio (M_R) is a similar measure, comparing the vehicle's dry mass (m_1) to its mass with propellant (m_0).

$$\zeta = \frac{m_p}{m_0} \tag{4-1}$$

$$M_R = \frac{m_1}{m_0} \tag{4-2}$$

A challenge when performing a mass analysis on a launch vehicle is deriving accurate mass estimates for the vehicle's subsystems e.g. avionics, separation systems, fasteners and payload adapters. Subsystem estimates obtained from literature are listed in Table 4-1. The averages of percentage masses in the table were calculated and used for part of the structural mass estimation.

Table 4-1: Spacecraft subsystem masses as percentage dry mass

Subsystem	**Percentage Dry Mass**			
	(Brown, 2002)	(Motiwala, 2014)	(de Weck, 2006)	(Gerberich, 2013)
Structure	29	20	21	24.2
Power	35	7	32	18.2
Cabling	4	-	-	-
Avionics	6	3	5	30.4

Chetty (2018) performed a preliminary CLVstudy for delivering a 75 kg payload to 500 km LEO. The study, based on the mission's required delta V, requires CLV's second stage to have a 0.85 mass fraction with 2055.9 kg propellant mass. A less conservative estimate yields a 1905.1 kg propellant mass requirement. This means the vehicle's dry mass limit is between 261 kg – 287 kg. The limit affects the analysis as it means the total mass of the sized components (i.e. propellant tanks, engine, battery pack, RCS, and pressurant storage vessels) must fall below this range in order to account for the subsystems that are not analytical sized. If the mass exceeds this, the 0.85 mass ratio will not be met.

4.1 Propellant Tanks

Mass is the key design constraint for the tanks. In this section, various tank materials are analysed and compared for blown-down and pump fed systems. The analysis assumes that each tank has 2 mm thick, 300 mm long fore and aft skirts. A tank skirt is a cylindrical structure that envelopes the tank end and allows the tank to interface with other structural components. Titanium is omitted from the analysis as it is financially infeasible to construct large propellant tanks from titanium, it is more commonly used for relatively smaller pressurant storage vessels. The statement is based on titanium's commodity price of $ 4800 per ton compared to aluminium and steel at $ 2446 per ton (Metalary, 2021) and $ 817 per ton (Trading Economics, 2021) respectively. Titanium is also incompatible with LOX (Jackson *et.al.*, 1961). For the pressure fed system, the tanks will be pressurised to 55 bar and 20 bar to account for the previous (Chetty, 2018) and (Singh, 2018) and current (Wunderlin, 2019) SAFFIRE chamber pressures. The pump fed system have 3 bar tank pressures. Figure 4-1 shows the design variables for a propellant tank and what output values they affect.

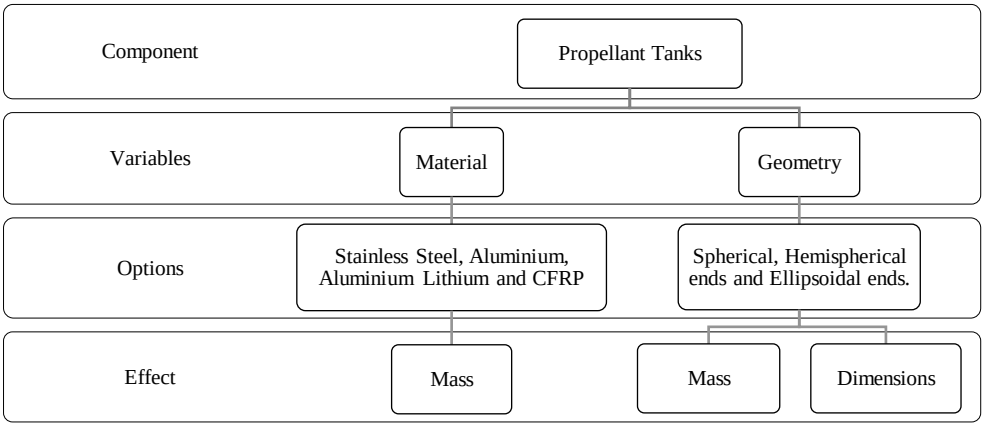

Figure 4-1: Propellant tank analysis parameters

A propellant tank consists of three structural main components: a cylindrical section, tank ends, and tank skirts. Once the thicknesses of each section has been determined (see Table 3-2 and Table 3-3), its mass can be calculated using the equations in Table 4-2.

Table 4-2: Propellant tank section mass formulae

Tank Section	**Formula**	
Cylindrical Section	$m = \pi l \rho [r_o^2 - (r_o - t)^2]$	(4-3)
Tank End (Ellipsoidal)	$m = \frac{4}{3}\pi\rho[r_o^2 h - (r_o - t)^2(h - t)]$	(4-4)
Tank End (Hemispherical)	$m = \frac{4}{3}\pi[r_o^3 - (r_o - t)^3]$	(4-5)
Skirt	$m = \pi l \rho [r_o^2 - (r_o - t)^2]$	(4-6)

4.1.1 Tank Geometry

Before the propellant tanks were compared based on material, the optimal geometric configuration was determined. To do this, aluminium lithium 2195 was assumed as a baseline propellant tank material and each configuration was compared based on overall mass and height. Considered geometries include: spherical (S), cylindrical with spherical end caps (CS), cylindrical with elliptical ends caps (CE), and combinations CS (LOX)/CE (kerosene) and CE (LOX)/CS (RP-1). The effect of a common bulkhead was also analysed.

The analysis found that the kerosene tank cannot have spherical tank ends if the outer diameter (OD) is 1.2 m (a design constraint). This is due to the spherical tank ends occupying more volume than the required fuel volume. Therefore, for the case of spherical end caps, the kerosene tank has a 1 m OD.

4.1.1.1 Tandem Tanks

This is the most common and least complex configuration, where the propellant tanks are separated by an intertank structure and plumbing can run externally or internally from the upper tank (LOX) to the engine. The mass and height of each tank geometry is listed in Table 4-3 and Table 4-4 respectively.

Table 4-3: Tank mass comparison for Al-Li 2195 for various geometries (tandem tanks)

Propellant Feed System	**Pressure (bar)**	**Mass (kg)**				
		S	**CS**	**CE**	**CS-CE**	**CE-CS**
Pressure	55	115	105	157	131	132
	20	58	54	73	63	64
Electric Pump	5	32	31	35	33	34

Table 4-4: Tank height comparison for various geometries (tandem tanks)

Height (m)				
S	**CS**	**CE**	**CS-CE**	**CE-CS**
2.43	2.79	2.36	2.50	2.66

4.1.1.2 Tandem with Common Bulkhead

For the common bulkhead tank configurations, two types of bulkhead geometry are considered: spherical (SB) and elliptical (EB). The endcap geometries will also be compared. The case of a spherical end cap (Se) and elliptical end cap (Ee) are compared.

Table 4-5: Tank mass comparison for Al-Li 2195 for various geometries (common bulkhead)

Propellant Feed System	**Pressure (bar)**	**Mass (kg)**			
		SB-Se	**SB-Ee**	**EB-Se**	**EB-Ee**
Pressure	50	92.4	115.1	113.3	121..3
	20	44.3	53.4	52.7	55.9
Electric Pump	5	20.2	22.5	22.3	23.0

Table 4-6: Tank height comparison for various geometries with a common bulkhead

Height (m)			
SB-Se	**SB-Ee**	**EB-Se**	**EB-Ee**
2.01	1.87	2.12	1.97

4.1.1.3 Summary

The results indicate that a cylindrical tank with spherical end caps offers the lowest mass while ellipsoidal ends occupy the least space. The addition of a common bulkhead reduces tank mass by 23% and height by 17%. A tank with a common bulkhead and spherical ends has the lowest mass of all tanks while using ellipsoidal ends with a spherical bulkhead produces the shortest tank. The masses of the various configurations are presented in Figure 4-2.

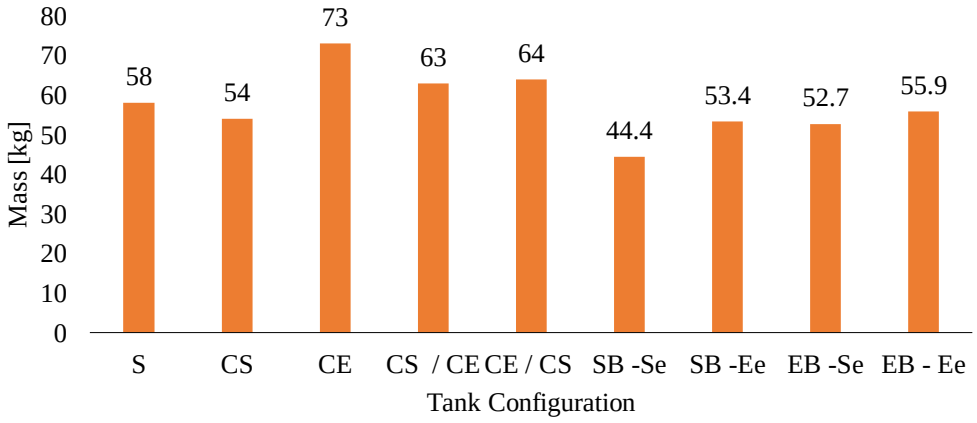

Figure 4-2: Tank configuration mass comparison for pressure fed Al-Li tanks

Historical industry trends show that cylindrical tanks with ellipsoidal ends are the most popular choice, probably due to the reduced height compared to hemispherical ends. However, recent vehicles seem to favour common bulkhead tanks with ellipsoidal ends for upper stage vehicles (e.g. Falcon 9 upper stage).

4.1.2 Tank Material

For the material comparisons the tanks were configured to be cylindrical with a spherical common bulkhead and spherical end caps. The materials are compared by mass and the results are presented in Table 4-8 to . The axial buckling stress of each tank is also provided. Lower the number the more likely it is to buckle under stress or collapse on its own weight. Aero-structural analyses are required to estimate the axial stress the propellant tanks will likely experience during flight.

4.1.2.1 Stainless Steel 301 FH

Last used on the Centaur upper stage "balloon tank", 301 stainless steel has since fallen out of favour as propellant tank material due to advances in the manufacture of tanks from composite materials and aluminium alloys.

Using stainless steel incurs a relatively large weight penalty compared to aluminium alloy and carbon fibre composite. However, its low cost, ease of machinability, availability and cryogenic strength make it a very attractive alternative to more exotic materials. Table 4-7 shows the estimated masses of tanks manufactured from 301 stainless steel, in fully work hardened (FH) form, for each vehicle configuration.

Table 4-7: Stainless Steel 301 FH tank masses

Propellant Feed System	**Storage Pressure (bar)**	**Tank Dry Mass (kg)**	**Min. Wall Thickness (mm)**	**Buckling Stress (MPa)**
Pressure Fed	55	159.36	3.10	169
	20	80.67	1.13	50
Electro-Pump	5	46.87	0.28	3 <

4.1.2.2 Duplex Stainless Steel

A recently developed grade of stainless steel, duplex stainless steel is characterised by a 50/50 austenite and ferrite ratio. The metal has improved corrosion resistance and some grades out perform their austenitic counterparts by twofold (Grocki, 2012). Duplex stainless steel is a cost saving alternative to most grades of stainless steel, however, stainless steel 301 FH still out performs this alloy based on mass. Table 4-8 shows the dry tank masses when Duplex steel is considers.

Table 4-8: Duplex stainless steel tank masses

Propellant Feed System	Storage Pressure (bar)	Tank Dry Mass (kg)	Min. Wall Thickness (mm)	Buckling Stress (MPa)
Pressure Fed	55	238.28	5.14	279
	20	109.28	1.87	122
Electro-Pump	5	53.79	0.47	11

4.1.2.3 Carbon Fibre Reinforced Plastic T700/Epoxy

Carbon fibre is a very attractive propellant tank material. It exhibits excellent mechanical properties, specifically an unsurpassed strength to weight ratio. However, the cost of tank fabrication is high given the complex manufacturing processes involved and the specialised resin systems required to achieve adequate LOX compatibility. The low dry masses achieved by CFRP are presented in Table 4-9.

Table 4-9: CFRP T700/Epoxy tank masses

Propellant Feed System	Storage Pressure (bar)	Tank Dry Mass (kg)	Min. Wall Thickness (mm)	Buckling Stress (MPa)
Pressure Fed	55	34.10	2.48	N/A
	20	18.16	0.90	N/A
Electro-Pump	5	11.32	0.23	N/A

4.1.2.4 Aluminium 7075-T6

Aluminium alloy 7075 in the T6 temper offers the inherent LOX compatibility and corrosion resistance of stainless steel while incurring less of a weight penalty. However, it is more expensive, more difficult to work and cannot easily be welded. Table 4-10 shows the resulting dry tank masses for each pressure

Table 4-10: Aluminium 7075-T6 tank masses

Propellant Feed System	Storage Pressure (bar)	Tank Dry Mass (kg)	Min. Wall Thickness (mm)	Buckling Stress (MPa)
Pressure Fed	55	110.87	6.92	< 74
	20	48.52	2.52	54
Electro-Pump	5	21.66	0.63	6

4.1.2.5 Aluminium 6061-T6

Similar properties to 7075 including excellent corrosion resistance and LOX compatibility. It is lower in strength compared to 7075-T6, however, it doesn't have the manufacturing challenges and cost associated with 7075-T6. Table 4-11 shows the tank dry masses when Al 6061-T6 is considered.

Table 4-11: Aluminium 6061-T6 tank masses

Propellant Feed System	Storage Pressure (bar)	Tank Dry Mass (kg)	Min. Wall Thickness (mm)	Buckling Stress (MPa)
Pressure Fed	55	185.52	12.77	70
	20	75.61	4.65	48
Electro-Pump	5	28.09	1.17	5

4.1.2.6 Aluminium Lithium 2195

Aluminium lithium alloys are touted as having the strength of steel with the weight of aluminium. The grade considered in this study is 2195; the dry masses of Al-Li tanks are presented in Table 4-12.

Table 4-12: Aluminium lithium 2195 tank masses

Propellant Feed System	Storage Pressure (bar)	Tank Dry Mass (kg)	Min. Wall Thickness (mm)	Buckling Stress (MPa)
Pressure Fed	55	100.34	6.51	148
	20	44.30	2.37	49
Electro-Pump	5	20.18	0.59	8

4.1.2.7 Dual Tank Material Options

From Table 4-9 it is clear that CFRP offers significant mass reductions compared to the other materials, however, finding and sourcing a LOX compatible resin system is a difficult task and likely to be costly. Table 4-13 and Table 4-14 present the results of a scenario where CFRP is used for the kerosene tank and aluminium alloy or stainless steel for the LOX tank. This compromise eliminates LOX compatibility issues while capitalizing on CFRP's mass savings. Unlike before, the tanks are in tandem without a common bulkhead to minimize manufacturing complexity. The common bulkhead reduces the overall tank dry mass.

Table 4-13: CFRP T700/Epoxy (CF) kerosene tank – aluminium 7075-T6 (Al) LOX tank masses

Propellant Feed System	**Storage Pressure (bar)**	**Propellant**	**Tank Dry Mass (kg)**	**Min. Wall Thickness (mm)**
Pressure Fed	55	LOX (Al)	45.05	6.92
		Kerosene (CF)	19.70	2.48
		Total Mass (kg)		**64.76**
	20	LOX (Al)	20.47	2.52
		Kerosene (CF)	10.05	0.90
		Total Mass (kg)		**30.52**
Electro-Pump	5	LOX (Al)	9.88	0.63
		Kerosene (CF)	5.90	0.23
		Total Mass (kg)		**15.78**

Table 4-14: CFRP T700/Epoxy (CF) kerosene tank - Aluminium 6061-T6 (Al) LOX tank masses

Propellant Feed System	**Storage Pressure (bar)**	**Propellant**	**Tank Dry Mass (kg)**	**Min. Wall Thickness (mm)**
Pressure Fed	55	LOX (Al)	74.42	12.78
		Kerosene (CF)	19.70	2.48
		Total Mass (kg)		**94.12**
	20	LOX (Al)	31.09	4.65
		Kerosene (CF)	10.05	0.90
		Total Mass (kg)		**41.14**
Electro-Pump	5	LOX (Al)	12.36	1.16
		Kerosene (CF)	5.90	0.23
		Total Mass (kg)		**17.96**

Table 4-15: CFRP T700/Epoxy (CF) kerosene tank – Stainless Steel 301 (SS) LOX tank masses

Propellant Feed System	Storage Pressure (bar)	Propellant	Tank Dry Mass (kg)	Min. Wall Thickness (mm)
Pressure Fed	55	LOX (SS)	66.59	3.10
		Kerosene (CF)	19.70	2.48
		Total Mass (kg)		**86.29**
	20	LOX (SS)	35.56	1.13
		Kerosene (CF)	10.05	0.90
		Total Mass (kg)		**45.61**
Electro-Pump	5	LOX (SS)	22.24	0.28
		Kerosene (CF)	5.90	0.23
		Total Mass (kg)		**28.14**

4.1.2.8 Summary

As expected, the results demonstrated that the low tank pressure associated with pump fed feed systems yield a significant mass reduction compared to the highly pressurized tanks of a pressure fed system with the mass of the 55 bar tanks nearing the dry mass limit of the entire vehicle. Figure 4-3 compares the tank masses of a 5 bar electric-pump fed system, a 20 bar pressure fed system and 55 bar system.

From Figure 4-3, the enormous mass saving potential CFRP tanks present is clear. The linerless CFRP tanks present a 59 % mass reduction compared to the nearest all metal competitor (i.e. Al Li 2195) and a 40 % reduction compared to the lightest material combination (i.e. CFRP-Al 7075).

The CFPR kerosene and Al 6061-T6 LOX tank combination is another attractive option, it is 7 % lighter than the Al Li 2195 tanks despite the mass penalty for not using common bulkheads. Al 6061 is cheaper and easier to source that Al Li and more forgiving, in terms of tank manufacture (i.e. rolling, spinning and welding), than 7075, which is notoriously difficult to weld. For similar reasons the case of a CFRP kerosene and SS 301 FH LOX tank is also compelling, although it is more difficult to source than 6061 (at least on a small scale less than 1 ton).

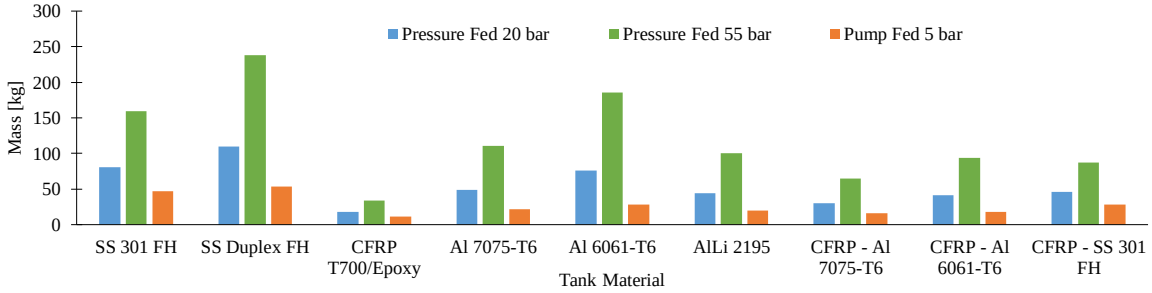

Figure 4-3: Feed system tank mass comparison for various materials and material combinations

4.2 Propellant Pressurization System

The mass of the pressurization system (helium and storage vessel) was analysed for the pressure fed and pump fed configurations. The analysis compared various tank materials, including CFRP (T700/Epoxy), titanium alloy (Ti6AlV), and aluminium (7075-T6). The effect that varying the tank geometries has on vessel mass and size was also analysed. The design variables for the helium storage tank and the parameters they affect are depicted in Figure 4-4 below.

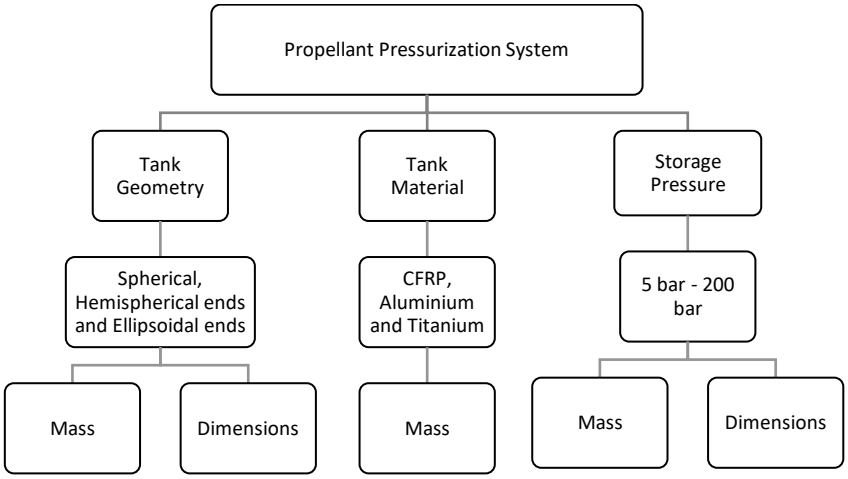

Figure 4-4: Propellant pressurization system variables and effects

For the first pressure fed case, the propellant tank pressure was specified as 20 bar, and required 6.8 kg of helium pressurant as per the calculations that were presented in Section 2.6. For the second pressure fed case, the propellant tank pressure was specified as 55 bar, requiring 18.8 kg of helium. For the electric pump fed configuration, the propellant tank pressure was specified as 5 bar, requiring 1.8 kg of helium.

The pressurant must be stored in a vessel at pressures exceeding 100 bar. As with the propellant tanks, the geometry of the tank is an important design variable. Especially considering that pressurant storage vessels generally occupy the empty space between components on an upper stage vehicle, typically around the engine. Mounting is another aspect to consider, some surfaces like a cylinder are easier to clamp compared to a sphere. Height and aspect ratio are other important metrics to consider. Figure 4-5 illustrates differences between each of the tank shapes considered.

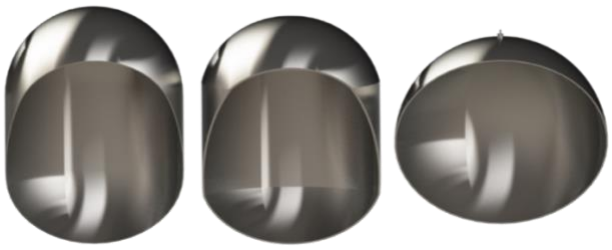

Figure 4-5: Pressurant storage tank geometry renders: hemispherical end (left), ellipsoidal end (middle), and spherical (right)

4.2.1 Spherical Vessel

Spherical vessels had the shortest total height in the axial direction (i.e. port-to-port) compared to cylindrical vessels for the same volume. Meaning the spherical vessel's diameter was less than the total length of the cylindrical vessel. However, when cylindrical vessels were "laid on their side" and the longitudinal axis considered (i.e. spherical vessel diameter vs cylindrical vessel diameter) the opposite is true. Table 4-16 lists the mass and geometries of a spherical vessel for each feed system.

Table 4-16: Spherical pressurant storage vessel mass analysis

Storage Pressure (bar)	**Feed System**	**Material**	**Tank Dry Mass (kg)**	**Thickness (mm)**	**Outer Diameter (mm)**
200	Pressure Fed (55 bar)	T700/Epoxy	30.28	5	1016
		7075-T6	121	13	1033
		Ti6AlV	107.7	8	1021
	Pressure Fed (20 bar)	T700/Epoxy	11	3.5	724
		7075-T6	44	9.5	737
		Ti6AlV	39.2	5.5	729
	Electric Pump (5 bar)	T700/Epoxy	2.8	2	457
		7075-T6	11	6	464
		Ti6AlV	9.8	3.5	459

4.2.2 Cylindrical Vessel with Elliptical Ends

Table 4-17 shows that the cylindrical vessel with elliptical ends was heavier than the spherical vessel for the various feed system pressure cases. The difference, however, is quite small with a 9 % difference for the 20 bar case.

Table 4-17: Cylindrical pressurant storage vessel with elliptical ends mass analysis

Storage Pressure (bar)	Feed System	Material	Tank Dry Mass (kg)	Thickness (mm)	Outer Diameter (mm)	Total Length (mm)
200	Pressure Fed (55 bar)	T700/Epoxy	31.4	4	808	1266
		7075-T6	125.8	15	821	1286
		Ti6AlV	111.7	9	812	1273
	Pressure Fed (20 bar)	T700/Epoxy	12.1	4	606	840
		7075-T6	48.4	12	616	855
		Ti6AlV	43	7	609	845
	Electric Pump (5 bar)	T700/Epoxy	3.2	3	404	488
		7075-T6	13	8	410	498
		Ti6AlV	11.5	4.5	406	492

4.2.3 Cylindrical Tank with Hemispherical Ends

This vessel was longer than the previous geometries, for the same feed system pressure case. Peculiar is that the mass is significantly lower than a spherical vessel, which is technically a stronger shape based on thin wall theory.

The phenomenon is in part due to the stress reduction expressions used in Huzel and Huang (1992) pressure vessel design calculations. This leads to hemispherical tank ends being stronger, and thus, thinner than a spherical tank at certain aspect ratios (k).

Another influence is due to the effect of reducing the internal radius of a cylindrical tank compared to a spherical vessel, whose radius is constrained. In other words, a cylindrical tank can have a larger aspect ratio (long with small diameter). Whereas a spherical tank will always have an aspect ratio of 1:1. The mass analysis for the hemispherical end vessel is presented in Table 4-18.

Table 4-18: Cylindrical pressurant storage vessel with spherical ends mass analysis

Storage Pressure (bar)	Feed System	Material	Tank Dry Mass (kg)	Thickness (mm)	Outer Diameter (mm)	Total Length (mm)
200	Pressure Fed (55 bar)	T700/Epoxy	20.2	4	808	1333
		7075-T6	80	7	821	1342
		Ti6AlV	71.5	4	812	1336
	Pressure Fed (20 bar)	T700/Epoxy	7.3	2	606	890
		7075-T6	29.1	8	616	896
		Ti6AlV	26	3	609	892
	Electric Pump (5 bar)	T700/Epoxy	1.8	1.5	404	522
		7075-T6	7.3	4	410	526
		Ti6AlV	6.5	4.5	523	523

4.2.4 Summary

The measures of interest from the above analysis are the tank masses, diameters length. The pressurant storage vessels of CLV upper stage should be compact in order to fit into the small unused spaces of the vehicle. Pressurant storage vessels are often located around the engine of small upper stages or inside the propellant tanks for large booster stages.

Figure 4-6 illustrates an interesting phenomenon. For a given material, vessel mass varies only slightly over a wide range of storage pressures. Between 20 and 160 bar there is a mass gain of only 0.7 % for a spherical vessel used for an electric-pump fed vehicle. This means the wall thickness doesn't vary much as pressure increases.

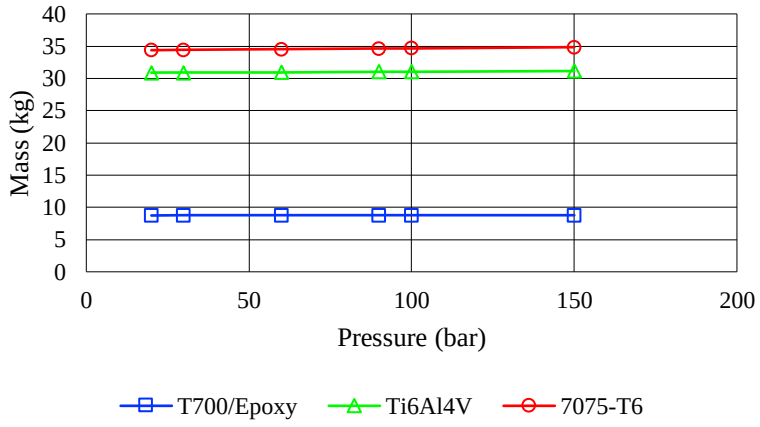

Figure 4-6: Spherical helium vessel mass vs storage pressure for electric pump fed system

However, the effect of pressure on tank dimensions is more pronounced, as per Figure 4-7, which shows the influence of storage pressure on vessel size. In pressurant storage pressures typically ranges between 200 and 300 bar (Hermsen and Zandbergen, 2017).

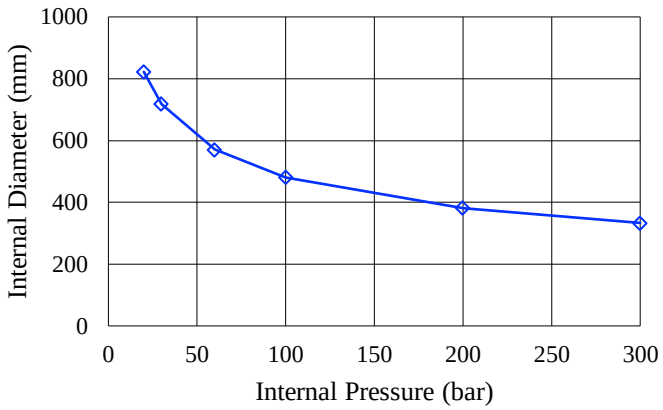

Figure 4-7: Spherical helium tank inner diameter vs pressure

Figure 4-8 illustrates how vessel mass is influenced by geometry for the 20 bar pressure fed and 5 bar pump fed cases. The pump fed tanks are appreciably lighter as they store less gas due to the low propellant tank pressure (5 bar). Cylindrical tanks with spherical ends are shown to offer the highest mass efficiency, while cylindrical tanks with elliptical ends occupy the least space. Spherical tanks are the most common for this application, however, ellipsoidal and spherical end composite and composite overwrap tanks are gaining popularity, as employed, for example, on the Rocket Lab Electron upper stage.

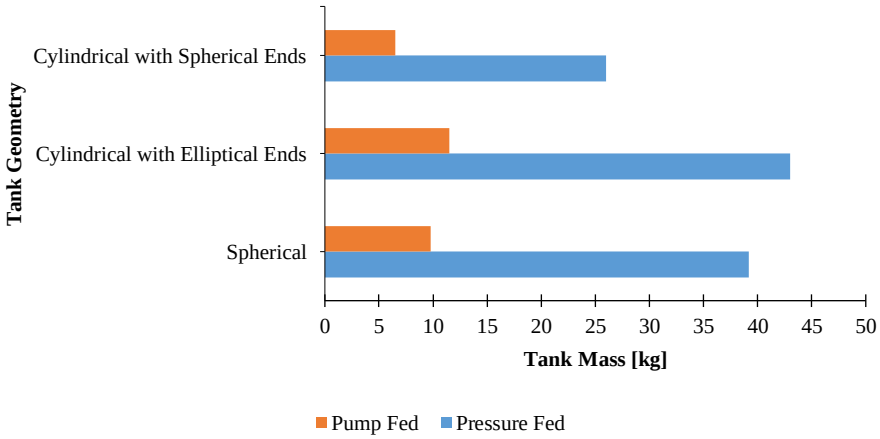

Figure 4-8: Ti6AlV helium tank geometry mass comparison

4.3 Electric-Pump Feed System

Using the equations in Section 3.4 and the parameters in Table 3-9, Table 4-19 lists the mass estimates for an electro-pump feed system and the various components.

Table 4-19: Electric pump feed system component mass estimates

Component	**Mass (kg)**
Pumps	4.5
Motors	18.7
Inverter	1.6
Battery Pack (Li-Ion)	162.9
Battery Pack (Li-Po)	49.57
Total Mass (Li-Ion)	187.7
Total Mass (Li-Po)	74.37

The mass of the pack can be reduced by using more power dense and energy dense Li-Po cells which yield a mass of ≈50 kg (69 % mass reduction) for the system requirements. The mass can be further reduced by redesigning the propellant pumps for a lower chamber pressure, the pumps in the analysis pressurize the chamber to 50 bar.

Figure 4-9 illustrates the mass allocation for the electric pump feed system. The battery pack is by far the largest contributor to mass and is thus the focus for mass optimization. As technology improves the energy and power densities of cells will increase thus further reducing pack mass making electric pump technology an attractive option given the simplicity (i.e. no turbine ignition, turbines, gas generators etc.).

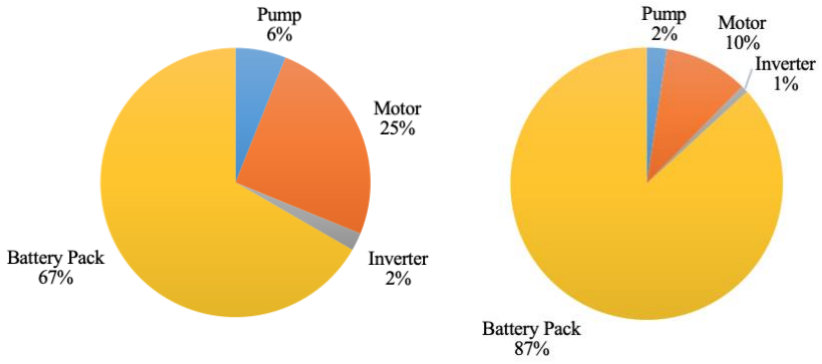

(a) Li-Po (b) Li-Ion

Figure 4-9: Electric feed system mass allocation for Li-Ion

4.4 Reaction Control System

For the reaction control system, the components of focus were the cold gas storage tanks and the cylindrical structure housing the cold gas system (see Figure 3-12 and Figure 3-13 in Chapter 3.3). The overall system mass depends on the required thrust magnitude and burn time; the thrust determines the required mass flow rate while the burn time determines the total amount of gas required. Figure 4-10 displays the linear trend between thrust and mass flow rate for nitrogen cold gas.

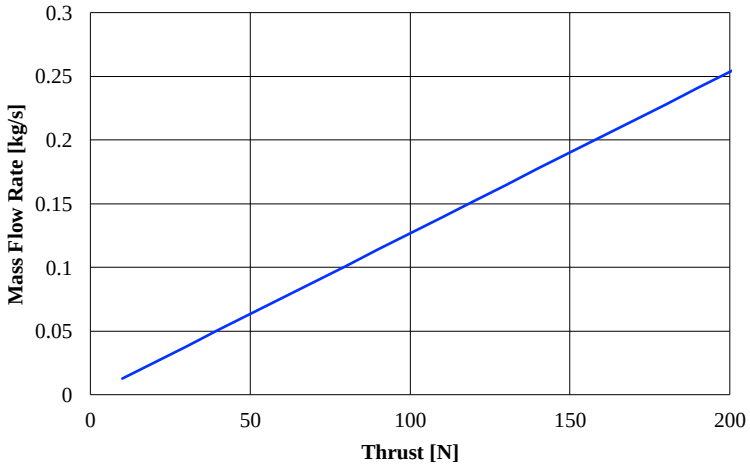

Figure 4-10: Mass flow rate vs thrust for nitrogen

Figure 4-11 shows the relationship between thrust and angular acceleration. The required thrust was determined by setting the angular acceleration the thrusters must achieve based on their mounting position (i.e. lever arm) and the moment of inertia of the vehicle. Equation 3-36 (from Chapter 3.3) was used to calculate the thrust based on the vehicle's longitudinal moment of inertia and angular acceleration.

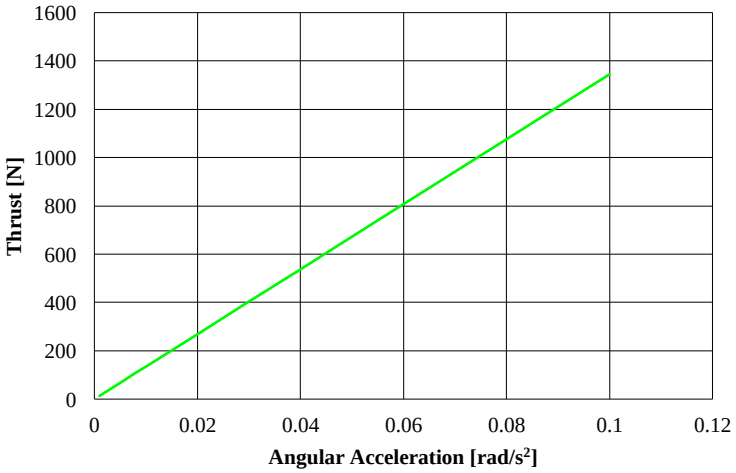

Figure 4-11: Thrust vs angular acceleration

Once the mass of gas required was determined, a storage vessel was designed. The pressure vessel followed the same design process described in Chapter 3.1. The number of pressure vessels for helium storage is an important decision. The relationship between number of spherical Ti6Al4V vessels and total mass is depicted in Figure 4-12. Figure 4-13 depicts the relationship between number of vessels and vessel outer diameters. Figure 4-14 shows how the wall thickness of each vessel decreases as more tanks used. The effect of reducing the diameter appears again, more tanks used means each tank stores a smaller volume and is thus smaller in diameter. A smaller radius vessel requires thinner walls for the same storage pressure.

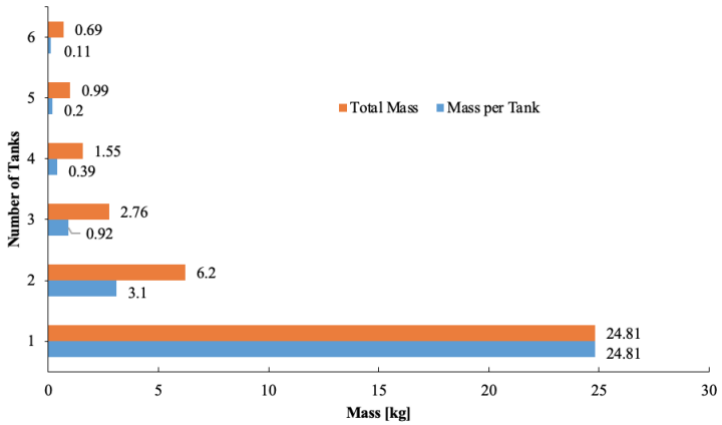

Figure 4-12: Mass vs number of spherical tanks

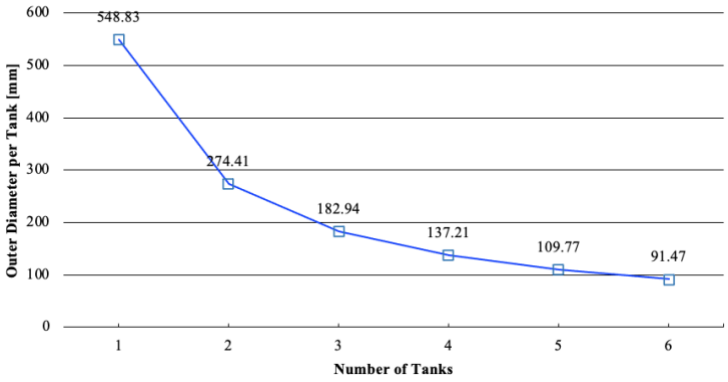

Figure 4-13: Outer diameter vs number of spherical tanks

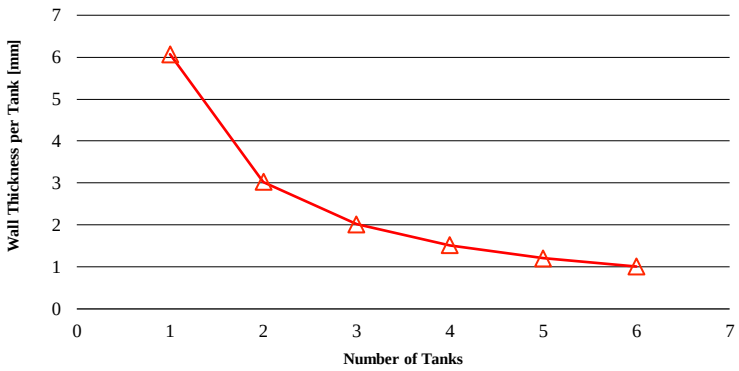

Figure 4-14: Wall thickness vs number of spherical tanks

4.4.1 Summary

Acquiring a mass estimate for the reaction control system is a challenge as the launch vehicle's flight plan and required manoeuvres must be known in order to optimize the system. A trajectory analysis will provide the necessary information to better predict RCS performance requirements.

In the interim the RCS system will consist of four of the 94 N thruster designed in Chapter 3.3, which are analogous to monopropellant thrusters sold by Moog inc. and flown on the ESA's Vega upper stage. The system will store enough nitrogen cold gas for a 200 s continuous firing of a single 94 N thruster, assuming the thrusters will be used in short bursts, each can have five 10 s bursts. The system will achieve a theoretical roll rate of 0.0016 rad/s^2, providing 188 N of moment force per thruster pair. Four CFRP vessels will store the nitrogen cold gas, one vessel per thruster. The mass estimates for the system are presented in Table 4-20.

Table 4-20: Reaction control system mass estimates

Component	**Mass (kg)**
Storage Tanks	1.55
Cold Gas	27.27
Cold Gas Thrusters (CAD model)	1.6 (0.4 per thruster)
RCS Bay	10
System Total	40.42

4.5 Upper Stage Mass

The upper stage design must achieve a 0.85 mass fraction, which means that for an estimated propellant mass of between 1961 kg (from hand calculation) and 1966 kg (reported by Chetty, 2018), the second stage should have a dry mass less than 300 kg. This analysis will compare a pressure fed vehicle to an electric pump fed vehicle. Each vehicle will comprise the following standard components: payload fairing, payload adapter, propellant tanks, pressurization tanks, reaction control propellant tanks, SAFFIRE - V engine and mounts, and thrust frame.

The outcome will determine how much mass budget remains for the auxiliary components (separation systems, plumbing, regulators, valves, avionics, fasteners etc.). The universal mass parameters, which apply to all analysis cases, are given in Table 4-21.

Table 4-21: Universal mass parameters.

Component	**Selection**	**Mass (kg)**	**Comment**
Payload	Small Satellite	75	-
Propellant	LOX and Kerosene	1905	240 s burn time
RCS System Tanks	CFRP	1.55	Custom linerless CFRP pressure vessels
Cold Gas	Nitrogen	27.27	94 N thrust (50 s per thruster) (x 4)
Engine	SAFFIRE - V	85	Vacuum expanded SAFFIRE
Fairing and Payload Attach	CFRP	40	3 mm thick fairing, 2.5 m tall, 600 mm base OD. (Mass from CAD)
Inter-tank	Al 7075-T6	1.5	3 mm thick, 47 mm tall, 600 mm OD. (Mass from CAD)
RCS bay	CFRP	10	3 mm thick, 380 mm tall, 0.6 OD. (Mass from CAD)
Thrust Frame	SS 316	11.2	Mass from CAD model
Universal Structural Total	64.25		

The universal structural mass is calculated using equation 4-16. The value features in both the pressure fed and electric pump system analyses.

$$m_{US} = m_{RCS\,Tanks} + m_{Fairing} + m_{Intertank} + m_{RCS\,Bay} + m_{Thrust\,Frame} \quad (4\text{-}16)$$

Various mass metric were calculated for each upper stage configuration. These metrics include: the dry mass of the upper stage "from factory" without a payload or fuel (m_d), the final mass at apogee just before payload ejection (m_f), upper stage wet mass when fuelled but without a payload (m_w), and the initial mass at take-off or "mass on pad" (m_i). The metrics were calculated using equations 4-8 to 4-11.

$$m_d = m_{tanks} + m_{engine} + m_{structural} \quad (4\text{-}8)$$

$$m_f = m_{tanks} + m_{engine} + m_{structural} + m_{payload} \quad (4\text{-}9)$$

$$m_w = m_{tanks} + m_{engine} + m_{structural} + m_{propellant} \quad (4\text{-}10)$$

$$m_i = m_{tanks} + m_{engine} + m_{structural} + m_{payload} + m_{propellant} \quad (4\text{-}11)$$

4.5.1 Pressure Fed Vehicle

This configuration uses the pressure fed cycle, with a presuure regulator, and maintains constant propellant tank pressure of 20 bar. Given the relativley high pressure at which the propellants are stored, this vehicle requires more helium and therefore a greater number of helium storage vessel compared to the pump fed vehicle. Table 4-22 to Table 4-31 list the individual component masses and vehicle mass metrics for the various tank materials used.

Table 4-22: Component masses of pressure fed vehicle.

Component	**Mass (kg)**	**Comment**
Engine	85	Mass of SAFFIRE-V engine
Propellant	1905	For 240 s burn time
Pressurization System Tanks	26	Ti6Al4V Cylindrical shell with elliptical ends
Pressurant	6.8	Helium
Total Propellant (m_p)	1966.8	LOX + Kerosene + He + N_2
Structural Total	91.8	Universal structural total + pressurization system tanks
Dry Mass Basic	176.8	Structural total + Engine
Wet Mass Basic	2143.6	Dry mass basic + total propellant
Final Mass Basic	251.8	Dry mass basic + payload

Table 4-23: Pressure fed vehicle mass metrics – SS 301 propellant tanks

Metric	**Value**
Tank Mass (m_{tanks})	80.67
Dry Mass (m_d)	257.47
Final Mass (m_f)	332.47
Wet Mass (m_w)	2224.27
Initial Mass (m_i)	2302.27
Mass Fraction ($\frac{m_p}{m_i}$)	0.854
Mass Ratio ($\frac{m_i}{m_f}$)	6.925

Table 4-24: Pressure fed vehicle mass metrics – Duplex SS propellant tanks

Metric	**Value**
Tank Mass (m_{tanks})	109.28
Dry Mass (m_d)	286.08
Final Mass (m_f)	361.08
Wet Mass (m_w)	2252.88
Initial Mass (m_i)	2327.88
Mass Fraction ($\frac{m_p}{m_i}$)	0.845
Mass Ratio ($\frac{m_i}{m_f}$)	6.447

Table 4-25: Pressure fed vehicle mass metrics – CFRP T700/Epoxy propellant tanks

Metric	**Value**
Tank Mass (m_{tanks})	18.16
Dry Mass (m_d)	194.96
Final Mass (m_f)	269.96
Wet Mass (m_w)	2161.76
Initial Mass (m_i)	2236.76
Mass Fraction ($\frac{m_p}{m_i}$)	0.879
Mass Ratio ($\frac{m_i}{m_f}$)	8.286

Table 4-26: Pressure fed vehicle mass metrics – Al 7075-T6 propellant tanks

Metric	**Value**
Tank Mass (m_{tanks})	48.52
Dry Mass (m_d)	225.32
Final Mass (m_f)	300.32
Wet Mass (m_w)	2192.12
Initial Mass (m_i)	2267.12
Mass Fraction ($\frac{m_p}{m_i}$)	0.868
Mass Ratio ($\frac{m_i}{m_f}$)	7.549

Table 4-27: Pressure fed vehicle mass metrics – Al 6061-T6 propellant tanks

Metric	**Value**
Tank Mass (m_{tanks})	75.61
Dry Mass (m_d)	252.41
Final Mass (m_f)	327.41
Wet Mass (m_w)	2219.21
Initial Mass (m_i)	2294.21
Mass Fraction ($\frac{m_p}{m_i}$)	0.83
Mass Ratio ($\frac{m_i}{m_f}$)	7.00

Table 4-28:Pressure fed vehicle mass metrics – Al-Li 2195 propellant tanks

Metric	**Value**
Tank Mass (m_{tanks})	44.30
Dry Mass (m_d)	221.1
Final Mass (m_f)	296.1
Wet Mass (m_w)	2187.9
Initial Mass (m_i)	2262.9
Mass Fraction ($\frac{m_p}{m_i}$)	0.869
Mass Ratio ($\frac{m_i}{m_f}$)	7.642

Table 4-29: Pressure fed vehicle mass metrics – CFRP T700-Epoxy/Al 7075-T6 propellant tanks

Metric	**Value**
Tank Mass (m_{tanks})	30.52
Dry Mass (m_d)	207.32
Final Mass (m_f)	282.32
Wet Mass (m_w)	2174.12
Initial Mass (m_i)	2249.12
Mass Fraction ($\frac{m_p}{m_i}$)	0.874
Mass Ratio ($\frac{m_i}{m_f}$)	7.967

Table 4-30: Pressure fed mass metrics – CFRP/Al 6061-T6 propellant tanks

Metric	**Value**
Tank Mass (m_{tanks})	41.14
Dry Mass (m_d)	217.94
Final Mass (m_f)	292.94
Wet Mass (m_w)	2184.74
Initial Mass (m_i)	2259.74
Mass Fraction ($\frac{m_p}{m_i}$)	0.84
Mass Ratio ($\frac{m_i}{m_f}$)	7.71

Table 4-31: Pressure fed vehicle mass metrics – CFRP T700-Eopxy/SS 301 propellant tanks

Metric	**Value**
Tank Mass (m_{tanks})	45.61
Dry Mass (m_d)	222.41
Final Mass (m_f)	297.41
Wet Mass (m_w)	2189.21
Initial Mass (m_i)	2264.21
Mass Fraction ($\frac{m_p}{m_i}$)	0.869
Mass Ratio ($\frac{m_i}{m_f}$)	7.613

4.5.2 Electric Pump Fed Vehicle

The electric pump fed vehicle will, in addition to the standard components, include the electric pump feed system comprising a battery pack, pumps, electric motors and an inverter. Table 4-32 to Table 4-41 that follow list the component masses and mass metrics calculated for the electric pump fed system with respect to the tank materials and battery pack cells used.

Table 4-32: Component masses of electric pump fed vehicle

Component	**Mass (kg)**	
Feed System	74.3 (Li-Po)	187.7 (Li-Ion)
Engine*	159.3 (Li-Po)	272.7 (Li-Ion)
Propellant	1905	
Pressurization System Tanks	6.1	
Pressurant	1.8	
Total Propellant (m_p)	1961.8	
Structural Total	71.9	

*Electric pump feed system + SAFFIRE-V engine

Table 4-33: Electric pump fed vehicle mass metrics –SS 301 FH

Metric	**Value**	
	Li-Po	**Li-Ion**
Tank Mass (m_{tanks})	46.87	
Dry Mass (m_d)	276.51	389.91
Final Mass (m_f)	351.51	464.91
Wet Mass (m_w)	2238.31	2351.71
Initial Mass (m_i)	2316.31	2429.71
Mass Fraction ($\frac{m_p}{m_i}$)	0.847	0.81
Mass Ratio ($\frac{m_i}{m_f}$)	6.590	5.23

Table 4-34: Electric pump fed vehicle mass metrics – Duplex SS FH

Metric	**Value**	
	Li-Po	**Li-Ion**
Tank Mass (m_{tanks})	53.79	
Dry Mass (m_d)	284.69	398.09
Final Mass (m_f)	359.69	473.09
Wet Mass (m_w)	2246.49	2359.89
Initial Mass (m_i)	2321.49	2434.89
Mass Fraction ($\frac{m_p}{m_i}$)	0.845	0.81
Mass Ratio ($\frac{m_i}{m_f}$)	6.454	5.15

Table 4-35: Electric pump fed vehicle mass metrics – CFRP T700/Epoxy

Metric	**Values**	
	Li-Po	**Li-Ion**
Tank Mass (m_{tanks})	11.32	
Dry Mass (m_d)	242.22	355.62
Final Mass (m_f)	317.22	430.62
Wet Mass (m_w)	2204.02	2317.42
Initial Mass (m_i)	2279.02	2392.42
Mass Fraction ($\frac{m_p}{m_i}$)	0.861	0.82
Mass Ratio ($\frac{m_i}{m_f}$)	7.184	5.56

Table 4-36: Electric pump fed vehicle mass metrics – Aluminium 7075-T6

Metric	**Value**	
	Li-Po	**Li-Ion**
Tank Mass (m_{tanks})	21.66	
Dry Mass (m_d)	252.56	365.96
Final Mass (m_f)	327.56	440.96
Wet Mass (m_w)	2214.36	2327.76
Initial Mass (m_i)	2289.36	2402.76
Mass Fraction ($\frac{m_p}{m_i}$)	0.857	0.816
Mass Ratio ($\frac{m_i}{m_f}$)	6.990	5.449

Table 4-37: Electric pump fed vehicle mass metrics – Aluminium 6061-T6

Metric	**Value**	
	Li-Po	**Li-Ion**
Tank Mass (m_{tanks})	28.09	
Dry Mass (m_d)	258.99	372.39
Final Mass (m_f)	333.99	447.39
Wet Mass (m_w)	2220.79	2334.19
Initial Mass (m_i)	2295.79	2409.19
Mass Fraction ($\frac{m_p}{m_i}$)	0.855	0.814
Mass Ratio ($\frac{m_i}{m_f}$)	6.874	5.385

Table 4-38: Electric pump fed vehicle mass metrics – Aluminium lithium 2195

Metric	**Value**	
	Li-Po	**Li-Ion**
Tank Mass (m_{tanks})	20.18	
Dry Mass (m_d)	251.08	364.48
Final Mass (m_f)	326.08	439.48
Wet Mass (m_w)	2212.88	2326.28
Initial Mass (m_i)	2287.88	2401.28
Mass Fraction ($\frac{m_p}{m_i}$)	0.858	0.817
Mass Ratio ($\frac{m_i}{m_f}$)	7.016	5.464

Table 4-39: Electric pump fed vehicle mass metrics – CFRP/Al 7075-T6

Metric	**Value**	
	Li-Po	**Li-Ion**
Tank Mass (m_{tanks})	15.78	
Dry Mass (m_d)	246.68	360.08
Final Mass (m_f)	321.68	435.08
Wet Mass (m_w)	2208.48	2321.88
Initial Mass (m_i)	2283.48	2396.88
Mass Fraction ($\frac{m_p}{m_i}$)	0.859	0.818
Mass Ratio ($\frac{m_i}{m_f}$)	7.099	5.509

Table 4-40: Electric pump fed vehicle mass metrics – CFRP/Al 6061-T6

Metric	**Values**	
	Li-Po	**Li-Ion**
Tank Mass (m_{tanks})	17.96	
Dry Mass (m_d)	248.86	362.26
Final Mass (m_f)	323.86	437.26
Wet Mass (m_w)	2210.66	2324.06
Initial Mass (m_i)	2285.66	2399.06
Mass Fraction ($\frac{m_p}{m_i}$)	0.858	0.818
Mass Ratio ($\frac{m_i}{m_f}$)	7.058	5.487

Table 4-41: Electric pump fed vehicle mass metrics – CFRP/SS 301 FH

Metric	**Values**	
	Li-Po	**Li-Ion**
Tank Mass (m_{tanks})	28.14	
Dry Mass (m_d)	259.04	372.44
Final Mass (m_f)	334.04	447.44
Wet Mass (m_w)	2220.84	2334.24
Initial Mass (m_i)	2295.84	2409.24
Mass Fraction ($\frac{m_p}{m_i}$)	0.855	0.814
Mass Ratio ($\frac{m_i}{m_f}$)	6.873	5.384

4.5.3 Summary

The values obtained for the two feed systems and the various tank material options are compared in Figure 4-15 and Figure 4-16.

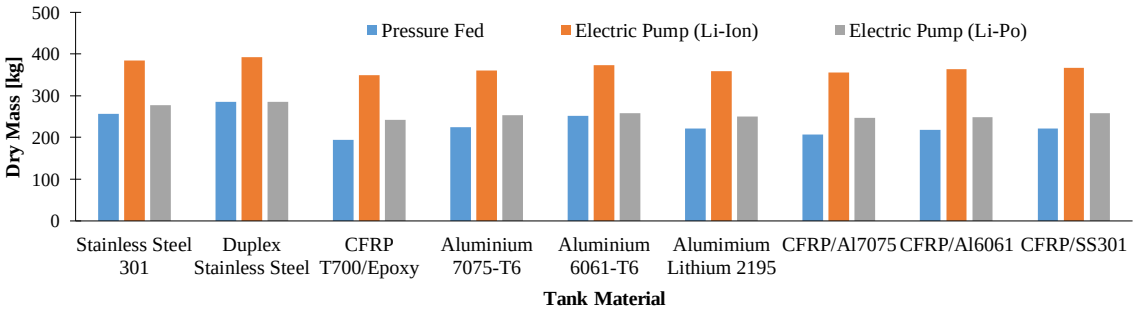

Figure 4-15: Vehicle dry mass comparisons

Given that the propellant tanks of an upper stage vehicle comprise a large portion of its total mass, the results follow a similar trend to that presented in Section 4.1.2. The CFRP based vehicle weighs the least, while the Duplex stainless steel vehicle weighs the most. As can be seen in Figure 4-15, upon comparing the feed systems it was found that the electric pump systems, using Li-Po battery packs, had a lower dry mass compared to pressure fed systems or when Li-Ion cells were employed.

Figure 4-16 shows that an electric pump fed vehicle employing a Li-Ion battery pack will not meet the target mass fraction, regardless of tank material. With a mass of 187.7 kg the Li-Ion battery pack is too heavy and offsets the effect of the thin propellant tanks.

The results also show that using stainless steel 301 and duplex for the propellant tanks is feasible for both the 20 bar pressure fed and Li-Po battery pack electric pump fed vehicles, with mass fractions of 0.869 and 0.847 obtained for each respectively.

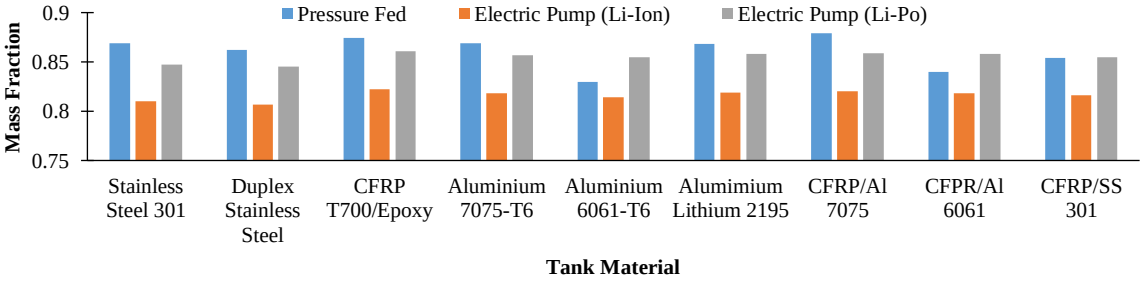

Figure 4-16: Vehicle mass fraction comparison

Figure 4-17 shows the approximate contribution of each vehicle configuration's main components to the overall mass; the values are based on the best performing configurations for each feed system type. For electric pump system, CFRP propellant tanks with Li-Po cells as the best preforming. For the pressure fed system, CFRP propellant tanks at 20 bar was the best performing configuration. It was found that for the electric pump fed vehicle the battery pack constitutes most of the mass. While for pressure fed vehicles, the mass is comprised mostly of the engine and propellant tanks.

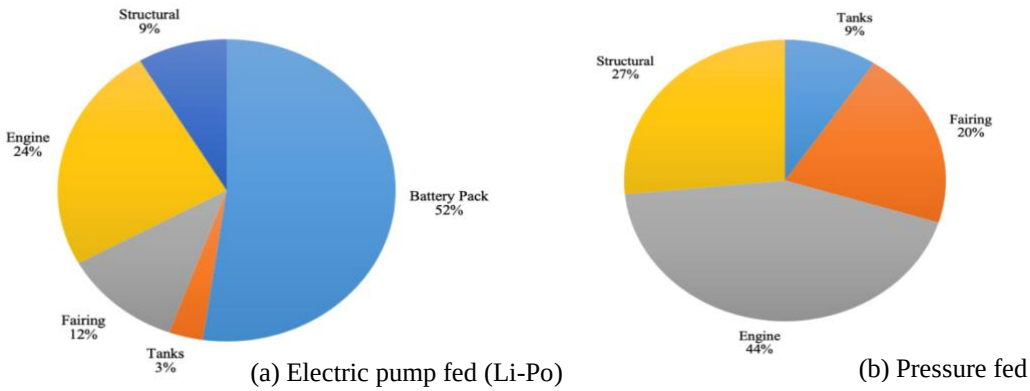

(a) Electric pump fed (Li-Po) (b) Pressure fed

Figure 4-17: Vehicle dry mass distributions

5 Conclusion

The primary aim of this work was to conduct a high level study and propose a preliminary design for the hypothetical Commercial Launch Vehicle 1's upper stage, designed for the orbital insertion of a 75 kg payload to a 400 km SSO. The upper stage was considered to be powered by a vacuum expanded derivative of the SAFFIRE engine. Specifically, he objectives required to complete the study were as follows:

1) Develop a preliminary methodology for upper stage design.
2) Compare various upper stage configurations based on a mass. Compare an electric pump fed system must also be assessed based on mass fraction.
3) Identify areas of future research based on findings.

The objectives, their fulfilment and a proposed design for the upper stage are discussed in the subsequent sections, followed by future recommendations and areas of focus.

5.1 Preliminary Design Methodology

The design methodology for the vehicle's components and systems was developed from the work of various authors including Bruhn and Bollard (1973), Humble (2007), Huzel and Huang (1992) and Sutton and Biblarz (2001). The intention is for the vehicle configuration results, obtained by using this methodology, to guide preliminary high level design decision making in deriving the most appropriate upper stage configuration. The components/systems accounted for by the methodology include the:

- Propellant tanks
- Reaction control system
- Propellant pressurization system

The methodology was presented in Chapter 3 for each component, accompanied by a flow chart to graphically represent each respective design process.

One of the major challenges of the design process was making assumptions regarding the yet-to-be-developed SAFFIRE-V engine's dimensions, which were necessary for designing structurally representative concept vehicles. The engine's performance specifications are necessary for component design; for example, the engine mass flow rate and O/F ratio determine the required quantity of propellants, which in turn affects the mass of the propellant tanks and pressurization system. Another challenge was keeping the process manageably simple yet detailed enough to derive representative mass values.

5.2 Mass Analysis

CLV's upper stage must achieve the 0.85 mass fraction requirement to meet the mission requirements. The mass fraction is affected by every design decision, and it thus guides these decisions from a preliminary, high level stand point.

To attain mass information, the major components and subsystems (i.e. those accounting for the majority of the stage mass) were designed. Various component architectures, construction materials and vehicle configurations were analysed and compared. In particular, the following aspects were assessed:

- The masses of the propellant tanks were compared by varying tank construction materials and tank endcap shapes. The effectiveness of common bulkheads was also assessed. A buckling analysis was also performed to gauge the buckling resistance capacity of the tanks for varying materials of construction.
- The mass of a nitrogen cold gas based RCS was compared at various thrust levels and burn times. These values influenced the maximum achievable roll speed, the cold gas mass and cold gas storage requirements.
- The mass of the electric pump feed system was analysed by varying the types of cells used for the battery pack. Li-Ion and Li-Po cells were compared.
- An analysis of two types of propellant feed system was also performed. Pressure fed and electric pump fed upper stages were compared; the choice of which had a noticeable effect on the minimum wall thickness of the propellant tanks.

One of the challenges of the analysis was factoring technological capabilities of South Africa into the process. For example, aerospace grade materials are notoriously difficult to acquire locally; large, flight weight, liquid propellant tanks have never been manufactured in Africa. Another challenge was making sensible assumptions regarding the electric pump feed system. The range of performance specifications, found in literature, for the classes of battery pack cells and the electric motors varies with each manufacturer. The works of Kwak et al. (2018) and Rachov (2014) were of critical importance for the mass analysis of the electric pump feed system. The mass analysis of upper stage iterations was conducted using a Microsoft® Excel spreadsheet, which comprised multiple interlinked calculators. In general, the design assumptions made were based on industry trends and prior research work.

The mass analysis revealed that for a given material and component architecture, pressure fed upper stage configurations exhibited better mass performance compared to electric pump fed configurations. The use of stainless steel as a propellant tank material was found to be feasible for the case of pressure fed designs, yielding mass fractions of 0.869 and 0.862 for 301 and Duplex stainless steels, respectively. This is an important observation, considering the comparatively low material and fabrication costs associated with stainless steels. The best performing configuration, based on minimum mass, upper stage resulted from all CFRP tankage, followed by the dual material option of an aluminium 7075-T6 oxidiser and CFRP fuel tank.

It was also determined that an electric pump fed upper stage did not meet the minimum mass fraction requirement with a Li-Ion based battery pack. Li-Ion cylindrical cells are notoriously heavy and space consuming given their long, cylindrical, leak-proof, plastic casing (resembling an AA battery) (Venkatasetty and Jeong, 2002). The Li-Ion battery pack was predicted to weigh 162 kg compared to the 45 kg mass of the Li-Po pouch cell battery pack. The Li-Po pouch cells (who had higher power and energy densities compared to Li-Ion cells) are therefore a better suited, with upper stages achieving mass fractions above 0.85, barring the upper stages with 301 or Duplex stainless steel propellant tanks. It is important to note that Li-Po pouch cells are easier to manufacture compared to cylindrical Li-Ion cells, however Li-Po cells are slightly more expensive (Rockett, 2018).

A pressure fed upper stage is a viable option based on mass, cost and complexity. While electric pump fed systems will become increasingly viable as cell, motor and material technology improves, or as more research emphasis is placed on the system, given that cells and motors can be customized. Improving the performance of the motors (i.e. increasing power density and efficiency) or decreasing SAFFIRE - V's chamber pressure (lower pump power) will decrease pump feed system's mass.

5.3 Proposed Design

Table 5-1 lists the proposed design decisions for the CLV upper stage based on the results from the mass analysis and the TRL of South Africa. Based on USA aerospace standards, a safety factor of 1.2 was selected for the tanks and other components with an additional blanket factor of 1.5 used for bolted connections.

Table 5-1: Upper stage design decisions

Component	**Choice**	**Motivation**
Propulsion		
Kerosene Tank Material	Carbon fibre T700/Epoxy	20% weight reduction vs AlLi. Tank will be linerless
LOX Tank Material	Aluminium 7075 T6	Light weight. Can withstand cryogenic conditions
Component	**Choice**	**Comment**
Propulsion		
Tank Configuration	Common bulkhead; ellipsoidal ends	Reduced mass and height
Propellants	Kerosene/LOX	I_{SP} = 353 s at vacuum
Feed System	Pressure regulated blow-down	Simple and robust. Best mass performance
Pressurant	Helium	Highest performance
Gimbal (Pitch & Yaw)	6 °	SAFFIRE specification
Ignition	Pyrophoric	Multiple starts and light weight
Reaction Control System		
Propellant	Nitrogen	Easy to obtain. Non-toxic. Best balance between molar mass and I_{SP}
Thruster (Roll)	Cold gas thruster (x4)	Simple to implement compared to mono/bipropellant systems.
Thrust	100 N (x4)	0.016 rad/s^2 roll rate
Position	Centre of mass	Easy translations
Separation Events		
Stage Separation	Electric actuation; Hydraulic latch	Low shock
Fairing Separation		
Payload Separation		

5.4 Recommendations and Future Areas of Focus

The propellant tanks contribute most to the dry mass of a pressure fed upper stage vehicle. An investigation comparing various tank design techniques (e.g. integral stiffening, composite

overwrapped tanks, and linerless composite tanks) would be beneficial. The investigation would require experimental testing of various materials and construction techniques; the buckling characteristics and cryogenic performance of the materials would be of particular importance. The propellant tank design and construction material(s) selection will depend on cost, availability, manufacturability, mass and TRL.

The components of the feed system contribute the most to the dry mass of the electric pump fed upper stage vehicle; it is therefore imperative that a more involved low-level study is performed to improve the accuracy of the associated mass analysis. The study should comprehensively qualify the performance specifications such as energy density, power density and efficiency of the system's various components (i.e. motors, cells, inverters and pumps) while optimizing the system with respect to mass and cost. Some specifications require independent testing, especially those regarding the battery pack, as quoted specifications are ambiguous or given over a large range. A test rig comprising the whole electrical feed system would provide a suitable platform to gauge performance.

A trajectory and orbital analysis will aid in the determination of the exact engine performance requirements while providing a platform to gauge the performance of design iterations. The analysis will also assist the establishment of a flight profile which is key for the design of the reaction control system.

Separation mechanisms should be another key area of future focus. The dynamics involving a separation event and the shock each event imparts on the vehicle are important measures of interest as they may affect the integrity of sensitive payload(s). Minimising vibration without increasing complexity and mass will prove challenging. Separation systems require detailed design, especially those that are electrically triggered.

A CFD-FEA coupled transient aerothermal structural analysis is a difficult but necessary exercise in order to determine the structural and insulation requirements of the upper stage and the launch vehicle as a whole. The "max q" —which is the maximum dynamic pressure imparted on an aerospace vehicle during its flight— is a key value the analysis must determine as it will influence the structural design of the launch vehicle.

Further studies on tank buckling is also required. Analytical buckling methods are unreliable as there is a large degree of variance between the different methods. Also, the analytics presented in this thesis are case specific (for the authors materials) and are heavily based on experimental data. Furthermore, the loads on the tanks are unknown, making it difficult to pass or fail a tank design based on buckling failure. FEA's and physical testing is necessary to give confidence on tank buckling. Finally, the analytics do not extend to the buckling of composite tanks, which is the likely material for the propellant tanks. In this thesis, a tank is passed if it can support it's own weight without buckling.

Given these considerations, the pursuit of a liquid rocket engine sounding rocket development programme, which would seek to design, manufacture and launch a sub-scale, sub-orbital version of CLV, is highly recommended. Such a programme would provide verification of simulation results and guide the development of an orbital launch vehicle. It would also provide a platform to develop and test flight-weight systems and components such as: the electric pumps, propellant tanks, pressurization systems, separation mechanisms, roll control systems, thrust vector control systems and avionics.

6 References

Aggarwal, P. and Hull, P. (2015). “Flight Vehicle Structural Design Processes for a Common Bulkhead and a Multipurpose Crew Vehicle Spacecraft Adapter”. *Proceedings of SciTech, 5-9 January*. NASA. DOI: 10.2514/6.2016-0158.

Alnaib, A. M. T. I. (2019) DC Motors. Northern Technical University.

Anderson, W., Boxwell, R., Crockett, D., Ross, R., Lewis, T., McNeal, C. and Verdarame, K. (1999). “Upper-Stage Flight Experiment”. *NASA Technical Report*. [online] Available at: https://ntrs.nasa.gov/search.jsp?R=20000004378 [Accessed 8 Jan. 2019].

Arianespace (2014). “Vega User’s Manual”. Issue 4. [online] Turin, Italy: Arianespace. Available at: https://www.arianespace.com/wp-content/uploads/2015/09/Vega-Users-Manual_Issue-04_April-2014.pdf [Accessed 20 Jan. 2020].

Assad Anis (2012). “Cold Gas Propulsion System - An Ideal Choice for Remote Sensing Small Satellites, Remote Sensing - Advanced Techniques and Platforms”. Boris Escalante-Ramirez, IntechOpen. DOI: 10.5772/37149.

Atkins, E. (2010). “Aerospace Avionics Systems”. *Encyclopaedia of Aerospace Engineering*. John Wiley & Sons, Ltd. DOI: 10.1002/9780470686652.eae451.

Avio. (2017). “VEGA: Payload Fairing”. [online] Available at: http:// www.avio.com/ en / vega / veg a / vega-payload-fairing/ [Accessed 30 Jan. 2020].

Balashanmugham, A. and Maheswaran, M. (2020) ‘Permanent-magnet synchronous machine drives’, *Applied Electromechanical Devices and Machines for Electric Mobility Solutions One*. doi: 10.5772/intechopen.88597.

Ballard, R. (2019) “Liquid Propulsion Systems – Evolution & Advancements: Launch Vehicle Propulsion & Systems’. Reston, VA: AIAA, pp. 1–31. Available at: https:// core. ac. uk/ download/ pdf/ 42733219. pdf.

Belluscio, A. (2016). “ITS Propulsion – The evolution of the SpaceX Raptor engine”. [online] Nasaspaceflight. Available at: https://www.nasaspaceflight.com/2016/10/its-propulsion-evolution-raptor-engine/ [Accessed 11 Dec. 2018].

Berger, E. (2019). “Blue Origin just validated the new space movement”. [online] Ars Technica. Available at: https://arstechnica.com/science/2016/10/blue-origin-just-validated-the-new-space-movement/ [Accessed 26 Dec. 2019].

Biskner, A. and Higgins, J. (2005). “Design and Evaluation of a Reinforced Advanced-Grid Stiffened Composite Structure”. *Proceedings of 46th AIAA/ASME/ASCE/AHS/ASC Structures, Structural Dynamics and Materials Conference*. *18-21 April. Austin, Texas*. DOI: 10.2514/6.2005-2153.

Biskner, A., Mehle, G. and Maly, J. (2007). “Design, Analysis, and Testing of the CASPAR Multi-Payload Adapter Bonded Composite”. [online]. *Proceedings of 48th AIAA/ASME/ASCE/AHS/ASC Structures, Structural Dynamics, and Materials Conference, 23-26 April, Honolulu, Hawaii*. Aerospace Research Central. DOI: 10.2514/6.2007-2191 [Accessed 31 Jan. 2020].

Brey, J. *et al.* (2017) “Use of Fuel Cells and Electrolyzers in Space Applications: From Energy Storage to Propulsion/Deorbitation”, *E3S Web of Conferences*, 16. doi: 10.1051/e3sconf/20171617004.

Brousseau, J., Maynard, R., Singaraju, A. and Richter, H. (2006). “A Testbed for Attitude Control Using Cold Gas Thrusters”. *Proceedings of ASME 2006 International Mechanical Engineering Congress and Exposition. 5-10 November. Chicago, Illinois*. DOI: 10.1115/IMECE2006-15307.

Brown, C. (2002). “Spacecraft Mission Design”. Reston, VA: American Institute of Aeronautics and Astronautics.

Brown, L., Martin, M., Aleck, B. and Landes, R. (1975). “Composite-Reinforced Propellant Tanks”. NASA Technical Report. Grumman Aerospace Corporation.

Bruhn, E. and Bollard, R. (1973). “Analysis and design of flight vehicle structures”. Carmel, IN: Jacobs.

Burghes, D. (1974). “Optimum Staging of Multistage Rockets”. [online]. *International Journal of Mathematical Education in Science and Technology, 5(1), pp.3-10*. DOI: 10.1080/0020739740050101. [Accessed 24 Jan. 2020]

Campbell, W. E. and Farquhar, J. (1974). “Centrifugal pumps for rocket engines”. NASA Technical Report. Aerojet Nuclear Systems Company.

Cao, W. et al. (2012) ‘Overview of electric motor technologies used for more electric aircraft (MEA)’, IEEE Transactions on Industrial Electronics, 59(9), pp. 3523–3531. doi: 10.1109/TIE.2011.2165453.

Chaker, N. et al. (2009) ‘Design of Axial-Flux Motor for Traction Application’, Journal of Electromagnetic Analysis and Applications, 01(02), pp. 73–84. doi: 10.4236/jemaa.2009.12012.

Chavez, T., Barrera, M. and Kanter, M. (2007). “Operational Satellite Concepts for ESPA Rideshare”. *Proceedings of 2007 IEEE Aerospace Conference*. 3-10 March. Big Sky, MT. [online] IEEE. Available at: https:// ieeexplore.ieee.org / abstract / document / 4161369 / authors # authors. DOI: 10.1109/AERO.2007.352892. [Accessed 21 Jan. 2020]

Chetty, C. (2018*). “*The Hydrodynamic Design and Analysis of an RP-1 Pump for a Liquid Rocket Engine”. Master of Science. University of KwaZulu-Natal.

Chindambaram, T., Krishan, A. and Agarwal, N. (2003). *"*Advances in Launch Vehicle Electronics in India". *IETE Technical Review, 20, pp.129-138*. DOI: 10.1080/02564602.2003.11417077.

Chu, M., De Jonghe, L. and Visco, S. (1996). "High specific power lithium polymer rechargeable battery". *Proceedings of 11th Annual Battery Conference on Applications and Advances. 9-12 Jan. Long Beach, CA*: I.E.E.E. Press. DOI: 10.1109/BCAA.1996.484988.

Civek-Coskun, E. and Ozgoren, K. (2013). "A generalized staging optimization program for space launch vehicles". *Proceedings of 2013 6th International Conference on Recent Advances in Space Technologies (RAST)*. *12-14 June. Istanbul, Turkey*. DOI: 10.1109/RAST.2013.6581333.

Clemens, K. (2018) A New Generation of Axial Flux EV Motors, Magnax. Available at: https://www.magnax.com/magnax-blog/a-new-generation-of-axial-flux-ev-motors (Accessed: 15 June 2021).

Crisp, N., Smith, K. and Hollingsworth, P. (2014). "Small Satellite Launch to LEO: A Review of Current and Future Launch Systems". [online]. *Transactions of the Japan Society for Aeronautical and Space Sciences, 12(29), pp.39-47*. Available at: https:// www.researchgate.net/ publication/ 264537134_ Small _ Satellite _ Launch _ to _ LEO _ A _ Review _ of _ Current _ and _ Future _ Launch _ Systems. DOI: 10.2322/tastj.12.Tf_39. [Accessed 21 Jan. 2020].

Crone, C. et al. (1993) "Combustion Instability in Small Earth Storable Bipropellant Rocket Engines", *Proceedings of AIAA / ASME / SAE / ASEE 25th Joint Propulsion Conference. 28 - 30 June*. Monterey, CA: American Institute of Aeronautics and Astronautics, Inc., pp. 1–9.

Crowell, G. (1996). "The Descriptive Geometry of Nose Cones". [ebook] Sao Paulo: University of Sao Paulo. Available at: http://www.if.sc.usp.br/~projetosulfos/artigos/NoseCone_EQN2.PDF [Accessed 17 Sep. 2018].

da Cás, P., Veras, C., Shynkarenko, O. and Leonardi, R. (2019). "A Brazilian Space Launch System for the Small Satellite Market". *Aerospace, 6(11), p.123*. DOI: 10.3390/aerospace6110123.

Dave Wilson Photography. (2010). "Second Stage Engine Detail, Saturn V". [online] Available at: http://www.davewilsonphotography.com/2010/11/02/second-stage-engine-detail-saturn-v/ [Accessed 3 Jul. 2019].

DEIMOS elecnor and OrbeX (2018). "AZuL - AZores Micro Launcher. ESA Micro-Launch Services Workshop". [online] Paris: DEIMOS Engenharia S.A. Available at: http:// esamultimedia.esa.int /docs/space_transportation/AZUL-ESA_Workshop-Export.pdf [Accessed 13 Feb. 2020].

Derammelaere, S., De Viaene, J., Verbelen, F., Haemers, M. and Stockman, K. (2016*). "*A quantitative comparison between BLDC, PMSM, brushed DC and stepping motor technologies". *Proceedings of*

19th International Conference on Electrical Machines and Systems (ICEMS). 13-16 November. Chiba, Japan: IEEE. Available at: http://hdl.handle.net/1854/LU-8544760 [Accessed 29 Apr. 2019].

Detloff, C. (2017) AC Induction Motors vs. Permanent Magnet Synchronous Motors - Empowering Pumps and Equipment, EM Powering. Available at: https://empoweringpumps.com/ac-induction-motors-versus-permanent-magnet-synchronous-motors-fuji/ (Accessed: 15 June 2021).

Deutsches museum. Deutsches Museum: Rocket engines. [online] Available at: https://www.deutsches-museum.de/en/exhibitions/transport/astronautics/rocket-engines/ [Accessed 3 Jul. 2019].

de Weck, O. (2006). "A Systems Approach to Mass Budget Management". *Proceedings of 11th AIAA/ISSMO Multidisciplinary Analysis and Optimization Conference. 6-8 September. Portsmouth, VA.* DOI: 10.2514/6.2006-7055.

Di Mauro, G., Lawn, M. and Bevilacqua, R. (2018). "Survey on Guidance Navigation and Control Requirements for Spacecraft Formation-Flying Missions". *Journal of Guidance, Control, and Dynamics, 41(3), pp.581-602.* DOI: 10.2514/1.G002868.

Dlugiewicz, L., Kolowrotkiewicz, J., Szelag, W. and Slusarek, B. (2012). "Permanent magnet synchronous motor to drive propellant pump". *Proceedings of International Symposium on Power Electronics Power Electronics, Electrical Drives, Automation and Motion. 20-22 June. Sorrento, Italy.* DOI: 10.1109/SPEEDAM.2012.6264431.

Doncaster, B., Shulman, J., Bradford, J. and Olds, J. (2016). "SpaceWorks' 2016 Nano/Microsatellite Market Forecast". [online]. *Proceedings of 30th Annual AIAA/USA Conference on Small Satellites. 8-13 August. Logan, UT*. Available at: https:// digitalcommons.usu.edu /cgi/ viewcontent.cgi? article=3336&context=smallsat [Accessed 8 Jan. 2020].

Draper, C., Wrigley, W., Hoag, G., Miller, J., Koso, D., Hopkins, A. and Vander Velde, W. (1965*). "*Apollo Guidance and Navigation. Space Navigation Guidance and Control". NASA Technical Report. Cambridge, Massachusetts: Instrumentation Laboratory of the Massachusetts Institute of Technology.

Duffy, K. (2015). "Electric Motors for Non-Cryogenic Hybrid Electric and Turboelectric Propulsion". *Proceedings of Joint Propulsion Conference. 27-29 July. Orlando, Florida:* AIAA. DOI: 10.2514/6.2015-3891.

Ermini, G. and Kaiser, F. (2002) "First Firing with the Regeneratively Cooled 2.5 kN LOX/Ethanol Engine". Langenthal, Switzerland: Swiss Propulsion Laboratory GmbH. Available at: http://www.spl.ch/old/news/first-LOX.html (Accessed: 16 April 2021).

Etherington, D. (2020). “Rocket startup Astra emerges from stealth, aims to launch for as little as $1M per flight”. [online] Techcrunch. Available at: https://techcrunch.com/2020/02/03/rocket-startup-astra-emerges-from-stealth-aims-to-launch-for-as-little-as-1m-per-flight/ [Accessed 4 Feb. 2020].

EUROCKOT Launch Service Provider (2011). “Rockot User's Guide”. Issue 5. [online] Bremen, Germany: EUROCKOT Launch Services GmbH. Available at: http://www.eurockot.com/wp-content/uploads/2012/10/UsersGuideIss5Rev0web.pdf [Accessed 21 Jan. 2020].

Ewig, R. (2009). “Vapour Pressurization (VaPak) Systems History, Concepts, and Applications”. WA, USA: Holder Consulting Group.

Fahem, M. (2020) ‘Axial and Radial flux permanent magnet machines – What is the difference?’ Montreal, Canada: EM Works. Available at: https://www.emworks.com/blog/motor-design/axial-and-radial-flux-permanent-magnet-machines-what-is-the-difference (Accessed: 15 June 2021).

Fatehi, M., Nosratollahi, M., Adami, A. and Taherzadeh, S. (2015). “Designing Space Cold Gas Propulsion System using Three Methods: Genetic Algorithms, Simulated Annealing and Particle Swarm”. *International Journal of Computer Applications, 118(22), pp.25-32*. DOI: 10.5120/20878-3624.

Fink, A., Camanho, P., Andrés, J., Pfeiffer, E. and Obst, A. (2010). “Hybrid CFRP/titanium bolted joints: Performance assessment and application to a spacecraft payload adaptor”. [online] *Composites Science and Technology, 70(2), pp.305-317.* DOI: 10.1016/j.compscitech.2009.11.002 [Accessed 31 Jan. 2020].

Firefly Aerospace Inc (2018). “Payload User's Guide”. [online] Cedar Park, TX: Firefly Aerospace Inc. Available at: https:// firefly.com / wp – content / themes/ firefly_ aerospace/ files / Firefly _ Aerospace _ Payload _ User' s_ Guide.pdf [Accessed 13 Feb. 2020].

Fletcher, E. and Morrell, G. (1960) “Ignition in Liquid Propellant Rocket Engines”, *Progress in Combustion Science and Technology*. Elsevier, 1, pp. 183–215. doi: 10.1016/b978-1-4831-9753-1.50010-5.

Ford, D. (2007). “Asymmetric Bulkheads for Cylindrical Pressure Vessels”. Marshall Space Flight Centre, Alabama. [online] Techbriefs. Available at: https:// www.techbriefs.com / component / content / article / tb / Techbriefs / mechanics-and-machinery / 1200 [Accessed 18 Jun. 2018].

Foust, J. (2019). “Foust Forward | Worldwide, there are 131 small launch vehicles in the works. Most of these will fizzle out”. SpaceNews.com. [online] SpaceNews. Available at: https:// spacenews.com/ foust-forward-worldwide-there-are-131-small-launch-vehicles-in-the-works-most-of-these-will-fizzle-out/ [Accessed 24 Jan. 2020].

Foust, J. and Smith, P. (2004). “Small Launch Vehicle Services: Supply and Demand Though 2010”. *Proceedings of Space 2004 Conference and Exhibit*. *28-30 September. San Diego, CA.* [online] Aerospace Research Central. DOI: 10.2514/6.2004-6000. [Accessed 20 Jan. 2020].

Gardiner, G., 2017. “SpaceX announces COPV’s role in September rocket explosion”. [online] Compositesworld.com. Available at: <https://www.compositesworld.com/articles/spacex-announces-copvs-role-in-sept-rocket-explosion> [Accessed 19 April 2021].

Generation Orbit Launch Services, Inc. (2014). “GOLauncher 2: Fast, Flexible, and Dedicated Space Transportation for Nanosatellites”. [online] Atlanta, GA: Generation Orbit Launch Services, Inc. Available at: https://pdfs.semanticscholar.org/d722/302894eb1a570769ba6ce608337c6885e2c8.pdf [Accessed 13 Feb. 2020].

Gerberich, M. and Oleson, S. (2013). “Estimation Model of Spacecraft Parameters and Cost Based on a Statistical Analysis of COMPASS System Designs”. *Proceedings of AIAA SPACE 2013 Conference and Exposition*. *10-12 September. San Diego, CA.* DOI: 10.2514/6.2013-5432.

Glassman, I., Yetter, R. A. and Glumac, N. G. (2015) “Ignition”, in *Combustion*. Elsevier, pp. 363–391. doi: 10.1016/b978-0-12-407913-7.00007-4.

Goodwin, J. and Wegner, P. (2001). “Evolved Expendable Launch Vehicle Secondary Payload Adapter - A New Delivery System for Small Satellites”. *Proceedings from: 15th Annual/USU Conference on Small Satellites*. *Logan, UT*. [online] Digital Commons. Available at: https://digitalcommons.usu.edu/smallsat/2001/All2001/74/ [Accessed 31 Jan. 2020].

Gopal, S. (2020) ‘Analysis of Different Types of Motors for the Use in Electric Vehicles’, International Research Journal of Engineering and Technology, (June), pp. 5247–5251. Available at: www.irjet.net.

Graf, N., Davis, K. and McBain, M. (2000). “Subscale Composite Liquid Oxygen Tank Testing”. *Proceedings of 32nd SAMPE International Technical Conference. 5-9 November. Boston, MA*. NASA Technical Report. New Orleans, LA: Lockheed Martin Michoud Space Systems.

Grobekatthöfer, K. and Yoon, Z. (2012). “Introduction into quaternions for spacecraft attitude representation”. Berlin: Technical University of Berlin.

Grocki, J. (2012). “A Primer for DUPLEX Stainless Steel”. [pdf] ArcelorMittal. Available at: https://www.steeltank.com/Portals/0/Pressure%20Vessels/SSWseminarOct2012/4%20A%20Primer%20for%20DUPLEX%20%20Corrosion%20Solutions%20presentation.pdf [Accessed 16 Jul. 2019].

Gündüz, D. E. *et al.* (2005) “Hypergolic ignition of liquid fuel and liquid oxidizer in a rocket motor”, *RAST 2005 - Proceedings of 2nd International Conference on Recent Advances in Space Technologies*, 2005, pp. 324–329. doi: 10.1109/RAST.2005.1512585.

Haidn, O. J. (2008) ‘Advanced rocket engines’, Advances on propulsion technology for high-speed …, pp. 6-1-6–40. Available at: http://www.rto.nato.int.

Haydock, J. (2018) “Introduction to Lithium Polymer Battery Technology”. B.C.E. Electronics. Sassuolo, Italy. Available at: https://www.bce.it/wp-content/uploads/2019/06/Jauch-battery-white_paper_introduction_to_lipo_battery_technology_11-2018_BCE.pdf.

Henry, C. (2016) Rocket Lab Completes Flight Qualification for Electron’s Rutherford Engine - Via Satellite -. Available at: https://www.satellitetoday.com/business/2016/03/23/rocket-lab-completes-flight-qualification-for-electrons-rutherford-engine/ (Accessed: 8 June 2021).

Hermsen, R. and Zandbergen, B. (2017). “Pressurization system for a cryogenic propellant tank in a pressure-fed high-altitude rocket”. *Proceedings of 7TH European Conference for Aeronautics and Aerospace Sciences (EUCASS). 3-6 July. Milan, Italy*.

Humble, R., Henry, G. and Larson, W. (2007). “Space propulsion analysis and design”. New York: McGraw-Hill.

Huang, D. H. and Huzel, D. K. (1992) “Modern Engineering for Design of Liquid-Propellant Rocket Engines”, *Progress in Astronautics and Aeronautics, AIAA*. Washington, DC: American Institute of Aeronautics and Astronautics, 147. doi: 10.2514/4.866197.

Huzel, D. K. and Huang, D. H. (1967) “Design of Liquid Propellant Rocket Engines”. 2nd edn. NASA.

Jackson, J., Vickers, J. and Fikes, J. (2015). “Composite Cryotank Technologies and Development 2.4 and 5.5M out of Autoclave Tank Test Results”. *Proceedings of Composites and Advanced Materials Expo (CAMX). 26-29 October. Dallas, TX*. NASA Technical Report. Huntsville, AL: NASA.

Jackson, J., Miller, P., Boyd, W., and Funk, F. (1961). “A Study of the Mechanism of the Titanium - Liquid Oxygen Explosive Reaction”. Technical Report ASD-TR-61-479. Battelle Memorial Institute.

Karunamoorthy, B. and Dhivyaa, D. (2017) ‘Design of PMSM and its Application’, International Journal of Current Research, 9(5), pp. 2015–2018.

Ketsdever, A. and Micci, M. (2000). “Micropropulsion for small spacecraft”. Reston, VA: American Institute of Aeronautics and Astronautics.

Kim, M., Kang, S., Kim, C. and Kong, C. (2007). “Tensile response of graphite/epoxy composites at low temperatures”. *Composite Structures, 79(1), pp.84-89*. DOI: 10.1016/j.compstruct.2005.11.031.

King, P., Weldon, A. and Braadford, A. (2016). “Firefly Alpha - A Mass Produced Small Launch Vehicle for the New Space Era”. *Proceedings of the 30th AIAA/USU Conference on Small Satellites. 8-13 August. Logan, UT*. [online] Small Satellite Conference. Available at: https://digitalcommons.usu.edu/smallsat/2016/TS2Launch/8/ [Accessed 20 Jan. 2020].

Kolondzovski, Z. et al. (2011) 'Power limits of high-speed permanent-magnet electrical machines for compressor applications', IEEE Transactions on Energy Conversion, 26(1), pp. 73–82. doi: 10.1109/TEC.2010.2089459.

Kovacs, L. (2018) 'Firefly Aerospace Overview'. Firefly Aerospace. Available at: http://www.michman.org/resources/Documents/4 - Kovacs - Firefly MAMA.pdf.

Krebs, G. (2018). "Kuaizhou-1A (KZ-1A)". [online] Gunter's Space Page. Available at: https://space.skyrocket.de/doc_lau_det/kuaizhou-1a.htm [Accessed 20 Jan. 2020].

Krivanek, T. and Yount, B. (2012). "Composite Payload Fairing Structural Architecture Assessment and Selection. NASA Technical Report". [online] Available at: https://ntrs.nasa.gov/search.jsp?R=20120009204 [Accessed 4 Jun. 2018].

Kwak, H., Kwon, S. and Choi, C. (2018). "Performance assessment of electrically driven pump-fed LOX/kerosene cycle rocket engine: Comparison with gas generator cycle". *Aerospace Science and Technology*, 77, pp.67-82. DOI: 10.1016/j.ast.2018.02.033.

LabTV Online (2015). "Space Hitchhikers: The ESPA Ring". [video] Available at: https://www.youtube.com/watch?v=S_5MlJh5g3o [Accessed 7 Jun. 2018].

Lathabai, S. (2011). "Joining of aluminium and its alloys". *Fundamentals of Aluminium Metallurgy, pp.607-654.* DOI: 10.1533/9780857090256.3.607.

Lane, S., Higgins, J., Biskner, A., Sanford, G., Springer, C. and Berg, J. (2011). "Out-of-Autoclave Composite Fairing Design, Fabrication, and Test". *Journal of Manufacturing Science and Engineering, 133(3), p.031020.* DOI: 10.1115/1.4004321.

Lee, J. et al. (2020) 'Performance Analysis and Mass Estimation of a Small-Sized Liquid Rocket Engine with Electric-Pump Cycle', *International Journal of Aeronautical and Space Sciences.* doi: 10.1007/s42405-020-00325-z.

Li, J., Yan, S. and Tan, X. (2014). "Dynamic-Envelope Analysis of Clamp-Band Joint Considering Pyroshock of Satellite Separation". *Journal of Spacecraft and Rockets, 51(5), pp.1390-1400*. DOI: 10.2514/1.A32382.

Linden, D. (2010) *Linden's Handbook of Batteries*. 4th edn. Edited by T. B. Reddy. Mc Graw Hill.

LJ Global Technology (2020) Product specification. Hong Kong.

Lopez, D. (2018). "Rocket Staging". [online] Grc.nasa.gov. Available at: https://www.grc.nasa.gov/WWW/K-12/rocket/rktstage.html [Accessed 27 Jan. 2020].

Marques, M. P. P. M. (2016) “Small Liquid Propellant Rocket Engine Design, Build and Test”. [Thesis] Instituto Superior Técnico. Available at: https:// fenix.tecnico.ulisboa.pt/ downloadFile/563345090415202/Thesis.pdf.

Mathew, L., Deepak, B.P, and Sabu, B. (2016). “Design and Analysis of a Metallic Ogive Payload Fairing for a New Generation Launch Vehicle”. *IOSR Journal of Mechanical and Civil Engineering, 13(05), pp.99-103*. DOI: 10.9790/1684-13050199103.

McLaughlan, P., Forth, S. and Grimes-Ledesma, L. (2011). “Composite Overwrapped Pressure Vessels A Primer”, Vol. 573 of NASA SP. Houston, TX: NASA, Johnson Space Centre.

Mei, J., Lee, C. H. T. and Kirtley, J. L. (2020) ‘Design of axial flux induction motor with reduced back iron for electric vehicles’, IEEE Transactions on Vehicular Technology, 69(1), pp. 293–301. doi: 10.1109/TVT.2019.2954084.

Messier, D., 2014. “Boeing’s Composite Tank Could Greatly Improve Launch Vehicles – Parabolic Arc”. [online] Parabolicarc.com. Available at: <http://www.parabolicarc.com/2014/04/05/composite-tank/> [Accessed 19 April 2021].

Metalary, 2021. “Titanium Price”. [online] Available at: <https://www.metalary.com/titanium-price/> [Accessed 10 August 2021].

Modlin, C. and Zipay, J. (2014). “The 1.5 & 1.4 Ultimate Factors of Safety for Aircraft & Spacecraft – History, Definition and Applications”. *NASA Technical Report.*

Morino, Y., Shimoda, T., Morimoto, T., Ishikawa, T. and Aoki, T. (2001). “Applicability of CFRP materials to the cryogenic propellant tank for reusable launch vehicle (RLV)”. [online] *Advanced Composite Materials, 10(4), pp.339-347*. DOI: 10.1163/156855101753415364 [Accessed 5 Feb. 2020].

Morring, F. and Norris, G. (2015) Rocket Lab Unveils Battery-Powered Turbomachinery, Aviation Week. Available at: https://aviationweek.com/defense-space/space/rocket-lab-unveils-battery-powered-turbomachinery (Accessed: 4 June 2021).

Motiwala, S., Mathias, D. and Mattenberger, C. (2014). “Conceptual Launch Vehicle and Spacecraft Design for Risk Assessment”. NASA Technical Report. [online] Hanover: NASA. Available at: https://ntrs.nasa.gov/search.jsp?R=20150000182 [Accessed 22 May 2019].

Miao, Y. et al. (2019) ‘Current li-ion battery technologies in electric vehicles and opportunities for advancements’, *Energies*, 12(6), pp. 1–20. doi: 10.3390/en12061074.

Mirshams, M., Taei, H., Ghobadi, M. and Haghi, H. (2014). “Spacecraft attitude dynamics simulator actuated by cold gas propulsion system”. *Proceedings of the Institution of Mechanical Engineers, Part G: Journal of Aerospace Engineering, 229(8), pp.1510-1530*. DOI: 10.1177/0954410014555167.

Mitchell, D.H. Flight separation mechanisms. “NASA Space vehicle design criteria”. [online] Available at: https://ntrs.nasa.gov/archive/nasa/casi.ntrs.nasa.gov/19710019510.pdf [Accessed 29 May 2018].

Mirza, U. (2013). “Face-Off: Lithium Ion Vs Lithium Iron Battery”. [online] Bright Hub Engineering. Available at: http:// www.brighthubengineering.com/ power-generation-distribution / 123906 – comparison -of-lithium-ion-to-lithium-iron-battery/ [Accessed 30 Apr. 2019].

Mikhaylik, Y. et al. (2018) “650 Wh / kg, 1400 Wh / L Rechargeable Batteries for New Era of Electrified Mobility”, *in 2018 NASA Aerospace Battery Workshop*. Huntsville, USA: NASA, pp. 1–20. Available at: https://www.nasa.gov/sites/default/files/atoms/files/650_whkg_1400_whl_recharg_batt_new_era_elect_mobility_ymikhaylik_0.pdf.

Mudunuri, V. (2005). “Aerodynamic Heating of Student Rocket Project-5 Sounding Rocket”. Master's. University of Alaska Fairbanks.

Nagendra, N. (2019). “Traditional space and new space industry in India ORF”. [online] ORF. Available at: https://www.orfonline.org/expert-speak/traditional-space-and-new-space-industry-in-india/ [Accessed 26 Dec. 2019].

NASA (1972). “ATLAS-Centaur AC-17 Performance for Applications Technology Satellite ATS-D” Mission. *NASA Technical Memorandum*.

NewSpace India Limited (2019). “Small Satellite Launch Vehicle Technical Brochure”. Version 2. [online] Bengaluru, India: Indian Space Research Organisation. Available at: http://nsilindia.co.in/sites/default/files/u1/SSLV%20Technical%20Brochure%20V12.pdf [Accessed 21 Jan. 2020].

Nguyen, X. (2018). Microgrid in USTH campus: Architecture and Power Management Strategies. Masters. University of Science and Technology Hanoi.

Niederstrasser, C. (2018). “Small Launch Vehicles – A 2018 State of the Industry Survey”. *Proceedings of 32nd Annual AIAA/USU Conference on Small Satellites. 4-9 August. Logan, UT.* [online] Dulles, Virginia: Northrop Grumman Corporation. Available at: https:// digitalcommons.usu.edu /cgi/ viewcontent.cgi?article = 4118&context=smallsat [Accessed 24 Jan. 2020].

Niederstrasser, C. and Frick, W. (2015). “Small Launch Vehicles - A 2015 State of the Industry Survey”. *Proceedings of 29th Annual AIAA/USU Conference on Small Satellites. 8-13 August. Logan, UT.* [online] Dulles, Virginia: Northrop Grumman Corporation. Available at: https://digitalcommons.usu.edu/smallsat/2015/all2015/12/ [Accessed 21 Jan. 2020].

Nothnagel, S., Streetman, B. and Hoffman, J. (2011). “Development of a Cold Gas Propulsion System for the TALARIS Hopper”. Master's. Massachusetts Institute of Technology.

Orbex Space. 2021. “Orbex Vehicle”. [online] Available at: <https://orbex.space/vehicle> [Accessed 13 April 2021].

Orbex (2019) Orbex Opens Doors to Europe’s Most Modern Rocket Factory. Available at: https://orbex.space/orbex-behind-the-scenes (Accessed: 4 June 2021).

Orbital ATK (2015). “Pegasus User's Guide”. [online] Dulles, Virginia: Orbital ATK. Available at: https://web.archive.org/web/20160113130631/https://www.orbitalatk.com/flight-systems/space-launch-vehicles/pegasus/docs/Pegasus_UsersGuide.pdf [Accessed 20 Jan. 2020].

Panasonic (2013) Specifications for NCR18650GA. Kadoma, Japan. Available at: https://datasheetspdf.com/pdf/955257/Panasonic/NCR18650PF/1.

Pallardy, R. (1998). “Cryogenics”. [online] Encyclopaedia Britannica. Available at: https://www.britannica.com/science/cryogenics [Accessed 4 Feb. 2020].

Park, S., Kim, Y. and Jeong, E. (2017) “Optimization of the Startup Sequence of a Liquid-propellant Rocket Engine”, *7th European conference for Aeronautics and Space Science*, (Cc), pp. 1–10. doi: 10.13009/EUCASS2017-293.

Pellegrino, G. et al. (2012) ‘Performance comparison between surface-mounted and interior PM motor drives for electric vehicle application’, *IEEE Transactions on Industrial Electronics*, 59(2), pp. 803–811. doi: 10.1109/TIE.2011.2151825.

Rabbitte, S. P. and Mohs, A. (2020) “Investigation of Ignition Systems for an 800 lbf Thrust Bipropellant Engine”. University of Alabama in Huntsville. Available at: http://space.uah.edu/assets/files/Rabbitte_Mohs_Ignition2020.pdf.

Radhika, M., Chandra, K. and Rao, G. (2014). “Design, Fabrication and Testing of Composite Overwrapped Pressure Vessel for CNG Storage”. *International Journal of Engineering Research & Technology (IJERT), 3(12)*.

Rawlins, L. (2019) ‘Low Cost , High Performance Easy to Use Drives for Permanent Magnet Synchronous Motors (PMSM)’. KB Electronics, pp. 1–4.

Rocket Lab (2016). “Payload User’s Guide”. 4th ed. Huntington Beach, California: Rocket Lab.

Rockett, D. (2018). “What’s the Better Battery for Your Portables—Li Ion or Li Poly?” [online] Electronic Design. Available at: https:// www.electronicdesign.com / power-management / article / 21806525 / whats-the-better-battery-for-your-portablesli-ion-or-li-poly [Accessed 13 Feb. 2020].

Ross, C. and Young, R. (1948). “The Design of Tanks for Liquid-Propellant Rocket Power Plants”. *Journal of the American Rocket Society, 00(75), pp.107-118*. DOI: 10.2514/8.4239.

Rudman, T. J. and Austad, K. L. (2002) ‘The Centaur Upper Stage Vehicle’, in *4th IAC on Launcher Technology, 3-6 December*. Liege, Belgium: Lockheed Martin Corporation.

Rycroft, M. (2018) The advantages of the small permanent magnet motor, EE Publishers. Available at: https://www.ee.co.za/article/the-advantages-of-the-small-permanent-magnet-motor.html (Accessed: 17 June 2021).

Sakunthala, S., Kiranmayi, R. and Mandadi, P. N. (2018) ‘A study on industrial motor drives: Comparison and applications of PMSM and BLDC motor drives’, 2017 International Conference on Energy, Communication, Data Analytics and Soft Computing, ICECDS 2017, (January), pp. 537–540. doi: 10.1109/ICECDS.2017.8390224.

Scarr, A. (1992).” Nested Tank Construction”. Patent: 5,085,343.

Seitzman, J. (2012). “Conical Nozzles”. Atlanta, GA: Georgia Institute of Technology.

Shen, F. and Pope, D. (1990). “Design and Development of Composite Fairing Structures for Space Launch Vehicles”. SAE Transactions - Journal of Aerospace, 99(1), pp.1447-1455. DOI: 10.4271/901836.

Shrivastava, K. (2016) ‘A Review on Types of DC Motors and the Necessity of Starter for Its Speed Regulation’, International Journal of Advanced Research in Computer and Communication Engineering, 5(4), pp. 4–6. doi: 10.17148/IJARCCE.2016.5416.

Singh, N. (2018). “The Hydrodynamic Design and Analysis of a Liquid Oxygen Pump Impeller for a Rocket Engine”. Master's. University of KwaZulu-Natal.

Štefan, D. et al. (2019) ‘Design of the Electrically Driven Fuel Pump for the Space Rocket Engine’, in Turbostroje 2019. Prague. Available at: https://www.researchgate.net/publication/339326266_Design_of_the_electrically_driven_fuel_pump_for_the_space_rocket_engine.

Stenzel, P., Baumann, M., Fleer, J., Zimmermann, B. and Weil, M. (2014*). “*Database development and evaluation for techno-economic assessments of electrochemical energy storage systems”. *Proceedings of 2014 IEEE International Energy Conference (ENERGYCON). 13-16 May. Dubrovnik, Croatia.* DOI: 10.1109/ENERGYCON.2014.6850596

Sutton, G. (2006). “History of liquid propellant rocket engines”. Reston, VA: American Institute of Aeronautics and Astronautics.

Sutton, G. and Biblarz, O. (2001). “Rocket Propulsion Elements”. Somerset: John Wiley & Sons, Incorporated.

Sutton, N. V. and Schneider, H. (1965) “Analysis of Hypergolic Igniters”, *Microchemical Journal*, 9(2), pp. 209–217. doi: 10.1016/0026-265X(65)90104-9.

SMAP (2018). “SMAP: Launch Vehicle”. [online] Available at: https://smap.jpl.nasa.gov/observatory/launch-vehicle/ [Accessed 31 May 2018].

Space Flight Systems. (2018). “Rocket Staging”. [online] Available at: https:// spaceflightsystems.grc.nasa.gov / education / rocket/rktstage.html [Accessed 28 May 2018].

Szelinski, B., Lange, H., Röttger, C., Sacher, H., Weiland, S. and Zell, D. (2012). “Development of an innovative sandwich common bulkhead for cryogenic upper stage propellant tank”. [online] *Acta Astronautica, 81(1), pp.200-213.* DOI: 10.1016/j.actaastro.2012.06.025 [Accessed 10 Feb. 2020].

“T1000G Data Sheet”. (2019). [pdf] Santa Ana: Toray Carbon Fibers America. Available at: https://www.toraycma.com/file_viewer.php?id=4465 [Accessed 27 Jun. 2019].

Tam, W., Ballinger, I. and Jaekle, D. (2006). “Conceptual Design of Space Efficient Tanks”. *Proceedings of 42nd AIAA/ASME/SAE/ASEE Joint Propulsion Conference. 9-12 July. Sacramento, CA.* DOI: 10.2514/6.2006-5058 [Accessed 5 Feb. 2020].

Teschler, L. (2013) What’s the Difference Between Asynchronous and Synchronous Motors?, Machine Design. Available at: https://www.machinedesign.com/motors-drives/article/21831717/whats-the-difference-between-asynchronous-and-synchronous-motors (Accessed: 15 June 2021).

Thesken, J., Murthy, P. and Phoenix, L. (2007). “Composite Overwrap Pressure Vessels: Mechanics and Stress Rupture Lifting Philosophy”. *Proceedings of 48th AIAA/ASME/ASCE/AHS/ASC Structures, Structural Dynamics, and Materials Conference. 23-26 April. Honolulu, HI.* DOI: 10.2514/6.2007-2145.

Torres, R., García, L. and Verdú, R. (2018). “Arion 2: The European and Reusable Rocket Launcher for Small Satellites”. *Proceedings of 2018 SpaceOps Conference. 28 May - 1 June. Marseille, France*. [online] Elche, Spain: American Institute of Aeronautics and Astronautics, Inc. DOI: 10.2514/6.2018-2467. [Accessed 20 Jan. 2020].

Trading Economics, 2021. Steel Historical Price and Forecast. [online] Available at: <https://tradingeconomics.com/commodity/steel> [Accessed 10 August 2021].

Tuttle, M E. (2009). “Moisture Diffusion in Honeycomb Core Sandwich Composites”. [online] Seattle, WA: University of Washington. Available at: http:// iccm-central.org/ Proceedings/ICCM17

proceedings/Themes/Applications/ SANDWICH%20STRUCTURES/B6.31%20Tuttle.pdf [Accessed 17 Sep. 2018].

United Launch Alliance (2006). “Delta II Payload Planners Guide”. [online] Littleton, Colorado: United Launch Alliance. Available at: https://www.ulalaunch.com / docs / default-source / rockets / deltaiipayloadplannersguide2007.pdf [Accessed 12 Feb. 2020].

United Launch Alliance. “Delta IV Launch Services User’s Guide”. (2013). Centennial, Colorado: United Launch Alliance. Available at: http://www.ulalaunch.com [Accessed 7 Jun. 2018].

United Performance Metals. (2019). “CP Grade 3 Titanium Sheet & Coil - AMS 4900”. [online] Available at: https://www.upmet.com/products/titanium/cp-grade-3#Physical-Properties [Accessed 28 Jun. 2019].

United Space in Europe. (2019). “Fairing separation system”. [online] Available at: https://www.esa.int/ESA_Multimedia/Images/2019/10/Fairing_separation_system [Accessed 31 Jan. 2020].

Venkatasetty, H. and Jeong, Y. (2002). “Recent advances in lithium-ion and lithium-polymer batteries”. *Proceedings of Seventeenth Annual Battery Conference on Applications and Advances (Cat. No.02TH8576). 18 January. Long Beach, CA*. [online] Available at: https:// ieeexplore.ieee.org / abstract/ document/ 986391. DOI: 10.1109/BCAA.2002.986391 [Accessed 15 Jan. 2020].

Virgin Orbit LLC (2019). “LauncherOne Service Guide”. 1st ed. [ebook] Long Beach, California: Virgin Orbit LLC. Available at: https:// virginorbit.com/ wp-content/ uploads/ 2019/09/ ServiceGuide_Sept2019.pdf [Accessed 20 Jan. 2020].

Vezzini, A. (2014) “Lithium-Ion Battery Management”. *Lithium-Ion Batteries: Advances and Applications*. Elsevier. doi: 10.1016/B978-0-444-59513-3.00015-7.

Wang, H. (2012) ‘Design and implementation of brushless DC motor drive and control system’, *Procedia Engineering*, 29, pp. 2219–2224. doi: 10.1016/j.proeng.2012.01.291.

Ward, T. (2010). “Aerospace propulsion system”. Singapore: John Wiley & Sons.

Waxenegger-Wilfing, G., dos Santos Hahn, R. and Deeken, J. (2018). “Studies on Electric Pump-Fed Liquid Rocket Engines for Micro-Launcher”. *Proceedings of Space Propulsion 2018. 14-18 May. Seville, Spain*. [online]: German Aerospace Centre. Available at: https:// www.researchgate.net / publication/324983438_Studies_on_Electric_PumpFed_Liquid_Rocket_Engines_for_Micro-Launcher [Accessed 29 Apr. 2019].

Wegner, P., Higgins, J. and VanWest, B. (2002). “Application of Advanced Grid-Stiffened Structures Technology to the Minotaur Payload Fairing”. *Proceedings of 43rd AIAA/ASME/ASCE/AHS/ASC*

Structures, Structural Dynamics, and Materials Conference. *22-25 April. Denver, Colorado*. DOI: 10.2514/6.2002-1336

Wekerle, T., Pessoa Filho, J., Costa, L. and Trabasso, L. (2017). "Status and Trends of Smallsats and their Launch Vehicles — An Up-to-date Review". *Journal of Aerospace Technology and Management, 9(3), pp.269-286.* Available at: http://www.scielo.br/scielo.php?script=sci_arttext&pid=S2175-91462017000300269 [Accessed 21 Jan. 2020]. DOI: 10.5028/jatm.v9i3.853.

Wiesehan, G. and Villegas, J. (2018). "Design of Augmented Spark Igniter". [online] Rocket Propulsion Laboratory. Available at: https://rocketproplab.org/news/2018/3/11/design-of-augmented-spark-igniter [Accessed 7 Jan. 2019].

Wunderlin, N. (2019) *Design of a Liquid Propellant Rocket Engine Combustion Chamber*. University of KwaZulu-Natal.

Wunderlin, N., Martin, D., Brooks, M. and Pitot, J. (2018). "Design Options for a South African Small-Satellite Launch Vehicle". *Proceedings of 2018 Joint Propulsion Conference*. *9-11 July*. *Cincinnati, Ohio.* Reston, VA: AIAA. DOI: 10.2514/6.2018-4462.

Yang, Y. P. and Lee, C. H. (2012) 'Multifunctional optimal design of axial-flux permanent magnet wheel motors for light electric vehicles', *World Electric Vehicle Journal*, 5(2), pp. 533–540. doi: 10.3390/wevj5020533.

Yazdi, M. A., Saied, S. A. and Mirimani, S. M. (2020) 'Design and construction of new axial-flux permanent magnet motor', *IET Electric Power Applications. Institution of Engineering and Technology*, 14(12), pp. 2389–2394. doi: 10.1049/iet-epa.2020.0126.

Yu, J. C., Cheng, M. Te and Yao, W. S. (2016) 'Design and Analysis of Axial Flux Permanent Magnet Motor with Variable Windings', *Journal of the Chinese Society of Mechanical Engineers, Transactions of the Chinese Institute of Engineers*, Series C/Chung-Kuo Chi Hsueh Kung Ch'eng Hsuebo Pao, 37(5), pp. 497–507.

Zhao, J. and Yangwei, Y. (2011) 'Brushless DC Motor Fundamentals Application Note', MPS, *The future of Analog IC Technology*, (July 2011), pp. 7–8.

Zelenka, J., Vlcek, T., Diaz, V., Rodriguez, J., Cardone, T. and Jaredson, D. (2012). "Leak Resistant Liners for Propellant Tanks - Space Application". *NanoCon*. [online] Available at: http://nanocon2014.tanger.cz/files/proceedings/04/reports/1250.pdf [Accessed 8 Jan. 2019].

Zheng, H., Zeng, X., Zhang, J. and Sun, H. (2018). "The Application of Carbon Fiber Composites in Cryotank". In book: *Solidification*. DOI: 10.5772/intechopen.73127

Appendix: Buckling Results

This analysis was performed in order to determine the minimum propellant tank wall thickness required for tank buckling to be avoided in an unpressurized state. Ideally, a vehicle should hold its own weight without external support or internal pressurization to reduce storage and transportation complexities. Only the buckling response for the kerosene tank is presented here, since a preliminary analysis found a negligible difference in performance between the LOX and kerosene tanks. The geometry of the tank was specified as follows: outer radius 600 mm; length 383 mm; thicknesses range from 0.1 mm – 10 mm. The results for the four analysis types considered in Section 2.7 are presented in Figures A-1 to A-3.

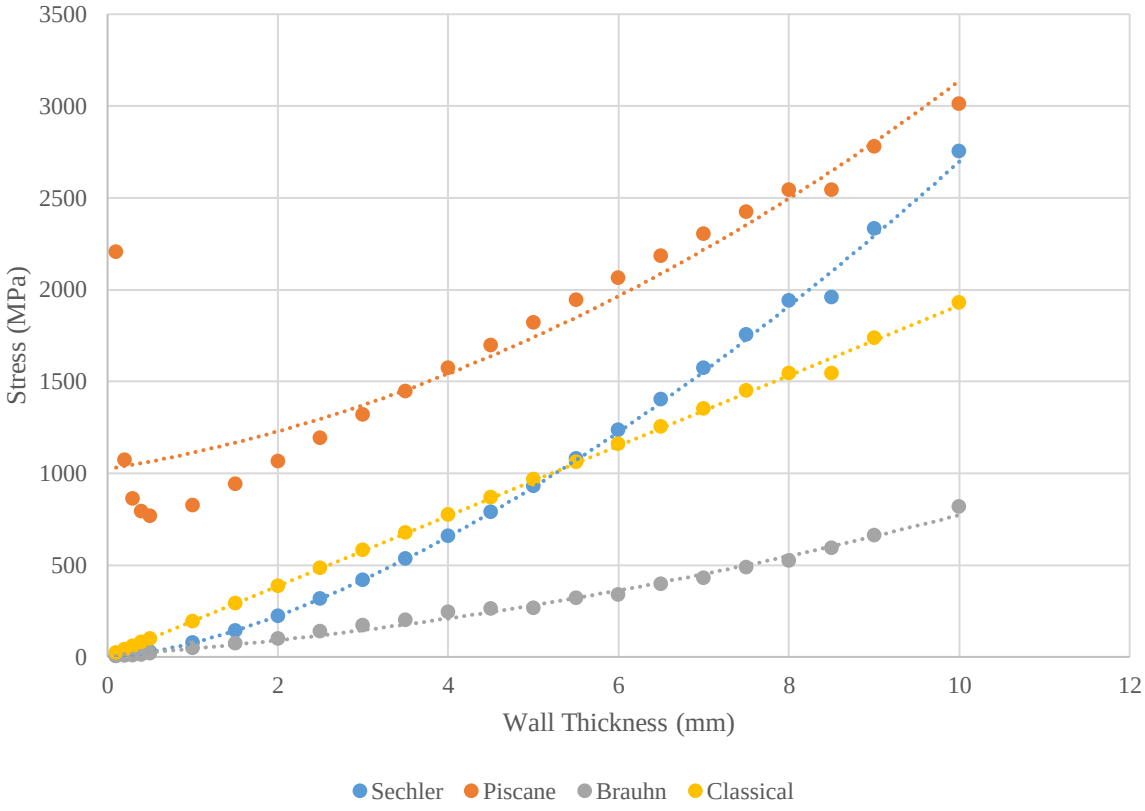

Figure A-1: Stainless steel 301 FH buckling stress analysis

A comparison of the various materials is given below. Brauhn's method is used in the comparison as it is the most conservative and his work focuses specifically on launch vehicles. Of particular interest is how similarly stainless steel 301and carbon fibre perform for thickness less than 5 mm.

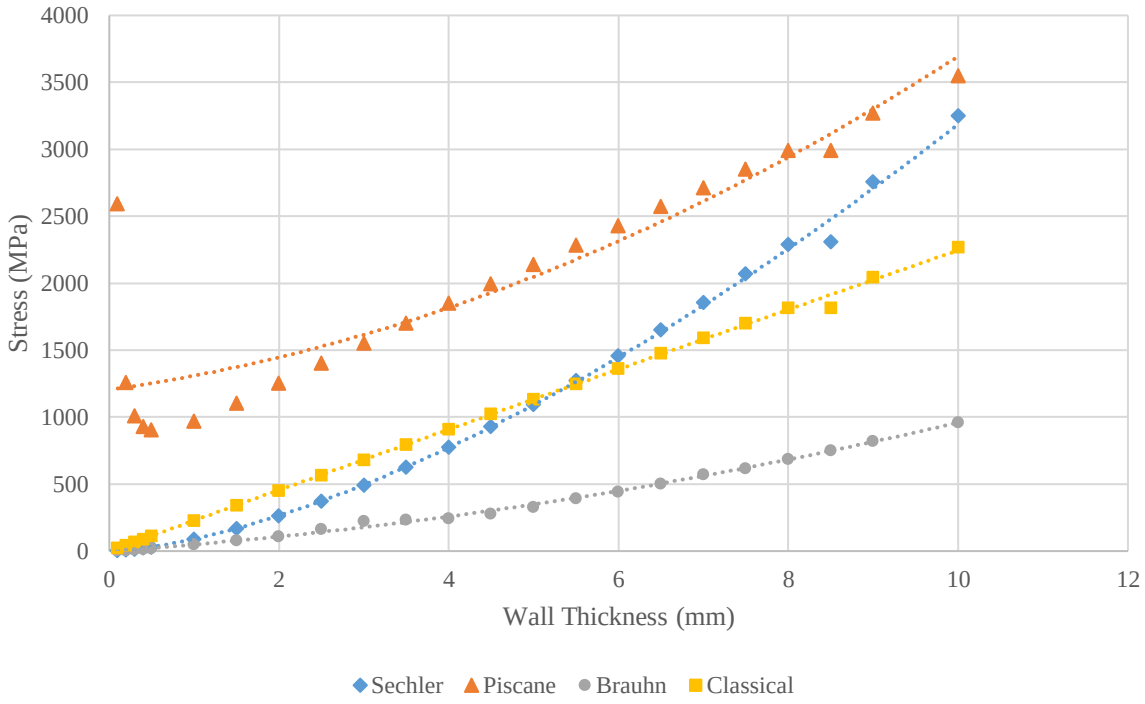

Figure A-2:CFRP T700/Epoxy buckling stress analysis

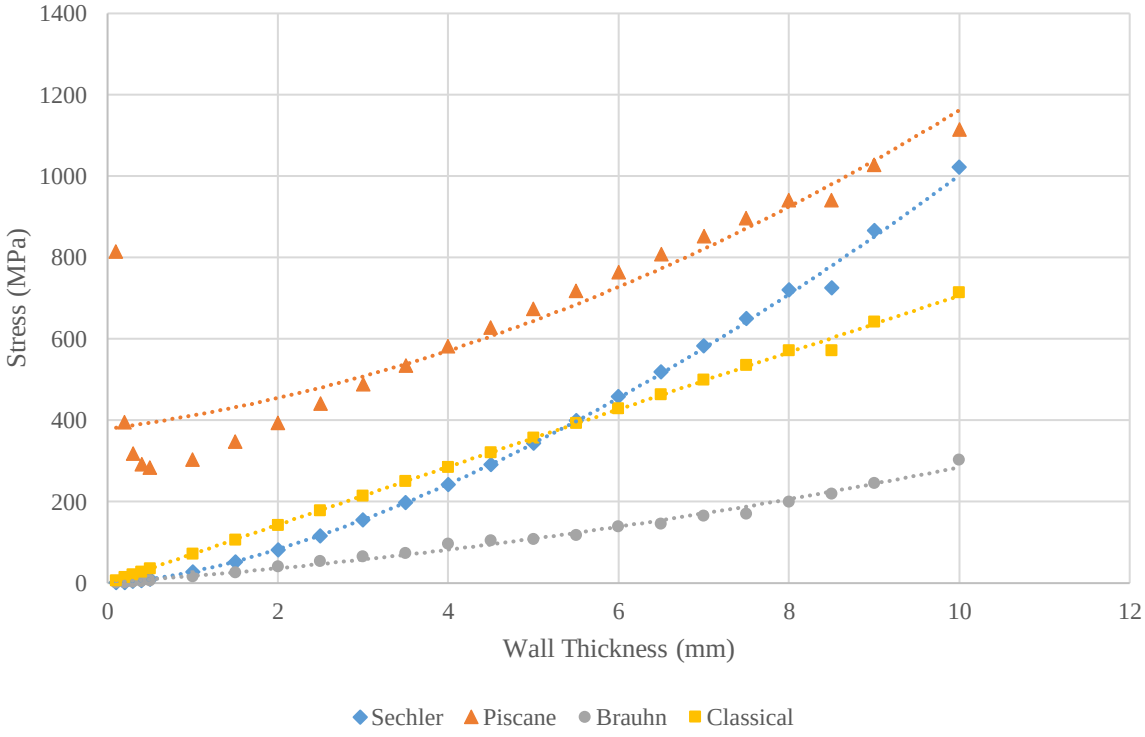

Figure A-3: Al 7075-T6 buckling stress analysis

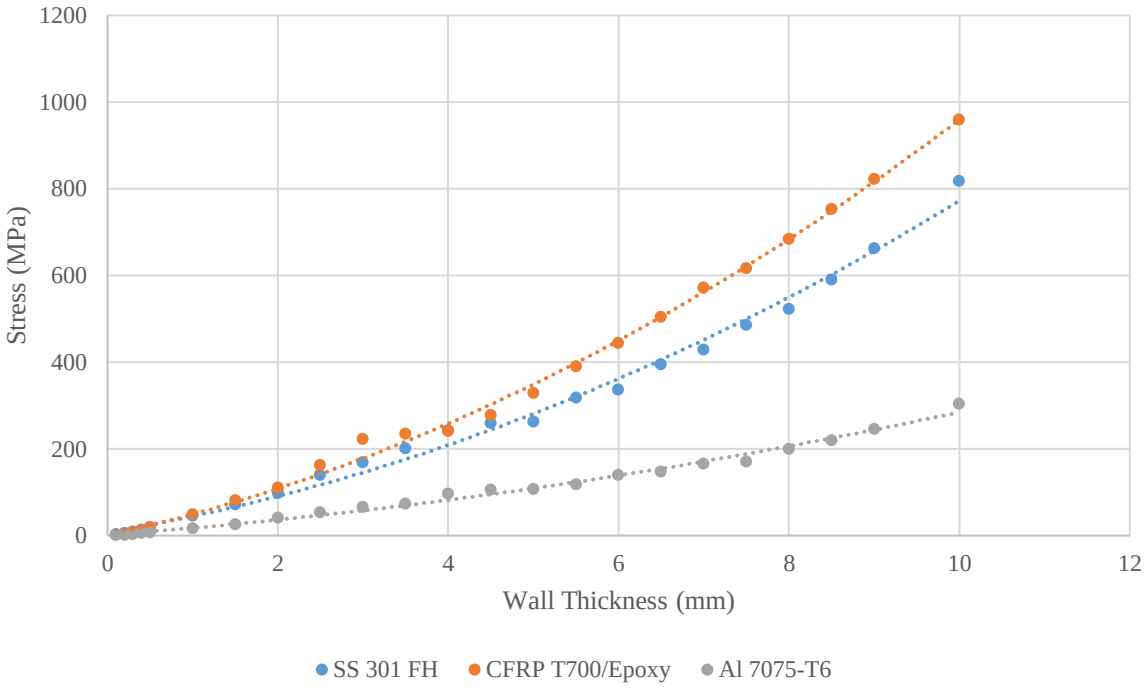

Figure A-4: Brauhn buckling stress comparison

The results suggest that tanks should be designed for failure due to internal pressure rather than buckling for the upper stage vehicle, however this may not be true for the booster stage which will have a larger aspect ratio and greater inertial loading in the axial direction.